Institute for Crop Science and Resource Conservation -
Plant Diseases and Plant Protection

# Phenotyping of barley resistance to plant diseases on the leaf and greenhouse scale through hyperspectral imaging and data analysis

Dissertation

zur
Erlangung des Doktorgrades (Dr. rer. nat.)
der
Mathematischen-Naturwissenschaftlichen Fakultät
der
Rheinischen Friedrich-Wilhelms-Universität Bonn

vorgelegt von

**Stefan Thomas**
aus
Bonn, Deutschland

Bonn, August 2020

Angefertigt mit Genehmigung der Mathematisch-Naturwissenschaftlichen
Fakultät der Rheinischen Friedrich-Wilhelms-Universität Bonn

1. Gutachter: Prof. Dr. Anne-Katrin Mahlein
Institut für Nutzpflanzenwissenschaften und Ressourcenschutz, Universität Bonn

2. Gutachter: Prof. Dr. Peter Dörmann
Institut für Molekulare Physiologie und Biotechnologie der Pflanzen, Universität Bonn

3. Gutachter: Prof. Dr. Uwe Rascher
IBG-2: Plant Sciences, Forschungszentrum Jülich GmbH

Tag der mündlichen Prüfung: 15.12.2020
Erscheinungsjahr: 2021

# Abstract

Optical sensors become increasingly interesting as means to perform automated, non-invasive and objective monitoring in agriculture, but also have immense potential as tools for research and development. Especially hyperspectral sensors have proven to extract a multitude of relevant parameters about the interaction of plants with biotic and abiotic stresses alike through the large amount of precise information about changes in the plant spectral signature they can detect. However, despite multiple research studies, there are still areas within the field of hyperspectral imaging which have barely been investigated.

This study focusses on three such areas, the potential of transmission based hyperspectral imaging for early disease detection and quantification, the early detection and quantification of disease symptoms on canopy scale in high-throughput, and the question of data compatibility of hyperspectral data from different scales.

In order to achieve those goals three barley pathogens – *Blumeria graminis* f. sp. *hordei*, *Puccinia hordei* and *Pyrenophora teres* f. *teres* – were investigated in leaf scale time-series measurements, during which reflection and transmission data was gathered simultaneously through the HyperART setup. The effect of the distinct plant-pathogen interactions of the examined pathogens over the course of the inoculation were then used to evaluate the possibilities of transmittance hyperspectral images for early disease detection and quantification in direct comparison to the performance of reflectance data, giving valuable insights not only into the performance of transmission measurements but also about the underlying mechanisms through the interpretation of the results from the different pathogens.

A high-throughput hyperspectral measurement system, which is able to perform time-series measurements in the greenhouse under field-like conditions on canopy level while being independent from environmental factors, was developed during the study. With this system it was possible to accurately detect powdery mildew symptoms on barley canopies and quantify the disease development automatically over the course of 30 days long time-series measurement, showing the possible advantages of non-invasive and objective measurements for phenotyping applications. Additionally, it was possible to detect and quantify necrotic lesions on the most resistant barley cultivar. These necrotic lesions could be linked via microscopic studies to resistance reactions of the cultivar upon powdery mildew inoculation, showing the possibilities to precisely track the progression of resistant plant cultivars on canopy level via automated hyperspectral measurement setups.

Through the comparison of the hyperspectral data of time-series measurements investigating the plant-pathogen interactions of barley-powdery mildew, generated on both leaf and canopy level, through manual examination of the changes within the plant spectral profiles and the results of modern data analysis methods it was possible to confirm high similarities within both datasets. These results – and taking into account other recent studies with similar scope – support that hyperspectral data is comparable across multiple scales. These

findings allow the usage of the wealth of results from scientific studies with hyperspectral imaging for more practical applications on higher scales.

# Kurzfassung

Das Interesse an optischen Sensoren zum automatischen, nicht-invasiven und objektiven Monitoring im Bereich der Agrarwirtschaft steigt stetig an, wobei optische Sensoren auch großes Potential im Bereich Forschung und Entwicklung haben. Vor allem hyperspektrale Sensoren haben gezeigt, dass sie viele relevante Parameter über die Interaktion von Pflanzen mit biotischen und abiotischen Stressfaktoren durch die präzise Messung der spezifischen Änderungen in den spektralen Signaturen der Pflanzen erkennen können. Dennoch gibt es, trotz einer Vielzahl an Studien im Bereich optische Sensorik, immer noch Teilbereiche der hyperspektralen Sensoren die kaum untersucht sind.

In der vorliegenden Studie werden drei solcher Teilbereiche untersucht. Das Potential von bildgebenden Transmissionsmessungen zur Detektion und Quantifizierung von Pflanzenkrankheiten, Die Frühdetektion und Quantifizierung von Pflanzenkrankheiten auf Bestandesebene, sowie die Untersuchung der Kompatibilität von hyperspektralen Daten welche auf verschiedenen Skalenebenen aufgenommen wurden.Um diese Ziele zu erreichen werden drei verschiedene Gerstenpathogene – *Blumeria graminis* f. sp. *hordei*, *Puccinia hordei* und *Pyrenophora teres* f. *teres* – in Zeitreihenmessungen auf Blattebene mittels des HyperART bei gleichzeitiger Betrachtung von Reflexion und Transmission untersucht. Durch die Untersuchung der spezifischen Pflanze-Pathogen Interaktionen der drei Pathogene ist es möglich sowohl die Leistung von Transnittanzaufnahmen zur frühen Pathogendetektion und Quantifizierung im direkten Vergleich mit Reflektanzaufnahmen zu evaluieren, als auch Rückschlüsse auf die den Interaktionen zugrundeliegenden Mechanismen zu gewinnen.

Ein hyperspektralen hochdurchsatz Messsystem, dass Zeitreihen Messungen im Gewächshaus unter feldähnlichen Bedingungen auf Bestandesebene unabhängig von Umgebungsfaktoren durchführen kann wurde innerhalb der Studie entwickelt. Das System war in der Lage symptome des echten Mehltaus in Gerstenbeständen akkurat in frühen Entwicklungsstadien zu detektieren und über den Messzeitraum von 30 Tagen automatisch die Befallsstärke zu ermitteln. Dies zeigt die möglichen Vorteile des nicht-invasiven, objektiven Messsystems für Anwendungen in der Phänotypisierung. Außerdem war es ebenfalls möglich nekrotische Läsionen auf den Blättern des resistentesten Gerstencultivars zu detektieren und quantifizieren. Diese Läsionen konnten mittels mikroskopischer Studien als Resistenzreaktionen auf die Inokulation mit echtem Mehltau identifiziert werden, was die Möglichkeit eröffnet mittels des automatischen, hyperspektralen Messsystems auch das Auftreten und die Entwicklung von Resistenzreaktionen präzise über den Messzeitraum zu verfolgen.

Durch den Vergleich der Daten aus den hyperspektralen Zeitreihenmessungen, welche die Interaktionen zwischen Gerste und echten Mehltau auf Blatt- und Bestandesebene dokumentierten, indem die spezifischen Änderungen der spektralen Signaturen manuell untersucht wurden und die Ergebnisse der angewandten Datenanalysemethoden war es möglich eine hohe Ähnlichkeit zwischen den Datensätzen zu bestätigen. Diese Ergebnisse – zusammen mit Ergebnissen von Studien mit ähnlichem Thema – unterstützen die These, dass hyperspek-

trale Daten über mehrere Skalenebenen vergleichbar sind. Hierdurch eröffnet sich die Möglichkeit die mannigfaltigen Ergebnisse wissenschaftlicher Studien im Bereich hyperspektraler Sensoren für praktische Anwendungen in höheren Skalenebenen zu verwenden.

# Publications published within CROP.SENSe.net

**Publications which have been used within this thesis:**

**Chapter 1.2:**

**Thomas S**, Kuska MT, Bohnenkamp D, Brugger A, Alisaac E, Wahabzada M, Behmann J, Mahlein A-K (2017) Benefits of hyperspectral imaging for plant disease detection and plant protection – a technical perspective. *Plant Disease and Protection* 125, 5. https://doi.org/10.1007/s41348-017-0124-6

**Chapter 3.1:**

**Thomas S**, Wahabzada M, Kuska M, Rascher U, Mahlein A-K (2017) Observation of plant-pathogen interaction by simultaneous hyperspectral imaging reflection and transmission measurements. *Functional Plant Biology* 44(1), 23-34.

**Chapter 4:**

**Thomas S**, Behman J, Steier A, Kraska T, Muller O, Rascher U, Mahlein A-K (2018) Quantitative assessment of disease severity and rating of barley cultivars based on hyperspectral imaging in a non-invasive, automated phenotyping platform. *Plant Methods* 14:45.

**Further publications:**

**Thomas S**, Behmann J, Wahabzada M, Rascher U, Mahlein A-K (2017) Non-invasive detection of barley powdery mildew on the leaf and canopy level through hyperspectral images and modern data analysis methods. *Borniimer Agrartechnische Berichte* 93, 216-222.

**Kuska** M, Wahabzada M, **Thomas S**, Dehne H-W, Steiner U, Oerke E-C, Mahlein A-K (2015) Proximal sensing of barley resistance to powdery mildew. *Precision Agriculture* 15, 611-618.

**Kuska** M, Brugger A, **Thomas S**, Wahabzada M, Kersting K, Oerke E-C, Steiner U, Mahlein A-K (2017) Spectral Patterns Reveal Early Resistance Reactions of Barley Against *Blumeria graminis* f. sp. *hordei*. *Phytopathology* 107:1388-98.

**Mahlein** A-K, Kuska M, **Thomas S**, Bohnenkamp D, Alisaac E, Behmann J, Wahabzada M, Kersting K (2017) Plant disease detection by hyperspectral imaging: from the lab to the field. *Advances in Animal Biosciences* 8(2), 238-243.

**Behmann** J, Acebron K, Emin D, Bennertz S, Matsubara S, **Thomas S**, Bohnenkamp D, Kuska MT, Jussila J, Salo H, Mahlein A-K, Rascher U (2018) Specim IQ: Evaluation of a New, Miniaturized Handheld Hyperspectral Camera and Its Application for Plant Phenotyping and Disease Detection. *Sensors* 18(2):441.

**Thomas S**, Behmann J, Rascher U, Mahlein A-K (submitted at 16.04.2021) Evaluation of the benefits of combined reflection and transmission hyperspectral imaging data through disease detection and quantification in plant-pathogen interactions. *Plant Disease and Protection.*

# Contents

# List of Abbreviations

| | |
|---|---|
| 3D | three dimensional |
| Ap | appressorium |
| *Bgh* | *Blumeria graminis* f. sp. *hordei* |
| C | cuticula |
| Co | conidium |
| Cp | conidiophores |
| cv | cultivar |
| dai | days after inoculation |
| dbi | days before inoculation |
| DC | distance classifier |
| DNA | Deoxyribonucleic acid |
| *Dt* | *Drechslera teres* |
| Em | epiphytic mycelia |
| Ep | epidermis |
| *gdp* | glyceraldehyde-3-phospahte dehydrogenase |
| Gt | germination tubes |
| H | hypha |
| Hm | haustorial mother cells |
| HR | hypersensitive response |
| Hs | haustorium |
| HSI | hyperspectral imaging |
| Ih | infection hyphae |
| LED | light emitting diode |
| *mlo* | mildew locus o |
| MR | manual rating |
| NDVI | Normalized Difference Vegetation Index |
| NIR | near infrared |

| | |
|---|---|
| PC | principal component |
| PCA | principal component analysis |
| PCR | polymerase chain reaction |
| *Ph* | *Puccinia hordei* |
| PLC | Programmable Logic Controller |
| Pm | palisade mesophyll |
| Pp | penetration peg |
| *Ptt* | *Pyrenophora teres* f. *teres* |
| qPCR | quantitative real time polymerase chain reaction |
| RGB | red, green and blue color image |
| RH | relative humidity |
| SAM | spectral angle mapper |
| SD | spectral decomposition |
| SiVM | simplex volume maximisation |
| Sm | spongy mesophyll |
| Sp | urediospore |
| St | stomata |
| *std* | standard deviation |
| SVI | spectral vegetation index |
| SVM | support vector machine |
| Vb | vascular bundle |
| VIS | vidible range |
| Vs | vesicle |
| WT | wild type |

# List of Figures

# List of Tables

# 1 Introduction

Plant diseases have a considerable impact on crop yield in modern agriculture. Monocultures of highly specialized crops tend to lead to increased spread of diseases, with the possibility to cause large losses in yield when untreated. This not only leads to financial losses, but also is concerning when taking the growing world population and the shrinking amount of available farmland into consideration (Oerke and Dehne 2004). Furthermore, there are numerous plant pathogens, which produce toxins that pose health risks for livestock and humans. It has been shown, that even with all tools which are currently available for plant protection being applied plant diseases still cause a yield loss of up to 30% (Oerke and Dehne 2004).

Chemical plant protection and the breeding of resistant cultivars are two of the key practices to minimize the occurrence of plant diseases in modern agriculture (Oerke and Dehne 2004). However, due to developments in recent years, chemical plant protection has fallen out of favour within the public opinion (Gullino and Kuijpers 1994; Kildea *et al.* 2017). This – in addition to the development of resistances in plant pathogens against highly used chemical treatments through rapid mutation – has caused a high demand for alternative treatments, such as biological antagonists, new resistant plant cultivars and improvements in precision farming.

The breeding of new plant cultivars is a lengthy process in which especially the step of phenotyping of promising genotypes is a time intensive bottleneck, that requires manual rating by experts (Fiorani and Schurr 2013). A similar problem presents itself when applying precision agriculture – in order to locate pathogen infection sides within a field in a timely manner a high human effort is required.

Optical sensors can act as a way to drastically reduce the required human workload in both techniques, while improving the reliability of the processes due to them being objective and the possibility of automated measurement procedures (Mahlein 2016). Especially hyperspectral imaging has been shown as a promising technique, due to the possibility to not only detect biotic and abiotic stresses, but also differentiate between different causes through distinct changes in the plants spectral profiles (Delalieux *et al.* 2009; Mahlein *et al.* 2010).

Despite multiple studies in laboratories and under field conditions showing the potential of hyperspectral imaging for plant disease detection (see Chapter 1.2.4 for a detailed analysis of applications on different scales) there are two aspects which are left out of the main scope of investigation and thus chosen as research topics for this study: The measurement of light which has been transmitted through the plant tissue and the practical application of hyperspectral measurements on canopy scale.

When light interacts with plant tissue it undergoes three distinct processes – reflection, absorption and transmission. Most studies with optical sensors, especially hyperspectral imaging related, are focussed on portion of the light, which is reflected by the plant tissue. The investigation of reflected light has been shown

as promising method for the detection of metabolic changes in plant tissue, as a portion of the light is reflected within the tissue – thereby transporting information about the whole plant (Brakke 1994). Nevertheless, a large portion of the reflected light comes from surface reflection and only contains information of the plant epidermis cell layers. Transmitted light in comparison has completely passed all cell layers of the measured plant. Within this study the potential of the measurement of transmitted light with hyperspectral imaging sensory is investigated through time series investigations of *Hordeum vulgare* (Barley) on leaf scale while being inoculated with three selected pathogens (*Blumeria graminis* f. sp. *hordei*, *Puccinia hordei* and *Pyrenophora teres* f. *teres*) via the HyperArt setup (Bergsträsser *et al.* 2015), allowing the simultaneous measurement of reflected and transmitted light. The unique interactions of the different pathogens with the host plant (see Chapter 1.1) permit a throughout investigation into the possibilities of transmittance based measurements for plant disease detection and disease severity estimation.

While the results of scientific studies for disease detection through hyperspectral imaging data indicate multiple possibilities for practical application the technologies are still not commonly applied for non-scientific purposes. The main hindrances are the difficulties to perform hyperspectral imaging measurements under practical conditions in the field and in greenhouses due to the requirements in measurement conditions for precision measurement (see Chapter 1.2.4), as well as the difficulty to transfer the results of laboratory studies onto scales which are useful for practical applications. Early disease detection through hyperspectral imaging is commonly achieved in controlled laboratory environments on leaf scale and below. In order to apply this information, it is necessary to provide information about the applicability of the results from such studies on canopy scale. The second part of this study focusses on the creation of a functional high throughput hyperspectral imaging system, which can be used for automated plant phenotyping on the canopy scale in field-like environments. The system allows the practical application of hyperspectral imaging data for an early disease symptom detection and quantification – as well as the detection of resistance reactions to specific pathogens – in an automated, easy to use setup for resistance breeding. Through a combination of the gathered data on leaf and canopy scale it is possible to correlate the results and provide further information about the applicability of studies gathering hyperspectral data on leaf scale for different scales of application.

## 1.1 *Hordeum vulgare* and selected pathogens as model organisms for the evaluation of transmitted light in plant disease detection with optical sensors

*Hordeum vulgare* (Barley) is one of the oldest cultivated crops in agriculture and is still cultivated in modern times, being used for brewing and animal feeding (Zohary and Hopf 2001). A further application is as model plant in scientific studies in which barley excels due to its relatively simple, diploid genome and its prominence as crop used in agricultural practice (Gobatz *et al.* 2007, Kleinhofs *et al.* 1993). Compared to other cereal crops, such as *Triticum vulgare* (wheat), the genome of barley is considerably smaller and allows comparatively simple generation of near-isogenic lines for scientific purposes due to its diploid nature (Kleinhofs *et al.* 1993, Schulte *et al.* 2009, Wicker *et al.* 2011). For studies with optical sensors it offers the additional advantage that its phenotype and plant architecture are similar to wheat, which is one of the most important crops worldwide (Tilman 1999).

Despite the long-term usage of agronomic cultivation strategies, such as the breeding of resistant plants, there are still a multitude of pathogens, which can cause significant yield loss after infecting barley plants. Some of the most important fungal pathogens affecting barley production are *Blumeria graminis* f. sp. *hordei* (powdery mildew), *Pyrenophora teres* f. *teres* (net blotch), *Drechslera graminea* (stripe disease), *Puccinia hordei* (leaf rust), *Puccinia striiformis* f. sp. *hordei* (stripe rust) and *Rhynchosporium commune* (scald) (Walters *et al.* 2012). Three of these pathogens – *B. graminis* f. sp. *hordei* (*Bgh*), *Puccinia hordei* (*Ph*) and *Pyrenophora teres* f. *teres* (*Ptt*; anamorph: *Drechslera teres* (*Dt*)) – and their interactions with barley upon disease progression were investigated within this study, due to the different plant-pathogen interactions of the fungal pathogens allowing for a close evaluation of transmitted light as source for disease detection, as well as their importance in modern agriculture.

*B. graminis* f. sp. *hordei*, the causative agent of barley powdery mildew, is an obligate biotrophic fungus. The fungus uses airborne conidia for its asexual reproduction, which – upon contact with plant tissue – develops a primary germ tube to anchor itself onto the tissue. Then a secondary germ tube is developed, which forms an appressorium from which a penetration peg breaks through the cell wall of the underlying epidermis cells in order to form out the haustorium – the primary feeding organ of the fungus (Hückelhoven and Panstruga 2011, Underwood 2012). This process is the only direct interaction of *Bgh* with its host plant, as the mycelium of the fungi develops upon the plant surface. This stays true for the entire lifecycle of *Bgh*, as conidia and – during sexual reproduction of the fungi – cleistothecia are developed outside of the plant tissue as well (Fig. 1.1). Thereby, the direct influence of powdery mildew infection is restricted entirely to the leaf surface and epidermis cells. This should make powdery mildew development relatively easy to be detected by hyperspectral reflection measurements, but challenging through the measurement of transmitted light.

*P. hordei* is an obligate biotrophic fungus, which is the causative agent of leaf rust (also known as brown rust) in barley plants. Like many rust fungi it

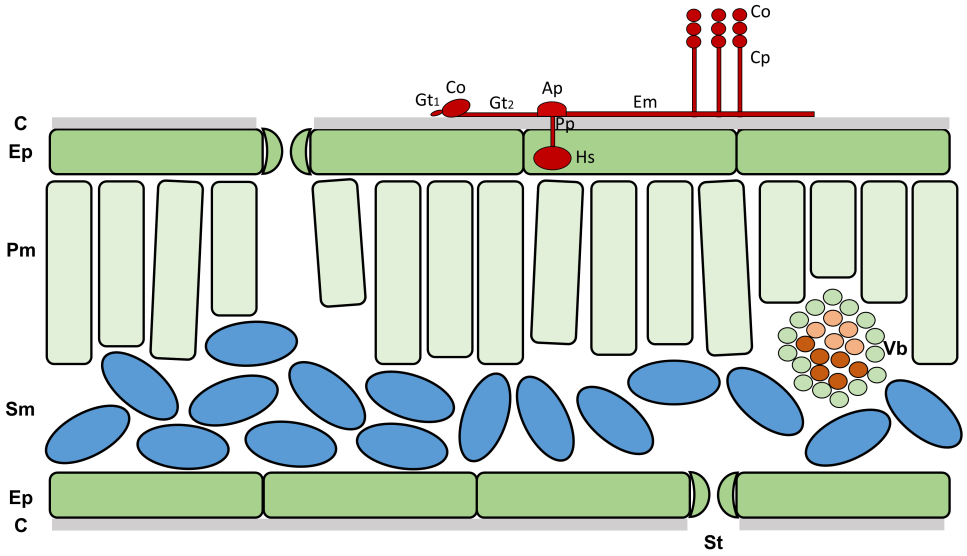


Figure 1.1: Infection of barley leaf with *Blumeria graminis* f. sp. *hordei*. The conidium (Co) lands on the leaf surface and develops germination tubes (Gt1 and Gt2). The second germination tube develops an appressorium (Ap). A penetration peg (Pp) is formed and breaks through the cuticula (C) as well as the cell wall of the underlaying epidermis cell, where a haustorium (Hs) devellops as primary feeding organ of the fungi. Epiphytic mycelia (Em) are developping and overgrowing the surface of the plant while conidiophores (Cp) are grown and produce new conidia. Ep = epidermis, Pm = palisade mesophyll, Sm = spongy mesophyll, St = stomata, Vb = vascular bundle.

has a complex life cycle, which includes five different types of spores and can include a secondary host plant on which the fungus survives while its primary host – barley – is unavailable (Anikster 1982, Lumbroso *et al.* 1977, Petersen 1974, Voegele 2006). Within the experiments of this study only urediospores were used. As shown in figure 1.2, the urediospores develop a germination tube when they come in contact with barley leaves. *Ph*, like most rust fungi, enters the leaf through the stomata when infecting the plant through urediospores by forming an appressorium once the germ tube reached it. A penetration peg is formed and used to enter the intercellular space of the barley leaf through the stomata opening, developing a vesicle, which in turn forms the infection hyphae that grows through the intercellular space (Anikster *et al.* 2004, Voegele 2006). Upon contact with mesophyll cells a haustorial mothercell is developed, which in turn forms out the haustoria as primary feeding organ of the fungi. During this phase the fungi are developing inside the intercellular space of the plant without causing notable tissue damage, despite feeding on nutrients from the host plant. This changes once the fungi develop spores for reproduction (either asexual with the development of urediospores during the summer, or sexual through the development of teliospores during autumn), as the spores are developed in colonies within the intercellular space before they are pushed out of the leaf tissue, breaking the overlaying epidermis cells in the process (Voegele 2006, Voegele *et al.* 2009). These stages make brown rust an excellent target organism for the evaluation of hyperspectral disease detection in reflection and transmission, as the fungus develops within the leaf tissue without causing tissue damage initially. As the fungus is not developing on the leaf surface a detection through direct reflectance is unfeasible, instead light which has been reflected through internal scattering and transmitted light should be the key factors in the detection of fungal tissue and metabolic changes upon plant-pathogen interaction.

*P. teres* f. *teres*, the causative agent of the barley net blotch disease, is a necrotrophic pathogen. The conidia of the fungus are moving with air currents and adhere on host plant tissue before developing a germination tube, which in turn forms an appressorium from which the fungus penetrates the cell wall of the underlying epidermis cell directly (Liu *et al.* 2011). The fungus then forms a primary and secondary vesicle within the epidermis cell while the function of the infected cell and nearby cells is being disrupted while the mycelium of the fungus grows into the intercellular space and spreads throughout the leaf tissue (Fig. 1.3). The mycelium of *Ptt* – unlike *P. teres* f. *maculata* – does not interact through direct contact with the nearby plant cells, but instead secretes effector candidates which induce cell death within the nearby plant cells (Liu *et al.* 2011, 2015). The necrotic fungi can then feed on the disrupted plant tissue and produce further conidia for asexual reproduction, as well as teleomorph pseudothecia at the end of the growing season for over seasoning (Liu *et al.* 2011). The development of the fungus causes a disruption of plant tissue through all layers of the leaf tissue, which hyperspectral imaging sensors should be able to measure equally well from both reflected and transmitted light.

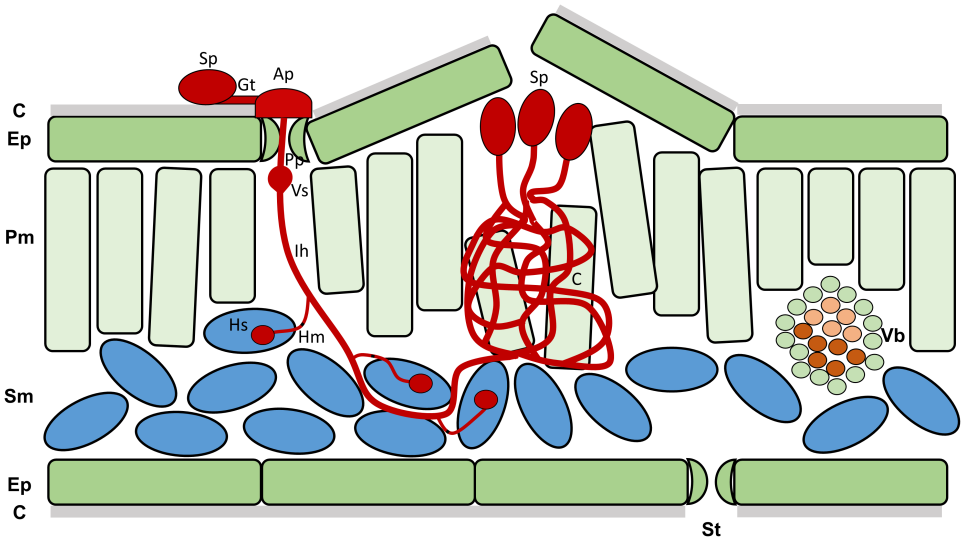


Figure 1.2: Infection of barley leaf with *Puccinia hordei*. An urediospore (Sp) lands onto the leaf surface where it forms a germination tube (Gt) and devellops an appressorium (Ap) over the stomata (St) of the leaf. A Penetration peg (Pp) enters through the stomata into the intercellular room of the leaf. A vesicle (Vs) is formed, from which infection hyphae (Ih) spread through the intercellular space and form haustorial mother cells (Hm), which attach to plant cells and break the cell wall without damaging the cell membrane to form a haustorium (Hs) as primary feeding organ of the fungi. Afterwards the fungi forms colonies (C) were new spores are developed. These break through the epidermis of the leaf. C = cuticula, Ep = epidermis, Pm = palisade mesophyll, Sm = spongy mesophyll, Vb = vascular bundle.

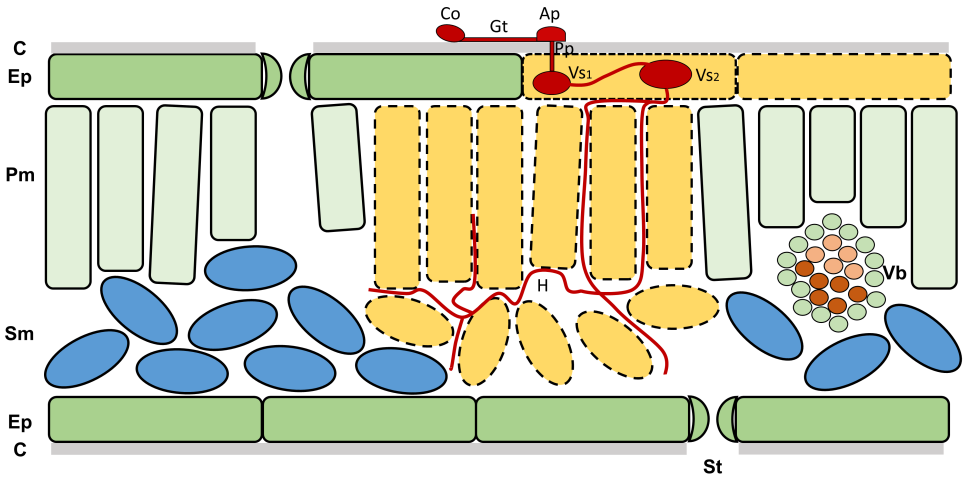


Figure 1.3: Infection of barley leaf with *Pyrenophora teres* f. *teres*. A conidium (Co) lands on the leaf surface and forms a germination tube (Gt). An appressorium is developed, which breaches the cuticular (C) and cell wall of the epidermis cell with a penetration peg (Pp), where the primary intracellular vesicle (Vs1) is formed. Shortly after a secondary vesicle (Vs2) devellops in the epidermis cell while the function of the infected- and nearby cells is disrupted. A hypha (H) emerges intracellular from the secondary vesicle and breaches into the intercellular space of the mesophyll, where it grows without making direct contact with the plant cells. The fungi's hyphae secrete toxins/effectors which lead to cell death, allowing the necrotic fungi to feed onto the tissue. Ep = epidermis, Pm = palisade mesophyll, Sm = spongy mesophyll, St = stomata, Vb = vascular bundle.

The three fungi should serve exceptionally well as model organisms for an evaluation of transmittance based imaging spectroscopy, as well as the comparison with reflectance based measurements, due to their unique interactions with their host plant. Powdery mildew symptoms developing on the leaf surface and epidermis, while brown rust symptoms develop within the intercellular tissue of the leaf after initial penetration of the stomata, should give insights about the possibilities of reflection and transmission measurements and their ability to detect plant-pathogen interactions on and within the leaf tissue respectively. The plant cell death through secreted proteins of *Ptt* affects all tissue layers in the infected area of the leaf for a further comparison of the performance of the two hyperspectral imaging methods, as well as granting insights about the detection of necrosis within plants – which is of high interest not only for pathogen detection, but also for the detection and quantification of plant resistance reactions through hypersensitive response upon pathogen inoculation.

## 1.2 Optical sensors - means to gather objective visual information within and outside of the human eye's visual spectrum

**Chapter 1.2 has been published:**

**Thomas S**[1,2], Kuska MT[1], Bohnenkamp D[1], Brugger A[1], Alisaac E[1], Wahabzada M[3], Behmann J[1], Mahlein A-K[4] (2017) Benefits of hyperspectral imaging for plant disease detection and plant protection – a technical perspective. *Plant Disease and Protection* 125, 5. https://doi.org/10.1007/s41348-017-0124-6.

[1]INRES-Phytomedizin, University Bonn, Bonn, Germany
[2]IBG2: Plant Sciences, Forschungszentrum Jülich GMBH, Jülich, Germany
[3]Bayer AG, Germany
[4]Institute of Sugar Beet Research (IfZ), Göttingen, Germany

**Changes made in the thesis chapter compared to the original publication:**

Chapter 1.2.5 has been rewritten. Furthermore, small changes have been made to adjust the cross-references of the article to the structure of the thesis. All changes have been marked by changing the colour of the respective text.

**Authors contribution**

Stefan Thomas, Anne-Katrin Mahlein, Matheus Thomas Kuska, Jan Behman and Mirwaes Wahabzada drafted and wrote the manuscript. Elias Alisaac, David Bohnenkamp, Jan Behman, Anna Brugger and Stefan Thomas designed figures and tables with support Anne-Katrin Mahlein.

Precise evaluation of plant disease incidence and severity, as well as of negative effects on yield quality and quantity is relevant for precision crop production and plant phenotyping. Within this context it is important to enable an accurate and timely assessment of plant disease occurrence and spread for planning targeted plant protection activities in field or greenhouse production and to forecast temporal and spatial disease spread. Traditional estimation methods for the detection, quantification and identification of plant diseases are visual monitoring, as well as microscopic, molecular, serological and microbiological methods (Bock *et al.* 2010, Martinelli *et al.* 2014). However, there is an increasing amount of non-invasive optical sensors available, which are able to assess reflectance properties of plants in different regions of the electromagnetic spectrum. These sensors can support plant disease detection and identification in different fields of application. Innovative sensor technologies can provide new insights into complex host-pathogen-systems and have the potential to substitute prevalent destructive investigation methods (Mahlein 2016, Mutka and Bart 2014). Especially precision agriculture and plant phenotyping for resistance breeding benefit from this development. Among the different sensor types (thermography, chlorophyll-fluorescence, RGB, multispectral and hyperspectral), hyperspectral sensors have significant potential and several advantages for monitoring plant diseases and host-pathogen interaction. Thermography and chlorophyll-fluorescence are able to detect plant stress without specification of the causal agent. With hyperspectral sensors, it is additionally possible to identify the responsible pathogen/disease (Bravo *et al.* 2004; Mahlein *et al.* 2010; Hillnhütter *et al.* 2012).

The application of hyperspectral imaging sensors on different scales - from investigating plant tissue on the tissue scale in laboratories over the individual plant scale in greenhouses or climate chambers to the canopy scale in field applications - comes with numerous advantages compared to classical visual monitoring or analytical methods. Unlike molecular or analytical methods, the process of hyperspectral imaging is non-invasive, thereby enabling researchers and breeders to perform time series measurements of the sample plants (Berdugo *et al.* 2014). This leads to a reduction of required samples and enables multiple repetitions. Moreover, hyperspectral imaging is an objective method in contrast to visual rating and can be implemented in automated systems, resulting in a considerably lowered workload (Walter *et al.* 2015; Mahlein 2016; Virlet *et al.* 2016). This leads to a reduction of economic and ecological costs in agricultural production.

### 1.2.1 Basic principle of hyperspectral sensors

The basic principle of hyperspectral sensors is comparable to the principle behind RGB cameras. Both systems measure the amount of light reaching the sensor and store the information. Unlike RGB cameras, which measure three bands of the visual part of the electromagnetic spectrum (red, green and blue light) a hyperspectral sensor measures up to several hundred bands of the electromagnetic spectrum in the wavelength range of the sensor. Each of these

spectral bands measures only a few nanometers of the electromagnetic spectrum, leading to a high spectral resolution for the hyperspectral sensor. Thereby each pixel in a hyperspectral image obtains a distinct set of information about the reflectance (or the transmittance) at each spectral band. The sum of these information is called a spectral signature (or spectral profile), which is measured by non-imaging hyperspectral sensors without further spatial information (Fig. 4.3). Imaging hyperspectral sensors measure the spectral bands for each pixel of the created image, thereby combining spectral and spatial resolutions. Each pixel of the image thereby has its own spectral signature, including reflectance values for all spectral bands measured by the hyperspectral sensor. From a different perspective, the resulting image is a hyperspectral data cube, containing two dimensions of spatial information and additionally one dimension of spectral information (Fig. 1.5; Jensen 2006). Besides assessing the visible part of the electromagnetic spectrum (400 – 700 nm), many hyperspectral sensors are also able to measure the near infrared (700 – 1000 nm) and short wave infrared (1000 – 2500 nm) part of the electromagnetic spectrum. Because of this procedure, high amounts of spectral data are collected with each hyperspectral image, making it difficult to extract relevant information from the images. This leads to the requirement of advanced data analysis methods in order to work efficiently with hyperspectral sensors (see Chapter 1.2.5; Behmann *et al.* 2015a).

### 1.2.2 Benefits of hyperspectral sensors for plant pathology, phenotyping and precision farming

There has been a long history of using spectroscopic methods for plant research. In laboratories, the analysis of natural compounds, cells, nucleic acid and metabolic processes based on their optical properties is an established standard procedure. The analyses of metabolites are made with photometrical applications after specific extraction and isolation procedures (Carocho and Ferreira 2013). The destructive nature of these methods prevents further investigation of the individual samples and makes time-series measurements impossible. Hyperspectral imaging sensors utilize a similar measuring principle (the absorption features and optical properties of biochemical compounds) to assess different plant parameters non-invasively over time (Berdugo *et al.* 2013; 2014).

Hyperspectral data can be linked to physiological processes in plants. Specific characterizations of the hyperspectral reflectance pattern were evaluated and validated by destructive methods e.g. determination of photo pigments (Zhao *et al.* 2016). This biological interpretation of hyperspectral reflectance can be achieved during plant-pathogen interactions, which influence the plant physiology, structure and water content. The spectral influence of fungal pathogens depends on the interaction type and way of nutrition (biotrophic, hemi-biotrophic, necrotrophic), growth type, pigmentation, developmental stage and disease severity. Changes in the photosynthesis apparatus during pathogen infection are indicated in wavelengths from 500 to 680 nm (Fig. 4.3). Pathogens, influencing the cellular structure of plants have a high influence in the near infrared wavelengths (700 – 1000 nm; Fig. 4.3). Changes in plant water content by

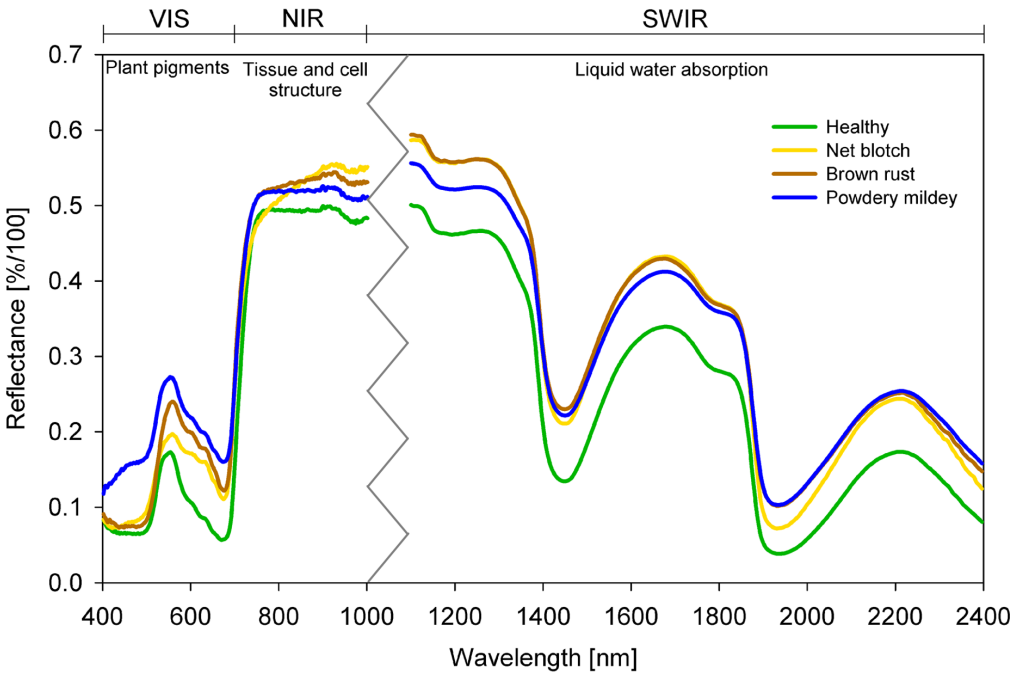


Figure 1.4: Spectral signatures of healthy barley leaves (green) and diseased barley leaves with net blotch (yellow), brown rust (brown) and powdery mildew (blue) respectively at 10 days after inoculation (dai). Sensors: "PS V10E" (400 – 1000 nm) and "SWIR" (1000 – 2500 nm) push broom scanners (Specim, Oulo, Finnland). All measurements were performed with the HyperART setup according to Thomas *et al.* (2017). VIS = Visual -, NIR = Near infrared -, SWIR = Short wave infrared part of the electromagnetic spectrum.

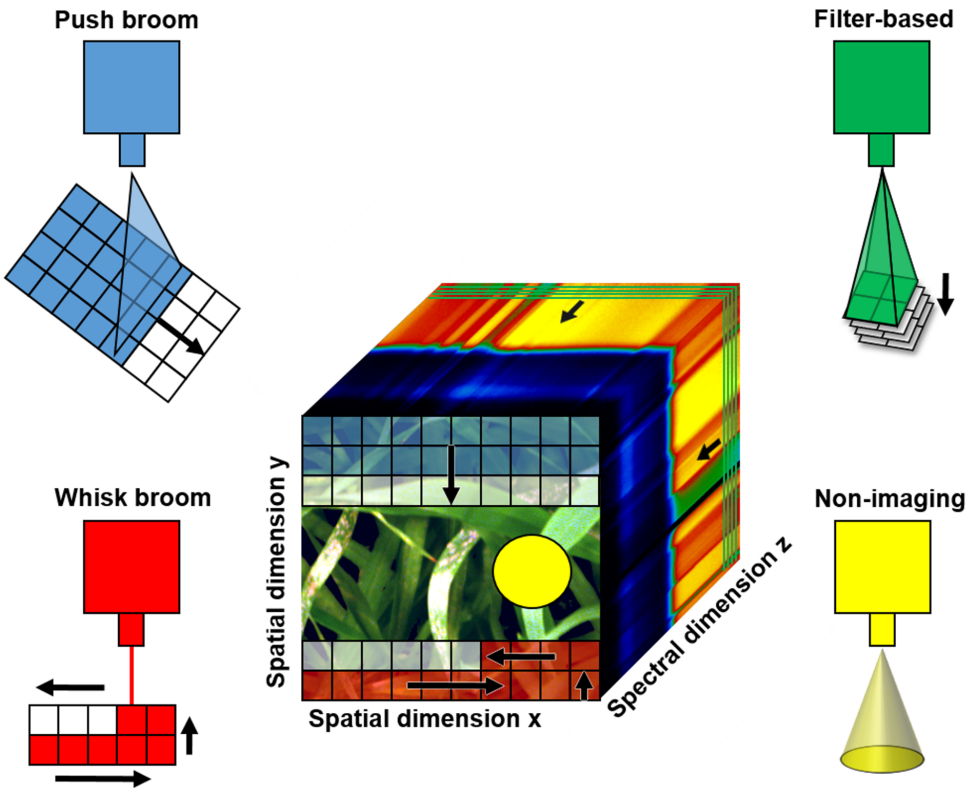


Figure 1.5: Various types of sensor systems for spectroscopic image acquisition. Push broom scanner (blue), whisk broom scanner (red), filter-based sensor (green) and non-imaging sensor (yellow). The measurement principle of each sensor type is illustrated at the hyperspectral data cube in the center.

necrotrophic pathogen caused necrosis e.g. are indicated by an increased reflectance intensity of specific water absorption bands in the short wave infrared at 1400 and 1930 nm (Fig. 4.3). These examples show that changes in plant physiology during pathogen attack can be linked to hyperspectral data by assigning specific changes of plant reflectance pattern during pathogenesis with known physiological processes. A correlation between hyperspectral reflectance signatures and metabolites during plant-pathogen interaction would improve the physiological analysis. Functional links of cellular processes to hyperspectral reflectance patterns will allow a deep phenotyping of the genotype and might improve existing crop physiological modelling (Yin *et al.* 2004).

In an agricultural context - such as plant breeding and precision farming - it is of high importance to determine changes in factors like the nutrient content, biomass or a disease infection. These parameters are commonly investigated either by visual rating, a time-consuming process which requires experts and is subjective, or by destructive investigations on laboratory scale as described earlier. In addition to afore mentioned benefits of hyperspectral imaging (non-invasive, objective, repeatable), hyperspectral sensors can be applied directly in greenhouses and fields, avoiding the step of extracting and transporting samples for analysis into a laboratory.

It could be shown, that metabolic changes in plants during pathogen attack can be detected by hyperspectral imaging (Arens *et al.* 2016), with different pathogens leading to characteristic changes in the plants reflectance profile (Mahlein *et al.* 2012; Fig. 4.3). Thereby it is possible to detect and identify disease outbreaks and dynamics through hyperspectral imaging on different scales (Bravo *et al.* 2004; Huang *et al.* 2007). This enables a timely detection of specific diseases and an early application of disease specific countermeasures in precision farming. Furthermore, the possibility of automated disease severity detection through hyperspectral imaging in combination with data analysis methods could be used to improve phenotyping applications (Kuska *et al.* 2015; Thomas *et al.* 2017).

While this review focusses on the usage of hyperspectral sensors for disease detection it should be mentioned briefly that other important parameters for plant health, such as abiotic stress and soil properties can be assessed as well. It could be shown that hyperspectral investigations of plants can detect multiple abiotic stress factors, such as drought stress or nitrogen deficiency (Asner *et al.* 2004; Vigneau *et al.* 2011), thereby allowing farmers to react by adjusting water and nutrient distribution during growing seasons. Hyperspectral sensors can also be used to gather non-plant specific information, like differences in the soil quality and create soil maps (Dematt$\hat{e}$ *et al.* 2001; Ben-Dor *et al.* 2009; Hbirkou *et al.* 2012). These maps can be used to plan ideal nutrient supplementation for different parts of the field according to the determined soil parameters.

In general, measurement methods, such as RGB, hyperspectral, lasers, etc., which provide the possibility for time series imaging, are suited to keep track of the plant biomass on the field. The plant growth rate and an estimation of the expected yield can be deduced from hyperspectral imaging data. This information can be applied to assess differences in the biomass and to adjust the

amount of pesticides required, depending on the crop stand density (Tackenberg *et al.* 2016).

### 1.2.3 Technical aspects of hyperspectral sensor systems

In this chapter the different types of hyperspectral sensors, as well as possible platforms for hyperspectral sensor systems, are explained in detail. The choice of sensor type and platform have a strong impact on the possible applications, as these components define the possible measurement scale, the spatial resolution and the throughput of the hyperspectral sensor system. Detailed information about these parameters and their importance for different applications in plant disease detection are provided in Chapter 1.2.4.

**Hyperspectral sensor types** Different kinds of hyperspectral sensors, based on different measurement principles, are available. Each method implies distinct advantages and disadvantages in certain hyperspectral sensor setups. It is possible to distinguish four basic types of hyperspectral sensors: (I) whisk broom, (II) push broom, (III) filter-based sensors - which are all imaging sensors - and (IV) non-imaging sensors (Fig. 1.5; Jensen 2006).

Non-imaging hyperspectral sensors measure the mean spectral reflectance, averaged on their area of view without spatial information. Basically, they are measuring the integral of a certain area with the full spectral profile, depending on their sensor range. The size of the assessed area is characterized by the focal lens, the viewing angle and the distance from the target (Fig. 1.5). Since early plant disease symptoms appear often in sizes below 1 mm, the detection sensitivity can be limited by non-imaging sensors, averaging signals of both healthy and diseased tissue in the measurement area (Mahlein *et al.* 2012).

Hyperspectral imaging sensors (hyperspectral cameras) have to capture the one-dimensional spectral information in addition to the two-dimensional spatial information of an image. The available illumination sensor arrays can only detect two dimensions of information though. Push broom and whisk broom scanners solve this discrepancy by simultaneously capturing the spectral information of a line or point on the measured object respectively. To compose the hyperspectral image, the object of interest is scanned through movement or rotation (Fig. 1.5). Both principles provide excellent spatial and spectral resolutions compared to other hyperspectral imaging sensors. However, this causes relatively long image acquisition times, depending on the size of the measured area, limiting the application of the sensor types to motionless objects.

Filter based sensors are another type of hyperspectral imaging sensors. They work similar to push and whisk broom sensors, with the notable difference that they measure the entire spatial image per spectral band at once. Filters, which allow only light of a specific wavelength to pass through, are interchanged rapidly during the image acquisition, allowing the hyperspectral information to be gathered over the two-dimensional image (Fig. 1.5). This system requires no movement of the sensor or the target during image acquisition. Thereby, the image acquisition time mostly depends on the exposure time and is in general

faster when compared to push- or whisk broom scanners. If the object is moving, this measuring principle can lead to inconsistent spectra as the single bands are observed at different points in time.

Recently hyperspectral/multispectral snapshot sensors have been introduced, which use the mosaic principle of common RGB cameras. Snapshot cameras provide a significantly higher image recording speed then traditional hyperspectral sensors. However, they have a significantly lower spatial resolution of the hyperspectral image when compared with hyperspectral scanners (Aasen *et al.* 2015). Nevertheless, the quick recording time and possibility to create hyperspectral image sequences in rapid succession make snapshot cameras very interesting for application under difficult environmental conditions (see Chapter 1.2.4) and UAV applications.

**Platforms for hyperspectral sensor systems** Hyperspectral sensors generally require to be installed on different platforms to form functioning measurement systems. Some examples for sensor platforms, sorted by altitude, are handheld sensors, rail systems, vehicle and tractor mounted systems, low altitude UAVs, as well as airplane and satellite mounted hyperspectral sensors.

If non-imaging hyperspectral data is sufficient, a variety of handheld sensors is available (Fig. 1.5). These allow for quick assessment of plants under greenhouse and field conditions. However, non-imaging systems provide the mean value over the measured area, resulting in a lower spatial resolution than imaging sensors at comparable distances (Huang and Apan 2006; Cao *et al.* 2013). Handheld non-imaging sensors are often used for hyperspectral scientific field projects, which investigate plant-pathogen dynamics, as they allow high throughput measurements and don't require a sophisticated measurement platform.

Until now, hyperspectral imaging sensors are too complex to be used as handheld devices. They require precisely steered line stages or mirror systems to provide accurate results. Additionally, the sensors should be kept stable during image acquisition, a process which can take up to several minutes depending on the spatial resolution and measured area. Thereby platform (stationary, rail system and vehicle based) mounted imaging hyperspectral sensors are used for observations on leaf, single plant and canopy scale, both under field conditions and in the greenhouse (Vigneau *et al.* 2011; Deery *et al.* 2014; Pinto *et al.* 2016). Such systems combine a high spatial resolution with the possibility for automatization and a reasonably high throughput. Because of these properties sensor based measurement systems are best suited for large scale approaches in plant disease detection and resistance phenotyping, which require a high measurement throughput and the option to perform fully automated and standardized measurement series (Virlet *et al.* 2017 ).

UAV based hyperspectral sensors can be used for monitoring fields and plots on the canopy scale, but in general lack the necessary spatial resolution for the detection of early plant disease symptoms or single plant analysis and are restricted by short flight times (Aasen *et al.* 2015). UAV´s have shown to be

a promising platform for multispectral and thermal sensors though, allowing evaluation of parameters such as drought stress, heat stress, nutrient content, plant biomass, yield and biotic stress under field conditions (Sankaran *et al.* 2015). It can be expected that with improvements in both hyperspectral sensors and UAV´s they will play a key role as platforms for field phenotyping and plant disease detection in the near future.

For large scale analysis of vegetation dynamics, it is also possible to mount hyperspectral sensors on zeppelins, airplanes and satellites. While hyperspectral sensors were originally mounted on satellites and airplanes for remote sensing or military applications, these setups are generally not able to generate a sufficient spatial resolution for the detection of plant diseases at an early stage (Mahlein 2016).

### 1.2.4 From the laboratory to the field: scales for hyperspectral applications and the tradeoff between spatial resolution and measurement throughput

When using hyperspectral imaging it has to be decided first on which scale the measurements should be performed. In this review, the scales tissue, leaf, single plant and canopy are in the focus. These scales are suited for investigating metabolic changes during plant pathogen interaction (tissue and leaf scale), resistance phenotyping, disease detection (leaf, single plant and canopy scale), disease distribution and patterns (canopy scale; Fig. 1.6). Tissue and leaf scale experiments are commonly performed in the laboratory in the context of basic research and to a certain amount for plant phenotyping, while leaf, single plant and canopy scale measurements in greenhouses and fields are required for more practical applications such as phenotyping or precision farming. The tissue scale can only be achieved by the usage of sophisticated hyperspectral microscope systems. It allows the observation of fungal spores or plant cells during early interactions and infection. Leaf scale measurements allow high resolution assessment of single parts of a plant (leaves, ears, stem, and roots) and are suited to observe specific changes in spectral characteristics of plants during pathogenesis. These measurements can be performed in the laboratory, greenhouse or even on the field. Laboratories provide the most stable environmental conditions for hyperspectral experiments, without risk of changing environmental factors, such as light intensity and direction, influencing the results. Single plant and canopy measurements can be performed in laboratories, greenhouses and the field. Hereby fields allow large scale applications, while investigations in greenhouses combine a controllable environment and the possibility for high throughput experiments.

The decision which measurement scale is required for an application is mostly dependent on the desired spatial resolution and measurement throughput. Spatial resolution and throughput are in an inverted relationship for hyperspectral measurements, with tissue scale having the highest resolution of being able to monitor subtle processes and small structures, but having a very low throughput. Meanwhile, canopy scale measurements in the field have low resolutions with

pixel sizes of up to several meters, but provide increasingly high throughputs. The need for high throughput is especially prominent for practical applications on greenhouse and field scale, such as plant breeding or non-invasive disease detection (Deery *et al.* 2014; Mahlein 2016).

Multiple studies using hyperspectral imaging stated, that high spatial resolution is crucial to avoid mixed spectral signals (Bravo *et al.* 2003; West *et al.* 2010; Mahlein *et al.* 2012). These investigations focused on fungal-plant disease detection in the field (Bravo *et al.* 2003; West *et al.* 2010) and in the laboratory (Mahlein *et al.* 2012). In these studies, it was possible to detect and differentiate plant diseases, in some cases in early stages before they were visible for the human eye (Table 1; Rumpf *et al.* 2010). The importance of the spatial resolution was shown by small-scale investigations of Mahlein *et al.* (2012) for the detection and identification of *Cercospora* leaf spot, sugar beet rust and powdery mildew on sugar beet. It could be shown, that differences in the reflectance signatures of healthy and diseased tissue were decreased in lower spatial resolutions. The increasing number of pixels with mixed information could be identified as cause for this development. Thereby it is of high importance in hyperspectral investigations, to select a sufficient spatial resolution.

Nevertheless, disease specific hyperspectral signatures seem to be transferable on different scales. This enables the transfer of results from experiments with high resolution data and highly controlled environmental conditions in laboratories to other scales. Subtle processes, e.g. plant-pathogen interactions, can be closely observed on tissue and leaf scales, allowing a detailed understanding of the metabolic and structural changes during the infection. This knowledge can then be applied to find corresponding changes in spectral patterns on plant and canopy scale during practical applications in greenhouses and fields. Such a combination of different methods could increase the possibilities for pathogen detection and phenotyping applications in the near future.

### The importance of light and environmental conditions in hyperspectral imaging

In order to achieve reliable results with hyperspectral sensors it is necessary to consider the environmental conditions and the technical setup during the measurement.

Under controlled conditions of a laboratory setup the prominent factor, which has to be closely monitored, are the light conditions during the measurements. Due to the requirement of a reference measurement with a material, which possesses known reflection (and possibly transmission) properties in order to normalize the images, it is important to have stable light conditions during the process. Moreover, most light sources do not provide illumination over a broad spectrum of wavelengths, resulting in the demand for specialized light sources.

Companies and researchers designed multiple solutions to provide sufficient light conditions for hyperspectral imaging. The commonly used artificial light source is a tungsten halogen lamp with different modifications e.g. mirrors,

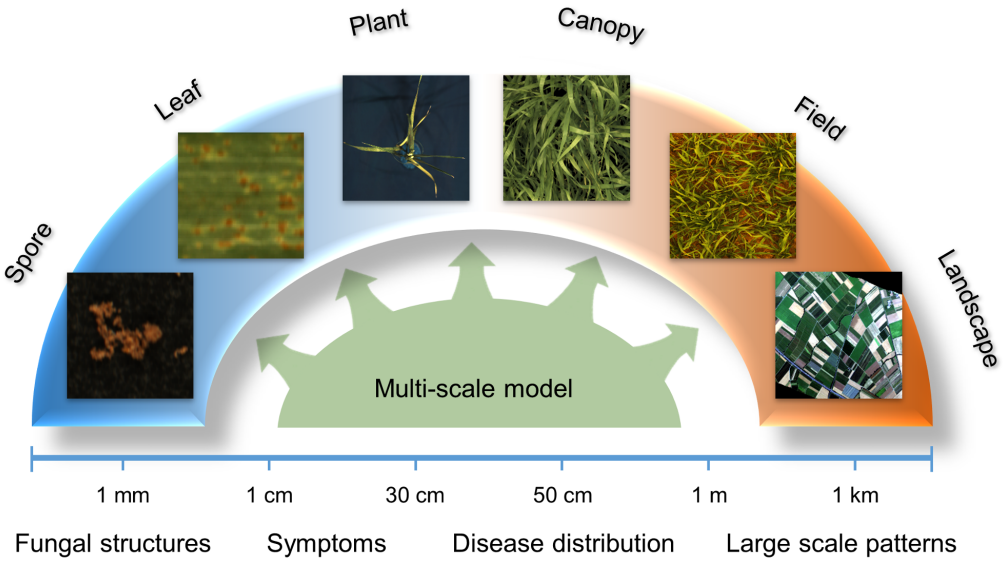


Figure 1.6: Vision of a multi-scale model integrating observations of the plant-pathogen interaction from the microscope up to airborne imaging. Such model derives a scale independent representation using physical models and machine learning methods and is able to analyze data from all scales supported by the wide data-base of observations.

Table 1: Overview of plant pathosystems and plant diseases assessed by hyperspectral imaging.
n.i. indicates a non-investigated aspect, * indicates nematodes.

| Host-Pathogen-System | Scale | Detection | Early Detection | Quantification | Reference |
|---|---|---|---|---|---|
| Apple - *Venturia inaequalis* | Leaf | ✔ | n.i. | ✔ | Delalieux *et al.* (2009) |
| Barley - *Blumeria graminis* f.sp. *hordei* | Tissue | ✔ | ✔ | n.i. | Kuska *et al.* (2015) |
| Barley - *Blumeria graminis* f.sp. *hordei* | Leaf | ✔ | ✔ | ✔ | Thomas *et al.* (2017) |
| Barley - *Blumeria graminis* f.sp. *hordei*, *Puccinia hordei*, *Pyrenophora teres* | Leaf | ✔ | ✔ | n.i. | Wahabzada *et al.* (2015) |
| Celery - *Sclerotinia sclerotiorum* | Canopy | ✔ | n.i. | n.i. | Huang & Apan (2007) |
| Cucumber - CMV, CGMMV, *Sphaerotheca fuliginea* | Leaf | ✔ | n.i. | ✔ | Berdugo *et al.* (2014) |
| Sugar beet - *Cercospora beticola* | Leaf | ✔ | n.i. | ✔ | Bergsträsser *et al.* (2015) |
| Sugar beet - *Cercospora beticola* | Tissue | ✔ | n.i. | ✔ | Leucker *et al.* (2016a, 2017) |
| Sugar beet - *Cercospora beticola*, *Erysiphe betae*, *Uromyces betae* | Leaf | ✔ | ✔ | n.i. | Rumpf *et al.* (2010) |
| Sugar beet - *Cercospora beticola*, *Erysiphe betae*, *Uromyces betae* | Leaf | ✔ | ✔ | ✔ | Mahlein *et al.* (2010, 2012) |
| Sugar beet - *Heterodera schachtii**, *Rhizoctonia solani* | Canopy | ✔ | n.i. | ✔ | Hillnhütter *et al.* (2011, 2012) |
| Oilseed rape - *Alternaria* spp. | Leaf | ✔ | n.i. | ✔ | Baranowski *et al.* (2015) |
| Wheat - *Blumeria graminis* f. sp. *tritici* | Canopy | ✔ | n.i. | ✔ | Cao *et al.* (2013) |
| Wheat - *Fusarium* spp. | Ear | ✔ | ✔ | ✔ | Bauriegel *et al.* (2011a) |
| Wheat - *Puccinia striiformis* | Canopy | ✔ | n.i. | ✔ | Bravo *et al.* (2003) |
| Wheat - *Puccinia striiformis* | Canopy | ✔ | n.i. | n.i. | Bravo *et al.* (2004) |
| Wheat - *Puccinia striiformis* | Canopy | ✔ | n.i. | ✔ | Huang *et al.* (2007) |
| Wheat - *Puccinia striiformis* | Canopy | ✔ | ✔ | n.i. | Moshou *et al.* (2005) |
| Wheat - *Puccinia striiformis*, *Puccinia graminis*, *Puccinia triticina* | Leaf | ✔ | n.i. | n.i. | Devadas *et al.* (2009) |

(hemi-) spherical diffusers, filters, optical fibers and conductors (Baranowski *et al.* 2015; Behmann *et al.* 2015b; Yeh *et al.* 2016; Thomas *et al.* 2017). The emitted light has a spectrum from 380 – 2500 nm with a peak at 900 nm and is influenced by the energy source and working temperature (Elvidge *et al.* 2010). Further light sources: mercury or metal halide lamps; which have smaller emitted wavelength ranges with peaks, typically at 365, 405, 436, 546 and 579 nm (Elvidge *et al.* 2010). For this reason, they are suitable as calibration light sources for sensors or confocal applications. All these common light sources share the disadvantage of heat development, which may have an influence on plant samples and the sensor sensibility over the course of the measurement period. It is possible to eliminate heat related discrepancies for studies in control environment through the use of halogen lamps in combination with non-absorbing fibers to redirect the light, increasing the distance between the heat generating light source and the samples. Supplemental Light-emitted diodes (LEDs) can be used to provide additional light in wavelength areas where halogen lamps and hyperspectral sensors have low light emitting / detection performance. This leads to an improved signal-to-noise ratio (Mahlein *et al.* 2015). LEDs do not cause heat buildup, due to passive cooling when installed on heat conductors, e.g. aluminum. However, LEDs have only small peaks at discrete wavelengths in the electromagnetic spectrum. In order to achieve an equal illumination over the measured spectrum with LEDs, a complex setup of different LEDs is required for hyperspectral measurements. A prototype version of a LED illuminated multispectral sensor system was developed by Grieve *et al.* (2015), using LEDs with five different emitted wavelength peaks. The system showed comparable quality in plant disease detection to a common hyperspectral system. Hyperspectral imaging is indispensable in the development of such low-cost sensors, as the high spectral resolution of hyperspectral sensors enables the identification and characterization of disease specific spectra. These spectra can then be used to develop an according low-cost multispectral sensor for the detection of specific diseases on the target plant.

In greenhouse and field applications, light conditions are more complex compared to laboratory setups. Sunlight proves to be an excellent light source for hyperspectral imaging, covering a broad spectrum of wavebands. The main problem results in the inability to control changes in the light intensity, usually caused through clouds covering the sun at varying degrees. A change in light intensity during the time between measuring the reference and the sample will result in measurement inaccuracies (Damm *et al.* 2015; Pinto *et al.* 2016). This becomes a problem due to the required image acquisition time of whisk broom, push broom and filter based hyperspectral imaging sensors, which is often up to several minutes per image. Therefore, it could be recommended to additionally measure the light intensity over the measured spectrum during hyperspectral image acquisitions under natural light conditions. This technique allows to calculate the differences in the illumination levels and integrate these data in the normalization of the image.

The possible measurement windows under natural light conditions are further restricted by the fact, that the angle between incoming light, plant and

hyperspectral sensor has an influence on the received spectral signature of the sample plant (Milton *et al.* 2009; Vigneau *et al.* 2011; Behmann *et al.* 2015b; Pinto *et al.* 2016). This influence depends on the time of the day and thereby on the individual movement of the sun over the course of the day and by the time within the year. The complex relations between the angle of the sun, plant surfaces and sensors are described through the bidirectional reflectance-distribution function (Milton *et al.* 2009; Cao *et al.* 2013). Due to the complex architecture of plants it is difficult to eliminate these factors in the normalization of the image. Thus, it is recommended to perform time series measurements at the same time each day to avoid inaccuracies between different measurement dates due to changes in the bidirectional reflectance-distribution function (Milton *et al.* 2009; Cao *et al.* 2013). Within this context, PROSAIL (PROSPECT optical leaves properties model and SAIL canopy bidirectional reflectance model) is an approach to deal with these issues by providing a model to describe spectral and directional variation in canopy reflectance (Jacquemound *et al.* 2009). The above described difficulties make it challenging to perform time-series-, or "on demand" measurements with hyperspectral sensors under natural light conditions. A different strategy, which is applicable on the vehicle or platform scale, is to block out the natural light through shading cabins and use artificial light sources for illumination. This creates controlled light conditions and allows measurement independent of the above-mentioned factors, but increases the complexity of the hyperspectral sensor system (Delalieux *et al.* 2008; Rodionov *et al.* 2015).

For field applications, wind and rain are further environmental factors, which have influence on the hyperspectral measurements. Wind as example does not influence the image acquisition by itself, but often causes the sample plants to move slightly during the measurement process. Due to the nature of the hyperspectral imaging sensors, this results in heavy distortions in the hyperspectral image (Pinto *et al.* 2016). The continued development of more advanced snapshot based hyperspectral sensors and thereby reduced image acquisition time could minimize the influence of changing environmental conditions in the future.

When changing from leaf scale to canopy scale in order to increase the measurement throughput, direct light causes further difficulties. The angles and shadowing of the different leaves in the architecture of the measured plants also affect the intensity of light being reflected. This leads to large discrepancies of the illumination levels for different leaves at canopy level and increases the challenge in analyzing the gathered data (Behmann *et al.* 2015b).

For the usage of hyperspectral imaging on UAVs or even larger scales, environmental effects, especially movement of plants, and the complexity of the plant architecture are less important, as one pixel of the image tends to represent several leaves or even plants due to the low spatial resolution (Nevalainen *et al.* 2017; Sankaran *et al.* 2015). Nevertheless, the general problem with changes in light intensity during the measurements stays relevant.

## Applications and limitations of hyperspectral sensors on different scales

Innovative technologies from robotics, new sensors and imaging technologies allow for a wide range of applications, from laboratory research to screening systems on the field scale (Fig. 1.6; Fiorani and Schurr 2013; Granier and Ville 2014). Currently, different measurement systems, as well as automated phenotyping platforms are available. The different types of sensors and measurement scales were briefly described earlier in this review (Fig. 1.5). At this point the review tries to give a more detailed overview on each scale, focusing on the use of scale specific parameters and relevant applications for plant disease detection. Furthermore, research articles, which applied hyperspectral imaging on different scales, will be critically evaluated in order to give an indicator about scale specific applications. The selected articles have a thematic focus on the observation of plant-pathogen interaction and disease detection (Table 1).

**Tissue scale – hyperspectral microscopy and assessment of subcellular processes** Hyperspectral imaging systems on the tissue scale provide controlled measurement conditions and work with high spatial resolutions, enabling the observation of small scale processes, for example disease resistance reactions on plant leaves (Kuska *et al.* 2015; Leucker *et al.* 2016a; 2017). The analysis of individual plant-pathogen interactions using hyperspectral imaging on the tissue scale enables the characterization of even subcellular processes in space and time. This could be used in the future to establish the link between phenomic data and known parameters from ´omic and physiological studies, which is highly demanded (Großkinsky *et al.* 2015; Mahlein 2016; Simko *et al.* 2017). A relation of hyperspectral data to gene expressions, protein activity, physiological processes and histological changes will improve our knowledge on a plant's phenotype and is fundamental for plant resistance breeding. The disadvantage of microscopic measurement setups on the tissue scale is a low throughput of probe samples over time.

Kuska *et al.* (2015) established a hyperspectral imaging microscope setup with a spatial resolution of up to 7.5 µm per pixel. This setup allows small-scale image analysis and has been used for plant disease detection and disease specific resistance characterization (Kuska *et al.* 2015; Leucker *et al.* 2016a, 2017). Early spectral changes on powdery mildew diseased barley were shown by microscopic hyperspectral studies before symptoms became visible for the human eye (Kuska *et al.* 2015). Furthermore, the pathogenesis of powdery mildew on barley could be described, including evidence of spectral properties of race and non-race specific resistances (Kuska *et al.* 2015; Kuska *et al.* 2017). Leucker *et al.* (2016a; 2017) performed detailed investigations of pathogenesis of *Cercospora* leaf spot on sugar beet through hyperspectral microscopy. The results of these measurements could be used to evaluate the sporulation density of the fungus on different host genotypes (Leucker *et al.* 2017). These findings show tissue scale measurements as a valuable tool to observe and estimate the spread of pathogenic fungal species over multiple generations depending on their

interaction with the host plants. Moreover, Leucker *et al.* (2016a) were able to identify different sugar beet genotypes through the application of a spectral angle mapper algorithm, used commonly in remote sensing, on the disease symptoms of the investigated plants. Previous studies on leaf scale showed similar hyperspectral characteristics for *Cercospora* leaf spot on sugar beet (Mahlein *et al.* 2012). The hyperspectral signature patterns were similar, but showed slight differences in the blue and green range of the reflectance intensity. These differences were dependent on the development stage of the leaf spots (Mahlein *et al.* 2012) and the disease susceptibility of different sugar beet genotypes (Leucker *et al.* 2016a; Leucker *et al.* 2017).

**Leaf scale – high resolution evaluation of processes during pathogenesis under highly controlled conditions** It is possible to measure multiple leaves with laboratory based hyperspectral measurement setups. Depending on the setup, reflection and transmission measurement on leaf scale are possible (Bergsträsser *et al.* 2015; Kim *et al.* 2015; Thomas *et al.* 2017). While the resolution is sufficient to detect changes in the plant metabolism and structure before they are visible by the human eye, they allow a higher throughput compared to microscopic systems on tissue scale. In general, leaf scale based setups are most suited for basic research to discover changes during specific stress responses under highly controlled conditions in the laboratory.

Delalieux *et al.* (2009) used non-imaging hyperspectral sensors to detect apple scab on apple tree leaves, Mahlein *et al.* (2010) used performed similar non-imaging hyperspectral measurements to detect three different diseases of sugar beet leaves (*Cercospora* leaf spot, powdery mildew and sugar beet rust). Both research groups performed time series experiments from shortly after the inoculation up to points were symptoms were visible with the naked eye. Despite the used non-imaging sensors and their field of view averaging over an area of 10 mm it was possible to not only detect the diseases on the leaves, but also to trace the differences in the spectral signatures of different diseases with increasing disease severity. Each disease showed a distinct spectral signature, allowing a distinction between different diseases based on spectral vegetation indices (SVIs). These observations match the results of Hillnhütter *et al.* (2012), where symptoms on sugar beet leaves caused by Heterodera schachtii and Rhizoctonia caused root rot could be accurately detected with different vegetation indices. Rumpf *et al.* (2010) used vegetation indices and classification through the Support Vector Machines algorithm to detect and distinguish three different diseases on sugar beets (*Cercospora* leaf spot, sugar beet rust and powdery mildew) automatically, based on training datasets. In this study, a detection and identification of the diseases before symptoms were visible was achieved. Bergsträsser *et al.* (2015) could demonstrate that the combined hyperspectral imaging measurement of reflection and transmission allows for an increased accuracy when detecting *Cercospora* leaf spot disease on sugar beet leaves. The experiments of Thomas *et al.* (2017) were not able to confirm an increased detection accuracy of combined reflection and transmission measurements for

powdery mildew detection on barley plants. Although, it could be shown that high resolution hyperspectral reflection images on leaf level allow a detection of powdery mildew up to two days before visible symptoms appear. Additionally, it could be demonstrated that transmission based imaging performs equally to reflectance based imaging when detecting spontaneous necrosis on resistant barley plants. The combination of reflection and transmission imaging allowed for a clearer distinction between late powdery mildew symptoms and small necrotic spots on barley leaves. From the results of the two above-mentioned studies it can be theorized, that the value of transmission imaging is depending on the interaction and invasiveness of the investigated pathogen. The results of Bauriegel *et al.* (2011a) suggest, that hyperspectral imaging can be used to identify diseases on other plant parts then the leaves as well. In their study, wheat ears, which were inoculated with Fusarium head blight, were investigated through hyperspectral imaging and fluorescence measurement in a time series experiment. It was possible to determine infected ears as early as seven days after inoculation through hyperspectral imaging. Wahabzada *et al.* (2015a) applied advanced data analysis methods on hyperspectral time series image datasets of barley plants, which were inoculated with powdery mildew, brown rust and net blotch. It was possible to differentiate between the symptoms of the three pathogens and to create time line based maps for an illustration of spectral key moments of the three pathogens during the pathogenesis on barley plants. These findings could be correlated with the pathogen specific biological processes over the course of the infection. Thereby it is possible to get an overview about the disease specific changes in the plants metabolism at given time points during the pathogenesis.

**Single plant and canopy scales – high throughput disease detection for phenotyping and precision farming** Despite providing the lowest spatial resolutions of the measurement scales, high throughput experiments in greenhouses and fields have shown to be promising tools for studying plant-pathogen interactions. Through the use of modern hyperspectral line scanner sensors and a viewing distance of 30 to 100 cm the spatial resolution is sufficient to detect biotic and abiotic stresses on single plants in early stages (Vigneau *et al.* 2011). This measurement scale still allows for a high throughput. Thereby greenhouse and field based approaches allow a rapid assessment of multiple plants on leaf or canopy scale, which cannot be matched in laboratories due to special restrictions. Additionally, greenhouses and fields provide environmental conditions, which are similar to those of actual farming or crop breeding procedures.

Moshou *et al.* (2005) applied hyperspectral imaging sensors and multispectral fluorescence measurement to detect yellow rust infection in winter wheat under field conditions with ambient light. They managed to develop a method, based on three spectral bands of the hyperspectral images, to classify diseased tissue with an error rate of only 11.3%. Through combination of the hyperspectral and fluorescence measurement data with advanced data analysis they were able to reduce the classification error to 1%, showing the possible application of

non-invasive, multisensory platforms for real-time phenotyping.

Huang *et al.* (2007) investigated yellow rust on winter wheat by means of airborne hyperspectral reflection image acquisition. Despite a low spatial resolution with pixel size of 1x1 m the results of the study show a strong negative correlation of the Photochemical reflectance index, a vegetation index based on two wavelengths (531 and 570 nm), and the disease severity after visual rating of $r^2 > 0.90$. It was possible to identify areas with high disease pressure in the observed field as well. Hillnhütter *et al.* (2011) made airborne hyperspectral imaging measurements of sugar beet plants to detect symptoms caused by Heterodera schachtii infestation and of Rhizoctonia caused root rot, which were compared with georeferenced control data from ground based monitoring. Despite the two hyperspectral sensors, which were used for airborne data acquisition in this study, having a spatial resolution of 1.5 m and 2 m respectively it was possible to detect and quantify both pathogens with airborne measurements, based on the close correlation between disease severity and pathogen infestation. While early detection of pathogens before visible symptoms appear is not possible for current airborne hyperspectral imaging systems due to limitations in the spatial resolution, the results of these studies are good examples for possible uses in containing disease outbreaks by identification of the areas with initial symptoms to prevent the disease from spreading over the entire field.

While this review focuses on disease detection, hyperspectral imaging has potential to detect other parameters, which influence the plant health, reliably on different scales. Mirik *et al.* (2006) investigated changes in the spectral reflectance of wheat plants during greenbug infection on canopy scale in both greenhouses and fields. They were able to determine characteristic changes in the spectral signatures of the wheat plants during greenbug infection. Multiple tested spectral indices showed high correlation with greenbug damaged wheat as well, allowing an easy detection of greenbug infection on wheat canopies through hyperspectral imaging. Hyperspectral imaging found use as well to detect abiotic stress factors, such as drought stress (Winterhalter *et al.* 2011), or estimate plant biomass directly in the field (Montes *et al.* 2011).

### 1.2.5 Advanced data analysis: from hyperspectral data to information on plant health

The three-dimensional nature of hyperspectral datacubes makes manual processing of the high density information within hyperspectral imaging data not feasible for modern applications. This leads to the application of modern data analysis methods to extract relevant information from the large number of highly correlated features. Hereby the application in plant disease detection is linked to scale-dependent features on specific bands, preventing established data analysis techniques on single bands. Furthermore, hyperspectral datasets of time-series measurements to detect biotic and abiotic stresses generates large amounts of high-dimensional data (up to terabytes scale within high-throughput settings) (Furbank and Tester 2011, Mahlein 2016. Wahabzada *et al.* 2016, Thomas *et al.* 2018).

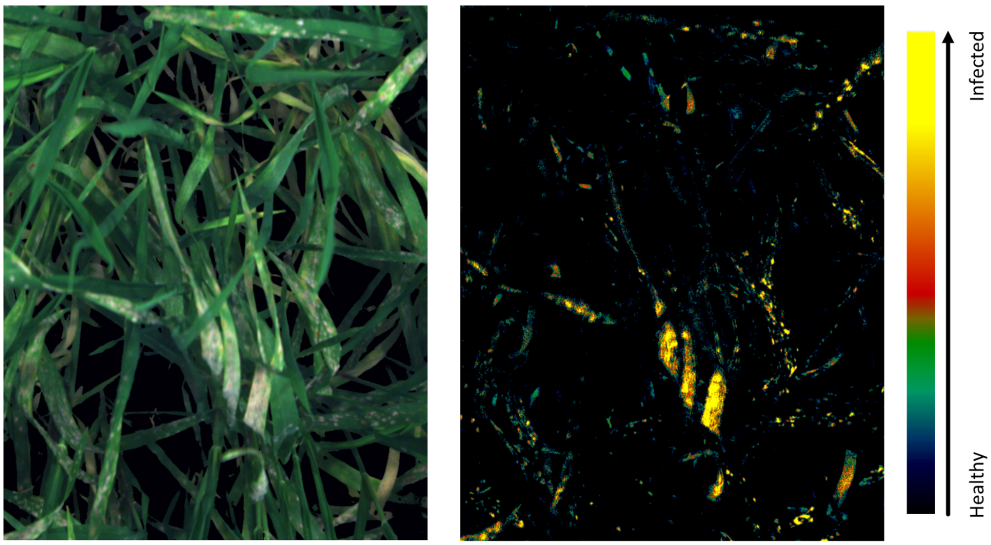


Figure 1.7: Powdery mildew infested canopy of barley cultivar Grace. Powdery mildew infestation can be observed in the pseudo RGB image (left). After application of Simplex Volume Maximization, a false color image (right) was created based on the abundance level of one archetype with high relevance for powdery mildew symptoms. Hyperspectral imaging was performed under greenhouse conditions with artificial light sources (diffuse light; Specim V10 hyperspectral sensor).

Despite this challenges it was possible to adopt efficient data analysis methods, which have been established for image analysis within the remote sensing community(Fig. 1.7; Moshou *et al.* 2005, Plaza *et al.* 2009, Ustin and Gamon 2010, Rumpf *et al.* 2010, Behmann *et al.* 2014, Wahabzada *et al.* 2015a). A main goal is the dimensionality reduction of the hyperspectral data in order to enable an easy to interpret visualization of the results, which allows researchers with different backgrounds sufficient access to the results to combine their expertise for plant phenotyping. Common methods range from relatively simple spectral vegetation indices which work by manually selecting the most relevant bands in the dataset to investigate the required parameters of the dataset, to advanced machine learning approaches (reviewed by Behmann *et al.* 2015a). Machine learning approaches are generally differentiated into supervised and unsupervised methods, depending on the requirement of annotated training data.

**Spectral vegetation indices** Spectral vegetation indices (SVIs) are an established method in remote sensing to relate plant-physiological parameters with airborne hyperspectral data (Jensen 2006, Govender *et al.* 2009). In general

principle SVIs are created by researchers who select specific bands to a single index that correlates with specific changes in the plants physiological state and metabolism. Over the years an immense variety of SVIs for different applications has been developed within numerous studies. One of – if not the – most common SVI is the Normalized Difference Vegetation Index (NDVI) (Rouse *et al.* 1974). It is related to biomass and plant vitality by correlating with the greenness of measured plants and used in remote sensing to differentiate vegetation and soil (Bravo *et al.* 2003), but also applied in plant stress detection. Devades *et al.* (2009) did investigate ten different vegetation indices in order to separate yellow rust, stem rust and leaf rust. While no single SVI was ideal for the separation it could be shown, that a series of multiple SVIs was able to identify specific rust types reliably. Finding new SVIs has become a challenging process, due to the increasing complexity of possible candidates. Through the usage of filter algorithms to identify relevant bands within the given dataset in order to perform an in-depth evaluation with a reduced computational load allowed Mahlein *et al.* (2013) to establish scale-specific indices for the detection and identification of sugar beet diseases.

While specific spectral vegetation indices have sharp limitations in their application to specific stress factors they offer the advantage of only considering few, distinct wavelengths in the analysis. This leads to low computational load when SVIs are applied to large datasets, but also has the risk of the SVIs giving misleading results when the dataset includes new factors, such as new stress factors or differing environmental conditions.

**Supervised methods** Supervised data analysis models classify each datapoint within a given scope – the can be applied on image or pixel level – based on a given set of training data for the separate classes. For the detection of plant stress, the pixel based approach is generally used and assigns each pixel within the hyperspectral image to one of the provided classes, such as "healthy" or "disease symptom". Another possible application is the use of regression models, which – contrary to classification – derive continuous predictions (Bishop 2006).

The spectral angle mapper (SAM) is a commonly used supervised data analysis method, which assigns pixel into classes based on the cosine range in the feature space relative to the training data (Kruse *et al.* 1993). The advantage of cosine distance as base for the classification is that it removes scale differences, thereby compensating for factors – such as varying illumination intensity. Spectral angle mapper was used by Mahlein *et al.* (2012) to detect and localise different sugar beet leaf diseases. Hillnhütter *et al.* (2011, 2012) used SAM to identify *Rhizoctonia*-caused root rot and *Heterodera schachtii* infection. Li *et al.* (2014) could detect Citrus canker through the application of SAM on airborne measurements. Bauriegel *et al.* (2011a) successfully detected *Fusarium* head blight on wheat ears.

Partial-Least Squares Regression is another common method for hyperspectral image analysis and well suited for cases where large numbers of highly

correlated bands are found within the dataset. Zhao *et al.* (2016) quantified the progressing degradation of chlorophyll and carotenoids on plants infected with angular leaf spot disease, visualizing the spatial distribution through the application of Partial-Least Squares Regression on hyperspectral images of the plants.

Support vector machine (SVM) is based on the principle of empirical risk minimization, allowing it to reliably separate datapoints in high-dimensional datasets into different classes with comparatively low amounts of training data (Cortes and Vapnik 1995). AVM has been shown to perform exceptionally well for remote sensing applications (Melgani and Bruzzone 2004). Rump *et al.* (2010) was able to apply SVM on close range measurements of foliar diseases, showing that the classification with SVM could identify disease effects before they became visible to the human eye.

Probabilistic topic models are a variant of classification, which uses not only single classes but small numbers of topics. Thereby, they are highly efficient in identifying hidden topics in large datasets, such as document selections, allowing the organisation of large datasets (Blei 2012). Wahabzada *et al.* (2012, 2016) applied this method on hyperspectral datasets by viewing hyperspectral images as "documents" and spectral signatures as "words", allowing a representation of relevant data (plant stress, healthy tissue) as pairs of wavelength x reflectance pairs. This approach proved to be successful to detect drought stress (Wahabzada *et al.* 2012) and different barley foliar diseases (Wahabzada *et al.* 2016).

**Unsupervised methods** Unsupervised methods offer the advantage of not requiring labelled training data in order to separate pixels of given images within a dataset into different classes. As the generation of training data often requires manual input and training datasets are only fully applicable to data which were measured under similar conditions and contain similar measurement targets, the use of unsupervised data analysis methods is desirable for practical use and the processing of multiple datasets with varying parameters. Unlike supervised methods however, unsupervised methods do not operate on the baseline of training data when it comes to determining classes. This can lead to significant difficulties for disease detection in early stages when other factors within the images lead to higher variability within the dataset then the differences of healthy plant tissue and symptomatic tissue. Data clustering through unsupervised methods is thereby often applied as a preprocessing step in order to derive a more comprehensible interpretation of a dataset with reduced variables, which can then be interpreted through the operator.

An example for an unsupervised data analysis method is the principal component analysis (PCA), which sorts data based on their variability within given datasets, thereby reducing the variance and lowering the dimension of the dataset (Bishop 2006). Thomas *et al.* (2017) detected and quantified powdery mildew symptoms on reflectance and transmittance hyperspectral images of barley leaves through the application of PCA on the respective datasets.

They were able to derive the respective changes through the correlation with the first and second principal component, as within the highly controlled laboratory setup the differences between healthy and symptomatic plant tissue were the factors with the most variance within the dataset. The above example shows the application of PCA onto a relatively simple dataset. Within more complex datasets the inert difficulties when working with PCA become apparent, as the principal components do not directly correlate with the physical reality within a given dataset. Instead, abstract features based solely on variance are extracted, which can make a correlation of PCA results with the desired factors within the images difficult (Mahoney and Drineas 2009).

Simplex volume maximisation (SiVM) is a data-driven approach, which extracts interpretable data from the given datasets (Thurau *et al.* 2012). It has the advantage that it doesn't rely on abstract features – like the PCA – but instead uses the spectral signatures as archetypes to generate a new interpretation of the data with reduced dimensionality. This allows SiVM to represent large hyperspectral datasets in reduced dimensionality while still presenting the data based on real data points, allowing for an easier interpretation. Kersting *et al.* (2012a) showed that the impact of extreme signatures within SiVM can be quantified through the application of probabilistic interference. This technique was successfully applied by Whabazada *et al.* (2015a) and Kuska *et al.* (2015) to extract disease signatures of different plant diseases, as well as computing the footprints of plants over the time based on time-series hyperspectral images (Kersting *et al.* 2012b, Römer *et al.* 2012, Wahabzada *et al.* 2015a). An example of SiVM being applied on a hyperspectral image of barley plants with powdery mildew symptoms is shown in figure 1.7. The pseudo RGB representation of the hyperspectral image (left) allows the user to determine the presence of powdery mildew symptoms with the naked eye, but a determination of the disease severity requires expert knowledge. The representation of a SiVM archetype with high relevance for powdery mildew symptoms (right) meanwhile highlights areas with powdery mildew symptoms and can be used to quantify the amount of pixels showing symptomatic tissue based on the abundance values per pixel for the selected archetype. Thereby, it is possible to perform an automated and objective assessment of disease severity.

**Perspectives in data analysis** Modern data analysis methods have great potential for extracting relevant and easy to interpret information out of hyperspectral datasets. However, it has been shown that this is a challenging process, which increases in difficulty the more variance is present within given datasets. While hyperspectral data under stable conditions can be transformed into the required classes – such as healthy and symptomatic tissue in plant disease detection – with relatively low difficulty this task becomes increasingly complex the more non experiment specific variance is added in the dataset. This can be the case through inert variance of datacubes through factors like environmental conditions or plant architecture on canopy scale, as well as factors which become relevant within the entirely of an investigated set of datacubes – such as

differences in respective images of time series measurements or measurements on multiple scales.

In order to keep up with the rapidly developing sensor technologies and future applications it is important to expand and evolve the scope of current data analysis as well. One factor which is so far often overlooked is taking the given spatial information within a hyperspectral datacube into account (Behmann *et al.* 2015). Referencing the given changes in the spectral profiles of selected pixels with their location within an image by patch-based feature descriptors or texture filters has potential to differentiate if these changes are relevant for the current application and thereby increase accuracy of the data analysis. The correlation of 3D models of plant canopies with hyperspectral datacubes could be used to negate the variance which is introduced through the plant architecture within canopy images (Roscher *et al.* 2016). This process has the potential to increase cross scale compatibility of data analysis methods drastically.

The inclusion of multi-scale data is an important aspect for the generation of future prediction models within plant management. The combination of data from different sensors and scales in order to increase the amount of information gathered in order to increase accuracy. Environmental data and general data about plant growth and nutrient gradients within the soil can be gathered from UAV and satellite based sensors, whereas close range sensors on ground based vehicles can give high resolution hyperspectral images for early disease detection, which can be correlated with disease specific spectral signatures from fungi under the microscope as shown in Bohnenkamp *et al.* (2018) (Fig. 1.6).

Such powerful models include vast amounts of data, which are not feasible to be annotated manually. Thereby, unsupervised or semi-supervised methods will become increasingly important in the future. In recent years deep learning has shown to outperform other data analysis methods when it comes to the application on such difficult tasks (LeChun *et al.* 2015). Based on neural networks deep learning uses huge nets of billions of neurons to benefit from large amounts of training data. While used extensively for multiple applications they have not yet been applied to the detection of plant diseases in hyperspectral imaging. Using these approaches has a high potential for the detection of new plant-pathogen interactions in early development stages, as they do not rely on input from the user – which requires the user to be able to recognise relevant areas within the datacube – but obtain this information based on the raw data itself.

### 1.2.6 Conclusion and prospect

It has been shown that hyperspectral imaging can be performed on different scales, from the tissue level to the canopy level. This offers several new applications for plant phenotyping and precision agriculture. Nevertheless, the scalability between hyperspectral close-range-, greenhouse-, field- and remote imaging has to be investigated in more detail in future research. From the technical side, a calibration of camera systems and different kind of measuring setups is essential for a precise mapping of spectral information (Behmann *et al.*

2015b). The 3D structure of the object of interest influences the information in hyperspectral data as well. Thus, optical sensing benefits from combined hyperspectral and 3D measuring approaches (Wahabzada *et al.* 2015b; Behmann *et al.* 2016; Roscher *et al.* 2016). Another important factor influencing the information content of hyperspectral images, is the spatial resolution and the number of mixed pixels. This parameter strongly depends on the distance between the sensor and the object; thus, airborne or space-borne, far-range systems have lower spatial resolution compared to near-range or microscopic systems. Sensors with a spatial resolution of about 1 m are hardly suitable for the detection of single symptoms or diseased leaves and plants; here proximal sensor platforms are preferable (Oerke *et al.* 2014). The spatial resolution has a strong influence on the detection of plant diseases or plant–pathogen interactions (Mahlein *et al.* 2012). Increasing the distance between sensor and plant is challenging for the specificity and sensitivity. Nevertheless, identified characteristic hyperspectral signatures seem to be transferable on different scales. This enables a new approach for basic research in the laboratory and in the greenhouse to analyze the plant phenotype and genotype under different conditions and transferring this knowledge to remote sensing methods. Future research also has to consider improved sensor platforms and vehicles for field and high-throughput applications more intensively (Polder *et al.* 2014; Sankaran *et al.* 2015; Walter *et al.* 2015; Virlet *et al.* 2017). It is expected that new developments in the field of robotics will speed up this process.

# 2 Objectives of this thesis

The overall aims of this study were: (1) To evaluate transmission-based hyperspectral imaging and compare it with reflection-based imaging for the detection and quantification of plant disease symptoms on leaf scale. (2) The development of high-throughput – canopy scale – measurement systems to promote hyperspectral applications in agricultural practice and explore early disease detection on canopy scale. (3) To investigate the compatibility of hyperspectral data from different scales.

Simultaneous reflectance and transmittance hyperspectral datasets of time-series measurements from different pathogens were performed with the HyperART system in order to evaluate the efficiency of reflectance and transmittance data for early pathogen detection and quantification on leaf level. Additionally, a high-throughput hyperspectral measurement system and measurement protocol for the rapid measurement of crop plants under field-like conditions in Mini-Plots within the greenhouse were developed. The data of reflectance and transmittance were processed and correlated on leaf level, which allowed a detailed evaluation of the performance of transmission based measurements for the detection and quantification of barley diseases with different plant-pathogen interactions – permitting greater insight into this relatively unknown research area. Furthermore, the direct comparison between datasets of powdery mildew infected barley plants on leaf scale under laboratory conditions and canopy scale under greenhouse conditions allowed a direct estimation of hyperspectral data compatibility on different scales.

The main objectives were to:

- Design of a measurement setup to acquire hyperspectral datasets for reflection and transmission based images of different diseases to record the changes to the plants spectral signatures during their respective plant-pathogen interactions (Chapter 3).
- Determine suitable means of data analysis for both reflectance and transmittance hyperspectral images of the different barley diseases (Chapter 3).
- Compare the performance of reflectance and transmittance data for the early detection and quantification of the examined diseases (Chapter 3).
- Develop a high-throughput measurement system for disease detection on crop plants on canopy scale under greenhouse conditions (Chapter 4).
- Establish a measurement protocol for the canopy based measurement under greenhouse conditions that permits high-throughput time-series measurements without being influenced by environmental conditions (Chapter 4).

- Find a suitable data analysis pipeline for early disease detection of canopy scale hyperspectral images, which is robust enough to work despite the increased data complexity (Chapter 4).
- Compare the results of manual investigation of spectral signatures and data analysis procedures on leaf and canopy scale in order to evaluate data cross-scale compatibility (Chapter 3 and 4).

# 3 Evaluation and possible uses of combined reflectance and transmittance measurement on leaf scale

## 3.1 Powdery mildew development on inoculated barley leaves

**Chapter 3.1 has been published:**

**Thomas S**[1], Wahabzada M[1], Kuska M[1], Rascher U[2], Mahlein A-K[1] (2017) Observation of plant-pathogen interaction by simultaneous hyperspectral imaging reflection and transmission measurements. *Functional Plant Biology* 44(1), 23-34.https://doi.org/10.1071/FP16127

[1]INRES-Phytomedizin, University Bonn, Bonn, Germany
[2]IBG2: Plant Sciences, Forschungszentrum Jülich GMBH, Jülich, Germany

**Changes made in the thesis chapter compared to the original publication:**

Figures have been slightly optically improved, without changing their content. Abbreviations have been adapted in order to provide a united layout over the course of the thesis.

**Authors contribution**

Stefan Thomas, Anne-Katrin Mahlein, and Uwe Rascher designed the study and drafted the manuscript. Stefan Thomas, Matheus Kuska, Mirwaes Wahabzada, Anne-Katrin Mahlein, and Uwe Rascher interpreted the experiments. Stefan Thomas modyfied the HyperArt measurement setup, performed the experiments within the study and carried out manual and statistical analysis. Stefan Thomas and Mirwaes Wahabzada performed the data mining methods for automated hyperspectral data analysis.

### 3.1.1 Abstract

Hyperspectral imaging sensors are valuable tools for plant disease detection and plant phenotyping. Reflectance properties are influenced by plant pathogens and resistance responses, but changes of transmission characteristics of plants are less described. In this study we used simultaneously recorded reflectance and transmittance imaging data of resistant and susceptible barley genotypes that were inoculated with *Blumeria graminis* f. sp. *hordei* to evaluate the added value of imaging transmission, reflection and absorption for characterisation of disease development. These datasets were statistically analysed using principal component analysis, and compared with visual and molecular disease estimation. Reflection measurement performed significantly better for early detection of powdery mildew infection, colonies could be detected 2 days before symptoms became visible in RGB images. Transmission data could be used to detect powdery mildew 2 days after symptoms becoming visible in reflection based RGB images. Additionally distinct transmission changes occurred at 580–650 nm for pixels containing disease symptoms. It could be shown that the additional information of the transmission data allows for a clearer spatial differentiation and localisation between powdery mildew symptoms and necrotic tissue on the leaf then purely reflectance based data. Thus the information of both measurement approaches are complementary: reflectance based measurements facilitate an early detection, and transmission measurements provide additional information to better understand and quantify the complex spatio-temporal dynamics of plant-pathogen interactions.

### 3.1.2 Introduction

When light interacts with a plant it comes to a distinct set of physical processes, namely reflection, transmission and absorption. A part of the incoming light is reflected from the surface of the plant and after internal backscattering, some light is absorbed by plant tissue and another part of the light is transmitted through the plant tissue (Vogelmann 1993). In addition, there is internal scattering of the reflected and transmitted light involved while it interfuses the plant tissue. The portion of incoming light that is reflected, transmitted or absorbed varies with the wavelength of the incoming light and depends on the structural and chemical composition of a plant (Knipling 1970; Woolley 1971). This means that together, the structure of the leaf surface and the composition of the plant tissue produce a characteristic spectral profile (Vogelmann and Gorton 2014). Plant pigments, such as chlorophyll, carotenoids or anthocyanins, have well known absorption patterns in the visible range of the electromagnetic spectrum (Blackburn 2007). When a plant is subjected to stress, such as pathogen attack, metabolic processes and the cellular structure of a plant change. This leads to an altered spectral profile of the plant and provides a possibility to detect plant diseases through observation of the plants spectral characteristics (Bock *et al.* 2010; Mahlein *et al.* 2012).

Measuring the reflectance of plant material with hyperspectral sensors has

already been shown to be an effective tool to detect stress in plants (Carter and Knapp 2001; Rascher *et al.* 2011;Yuan *et al.* 2014). Furthermore, multiple studies have demonstrated that it is possible to identify specific plant diseases through hyperspectral reflectance measurement (Zhang *et al.* 2002; Mahlein *et al.* 2010; Hillnhütter *et al.* 2012). Pathogen-specific changes in the plant's spectral profile could be observed on the respective model plants. Mahlein *et al.* (2010) were able to identify three different fungal diseases (*Cercospora* leaf spot, powdery mildew and rust) on sugar beet through a combination of different spectral vegetation indices. Following investigations established disease specific vegetation indices for disease detection based on hyperspectral imaging (Mahlein *et al.* 2013). This enabled a classification of sugar beet leaf infections with an accuracy of over 90%. Zhang *et al.* (2002) showed that late blight in tomatoes could be readily detected through principal component analysis (PCA) and cluster analysis, whereby the disease symptoms correlated with the second principal component (PC). An important task is the characterisation of disease susceptibility or resistance reactions through sensor observations of plant-pathogen interactions on different plant genotypes (Kuska *et al.* 2015; Leucker *et al.* 2016a, 2016b; Mahlein 2016). Different resistance mechanisms of barley (*Hordeum vulgare* L.) against powdery mildew (caused by *Blumeria graminis* f. sp. *hordei*; *Bgh*) are well known, and work over several biochemical pathways. The resistance mildew locus o (*mlo*) confers resistance through fast papillae formation, which inhibit the *Bgh* conidium to penetrate the epidermal cell (Jørgensen 1977; Bhat *et al.* 2005). In contrast, *Mla* gene-based resistance induces a hypersensitive reaction in epidermal cells, which are penetrated by *Bgh* (Jørgensen and Wolfe 1994; Wei *et al.* 2002; Hückelhoven and Panstruga 2011).

Spectral observations of plant–pathogen interaction are performed through hyperspectral sensors that measure reflectance signatures of plants. In this case, both imaging and non-imaging sensors are available (West *et al.* 2003; Sankaran *et al.* 2010; Mahlein 2016). Hyperspectral imaging sensors provide a spectral profile for each pixel of the measured image in three-dimensional hyperspectral data cubes. Technical solutions for reflection and transmission with non-imaging hyperspectral sensors are well established. Those sensors use spot measurements from both sides of a certain area simultaneously. However, this method is not applicable for current hyperspectral imaging sensors and has the disadvantage that only a small area of the leaf can be assessed (Bergsträsser *et al.* 2015). Through the development of the HyperART measurement setup by Bergsträsser *et al.* (2015), simultaneous hyperspectral imaging measurements of reflection and transmission are possible. This is an advantageous progress for a detailed, non-invasive and objective assessment of different plant genotypes and plant–pathogen interactions in breeding processes, which aim to establish pathogen resistant varieties. In theory, the addition of new information gathered by transmission measurements could increase the precision of reflection based measurements.

Although hyperspectral measurement of reflected light has been investigated in multiple studies, few studies are available on the possible use of transmitted

light for the identification and determination of abiotic and biotic plant stress (Bergsträsser *et al.* 2015; Kim *et al.* 2015). The measurement of transmission shows a reduced noise ratio compared with the reflection measurement in the approach by Bergsträsser *et al.* (2015). In that study investigating *Cercospora* leaf spot disease on sugar beet plants, a combination of reflectance and transmittance data turned out to be best suited for differentiating between infected and healthy leaf tissue. Reflected light is mainly influenced by the upper epidermis of a leaf, the strength of the effect is depending on the reflected lights wavelength. Meanwhile, transmitted light has interacted with the whole-leaf tissue, giving integrated information across all cell layers of the leaf. Thus it can be expected that reflectance and transmittance data have complementary information. This leads to the hypothesis that a combination of reflection and transmission measurements can provide a more precise model for identifying plant pathogens and for evaluating different genotypes.

The aim of the present study was to investigate the potential of transmission measurements to analyse plant–pathogen interactions. The study was performed with the model system barley (*Hordeum vulgare* L.) – powdery mildew (caused by *Bgh*) in order to evaluate if simultaneous reflection and transmission measurement provides an improvement for the detection and identification of biochemical and structural changes during pathogenesis. Powdery mildew infection starts on the leaf surface then later affects the whole-leaf tissue, thus is well suited for the evaluation of reflectance and transmittance based measurements. The development of *Bgh* on a susceptible barley wild type and a *mlo3*-based resistant genotype was investigated through time-series measurements. A dataset for both reflectance and transmittance information was generated using the HyperART hyperspectral imaging setup, which uses a mirror system to allow simultaneous measurement of reflection and transmission in wavelengths between 400 and 2500 nm (Bergsträsser *et al.* 2015). The additional benefit of transmission measurements was investigated and evaluated based on this exhaustive dataset using further statistical analysis by PCA.

### 3.1.3 Material and Methods

#### Plant cultivation and pathogen material

*Hordeum vulgare* L. cv. Ingrid wild type (WT; susceptible) and the corresponding near-isogenic line M.C. 20 (including *mlo3* gene based resistance; further referred to as *mlo3*, or resistant genotype) were used for the experiments (Hinze *et al.* 1991). The plants were grown in TEKU VQB $7 \times 7 \times 8$ cm pots (Pöppelmann) and filled with commercial substrate (Klasmann-Deilmann GmbH) under greenhouse conditions at 23/20°C (day/night) 60% RH and daylight period of 16 h. At growth stage 12 according to BBCH scale (Hack *et al.* 1992) fungicide Vegas (active agent 53.1 g L–1 cyflufenamid, BASF) was applied to keep control plants healthy. For measurements plants were relocated in the laboratory with a daylight period of 16 h and 22/20C (day/night), where the second leaf of each plant was fixed within a custom plastic frame. Six plants per genotype were

inoculated with *Bgh* isolate K1 (Hinze *et al.* 1991) while six control plants per genotype remained untreated. The inoculation was performed through gently shaking *Bgh* isolate K1 infected plants over the plants.

### Reflection and transmission hyperspectral imaging measurement

Simultaneous measurements of reflection and transmission of individual leaves were performed with the HyperART spectral imaging system (Bergsträsser *et al.* 2015; patent no.: DE 102 012 005 477). A detailed description of the measurement setup is published in work by Bergsträsser *et al.* (2015; see Fig. 1 in the referenced article for technical drawing).The system was modified to achieve better image quality for barley leaves. Briefly, the distance between camera and mirror setup was set to 600 mm in order to improve the spatial resolution of the pictures, achieving a pixel size of 0.19 mm. All leaves were measured in a time series experiment from 1 day before inoculation (dbi) to 11 days after inoculation (dai) in the visible range (VIS) and in the near infrared (NIR) range (400–1000 nm). For each measurement a 99% reflectance white standard (Spectralon Labsphere Inc.) and a white diffuser lambertian transmission foil (Zenith Polymer ~50% transmission, SphereOptics GmbH) was acquired, before measuring the leaf sample. These measurements served as white references for reflection and transmission images for the image normalisation (Bergsträsser *et al.* 2015). Wavelength-dependent differences in the percentage of the reflected and transmitted light of the two white references were taken into consideration during the normalisation process. With each measurement a dark current image of the internal camera noise was measured by closing an internal camera shutter. An example of spectral profiles for reflection and transmission and the according hyperspectral images of healthy barley leaves in RGB bands is shown in Fig. 3.1. Through this setup it is possible to observe the full spectrum of incoming light interacting with the leaf in form of reflection, transmission and absorption.

### Data analysis of the hyperspectral images

The reflectance and transmittance of the images was calculated relative to the respective white reference standard with ENVI 5.1 + IDL 8.3 (ITT Visual Information Solutions). The normalised images were smoothened using the SavitzkyGolay filter (Savitzky and Golay 1964) in order to reduce noise in the hyperspectral images. As the images had a high noise in the extremes of the measured range only data from 450–1000 nm was analysed. The background was masked out and pixels containing the leaves were manually extracted for both, test and control plants, leading to ~1000–8000 pixels per leaf used in statistical analysis. All signatures/vectors were normalised to have the unit Euclidian norm, being treated as points on a high dimensional unit sphere (Dhillon and Modha 2001; Leucker *et al.* 2016b). This allows to capture the vectors direction while mitigating effects of varying reflectance values and allowing for more robust data clustering. The motivation behind this was to reduce a high,

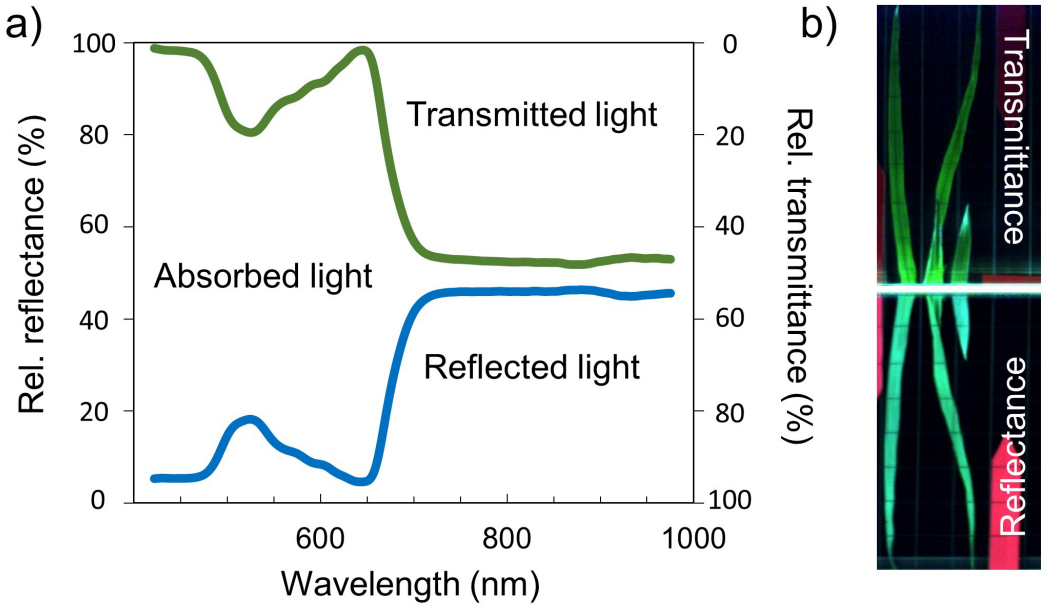


Figure 3.1: (a) Spectral signatures of reflectance and transmittance of a healthy leaf of barley cv. Leibniz plants, data are expressed as relative values. (b) Hyperspectral image of barley. The HyperART setup (patent no.: DE 102 012 005 477) allows one hyperspectral camera to gather reflection and transmission data of a sample at the same time as the camera view is split between the according mirrors. The interaction of all parameters (reflection, transmission, absorption) between incoming light and plant tissue can be observed.

Table 2: Percentage of explained variance of principal component (PC) eigenvectors for the PC analysis for susceptible wild type (WT) and resistant *mlo3* genotypes

| | PC 1 | PC 2 | PC 3 |
|---|---|---|---|
| WT reflectance | 86 | 6 | 3 |
| WT transmittance | 76 | 7 | 2 |
| *mlo3* reflectance | 77 | 5 | 3 |
| *mlo3* transmittance | 77 | 7 | 2 |

non-biologic variance in the reflectance data.

For further interpretation PCA was performed. PCA is a statistical method in which the data is transformed via the introduction of new axes along the greatest variance in the data (Wold *et al.* 1987). It is an unsupervised method that is often used for exploratory data analyses and tasks, such as data compression, noise and redundancy removal. In order to perform PCA, the spectral data cubes of all samples from a genotype were transformed into dense wavelength pixel matrixes and fused. PCA was implemented per genotype on the entire matrix, containing signatures of control and inoculated plants. The first three principal components (PCs) with the largest eigenvalues were selected for further analysis (Table 2).

All performed experiments, described in the material and methods, were repeated twice, using different datasets for the PCA in order to confirm the results.

**Disease severity estimation**

The disease severity of the test plants was estimated based on the hyperspectral reflectance images. In the PCA each pixel of the image is assigned a specific value in the PC, this value is similar for pixels in the same class. Based on the results of the PCA the values of healthy and inoculated pixels were assessed and a threshold was set to decide which pixel represent powdery mildew infected tissue. The percentage of pixels with powdery mildew infection was then calculated automatically.

Furthermore the percentage of powdery mildew DNA compared with total DNA of the barley leaves was measured through quantitative real time PCR (qPCR). The result was compared with the PCA based estimation of the same leaves. As the qPCR is a destructive method the comparison was handled as separate experiment with 18 leaves in total investigated (six leaves each at the time points 3, 6 and 9 dai). The leaves were measured with the HyperArt system according to the measurement protocol described above. Immediately after measurement the measured part of the leaf was removed and stored at -80°C for DNA extraction. DNA extraction of the leaves was performed with the DNeasy Plant Mini Kit (Qiagen) according to the manufacturer's instructions. The DNA of a known amount of powdery mildew spores was extracted with the same protocol

Table 3: PCR primers and probe for quantitative real-time PCR of powdery mildew *gdp* gene

| Designation | Sequence |
|---|---|
| Powdery mildew gdp forward primer | 5´-tgcctgtaatcaagtaacaacg-3´ |
| Powdery mildew gdp reverse primer | 5´-tgaggaaagaggggaagaag-3´ |
| Powdery mildew gdp qPCR probe | 5´-agattcagcaaccccaccatccgttat-3´ |

to serve as reference for the following qPCR. The qPCr was performed using the StepOnePlus TM RealTime PCR System (ThermoFisher Scientific) and Taq-Man Universal PCR Master Mix (Applied Biosystems). The target DNA was an 87 base pairs area of the powdery mildew specific glyceraldehyde-3-phospahte dehydrogenase (*gdp*) gene (Christiansen *et al.* 1997). Specific information on primers and qPCR probe are provided in Table 3.

#### Microscopic investigation

Leaf tissue samples for histological analysis were prepared from non-infected and *Bgh* infected Ingrid WT plants 6 dai, as well as non-inoculated *mlo3* plants with necrotic spots. Specimens were fixed with 8% paraformaldehyde and 8% glutaralaldehyde in 0.2 M sodium cacodylate buffer (pH 7.3) under vacuum for 4 h at room temperature. Samples were washed for 20 min within cacodylate buffer. The washing step was repeated three times before the samples were dehydrated in a graded ethanol series and embedded in London Resin White medium. The embedded samples were semi-thin sectioned on an ultra-microtome (Reichert Ultracut E, Leica Microsystems) and stained with 1% toluidine blue. Stained samples were observed using a Leitz DMR 6000b photomicroscope. Images were recorded with a digital camera (JVC, Ky-F75U) by using the Discus 4.6 (Technical Office Hilgers) software.

### 3.1.4 Results

#### Reflectance and transmittance profiles of susceptible and resistant genotypes

The first visible symptoms of powdery mildew developed 6 dai. From that day until 11 dai typical powdery mildew symptoms appeared on all inoculated leaves of the susceptible Ingrid WT genotype. However, as indicated in Fig. 3.2, the disease severity differed between the investigated individual leaves, ranging from ~10 to 80% at individual days. The observed variance in disease severity between different leaves is a natural effect when inoculating by shaking infected plants over the sample leaves. Due to air movements different amounts of spores will come into contact with the leaves, this effect is similar to powdery mildew infection under field conditions. Neither the inoculated plants of the *mlo3* genotype nor the control plants of both genotypes showed any powdery mildew symptoms.

The PCA based estimation of disease severity shows a correlation of over

0.72 with the qPCR based measurement of the powdery mildew DNA (Fig. 3.3). Total values differ in the case of strong powdery mildew infestation. However, this was expected, as the powdery mildew is only present in the epidermis layer of the leaf, which is measured by hyperspectral imaging. Meanwhile the qPCR measures the total amount of DNA of the leaf, including lower layers of the leaf, which are free of powdery mildew infection.

Fig. 3.4 displays the mean values of all inoculated leaves from susceptible Ingrid WT per day showed only minor changes over the course of the experiment. However, when the standard deviation (*std*) is taken into account, distinct changes in the reflectance spectral signature become visible during pathogenesis (Fig. 3.4). The powdery mildew infestation lead to a characteristic raise in the spectral reflection signature, which is prominent in the range between 550 and 680 nm. Spectral signatures of the transmission showed less prominent changes (Fig. 3.4). Of those, the most noticeable effect was a slight raise of the spectral signature in the range from 580 to 650 nm during the later pathogenesis, when larger symptoms had developed (8–10 dai). It is noteworthy that in both cases the *std* indicates the greatest variability of the data in the near infrared from 780 to 950 nm. The resistant *mlo3* genotype and the non-inoculated control plants of both genotypes showed the highest variability in the near infrared range of the spectrum, which was present consistently throughout all measurements during the experiment (Fig. 3.4). The reflectance and transmittance profiles of the resistant *mlo3* genotype did not change over the course of the experiment (Fig. 3.4). Thereby maintaining typical spectral profiles for barley leaves (Fig. 3.1) over the course of the experiment, which was also observed for the control plants.

### Analysis of powdery mildew in early stages through PCA

The first analysis of the hyperspectral datasets via mean values and standard deviations showed that the variance in the dataset is the most reliable factor for disease detection. Thus PCA analysis was performed in order to get a better representation of the biological variance. The eigenvalue of the PCs showed that the first and second PC were suitable for further investigation, while eigenvalues of higher PCs tended towards zero.

The first PC had a strong correlation with the reflection- and transmission-wavebands from 550 to 700 nm of the spectral signature, which was related to powdery mildew symptom development (Fig. 3.5a). The comparison of the RGB image and the false colour image, representing the values of the first PC per pixel, illustrated that the first PC is highly correlated with disease symptoms on barley leaves whereas the leaf structure showed no correlation (Fig. 3.5b).

The second and third PCs were difficult to interpret as they correlated positively and negatively over several wavelengths of the spectral profile (Fig. 3.5a). The second PC, when compared with the RGB image of the same leaf area, correlates strongly with the structure of the represented leaf (Fig. 3.5b). However, it also exhibits correlation with disease symptoms during the later stages of the disease progression, whereas the third PC with its strong correlation in the NIR

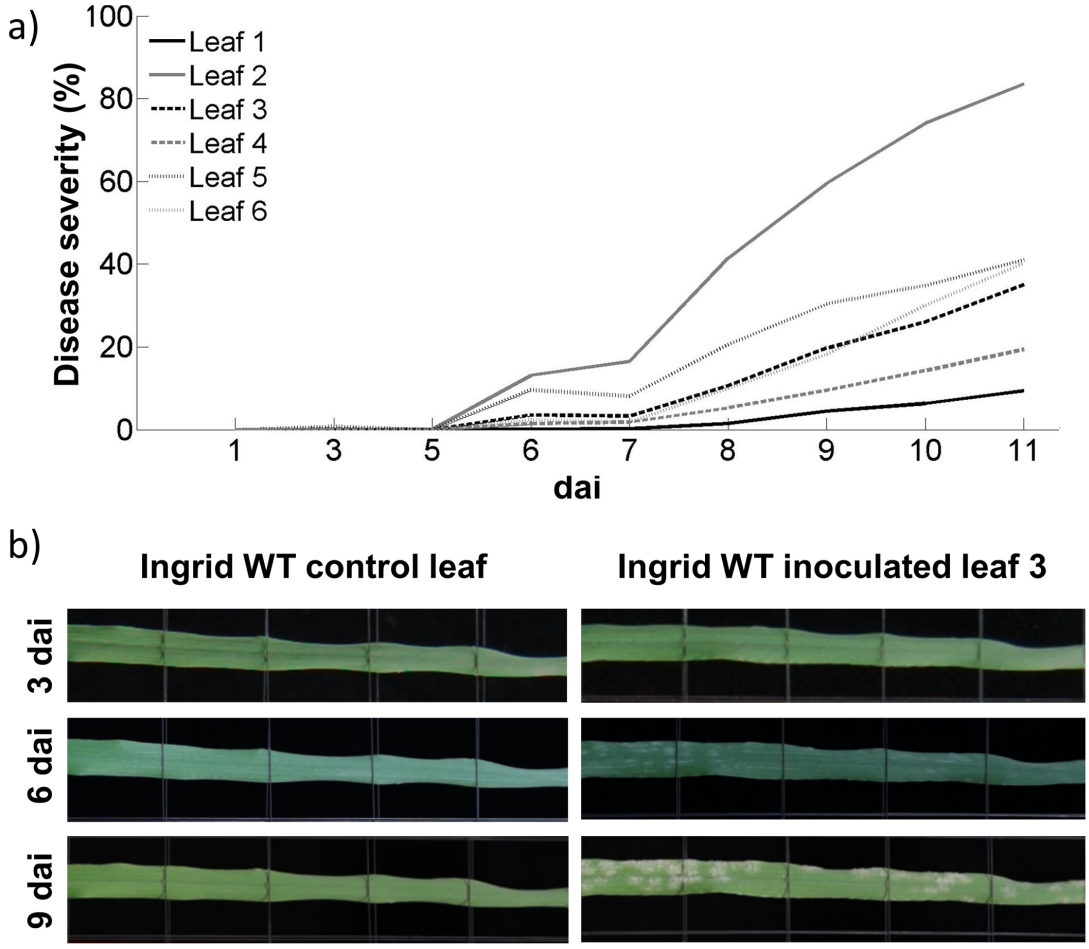


Figure 3.2: (a) Disease severity expressed as percent diseased leaf area for each barley leaf of susceptible line Ingrid wild type (WT) over the course of the experiment. Disease severity was estimated through the values of the second principal component in the statistical analysis of the reflection data, were every pixel with values over a threshold of 0.04 was classified as disease symptom. (b) RGB images of a healthy control leaf and a powdery mildew inoculated leaf (no. 3) at 3, 6 and 9 days after inoculation.

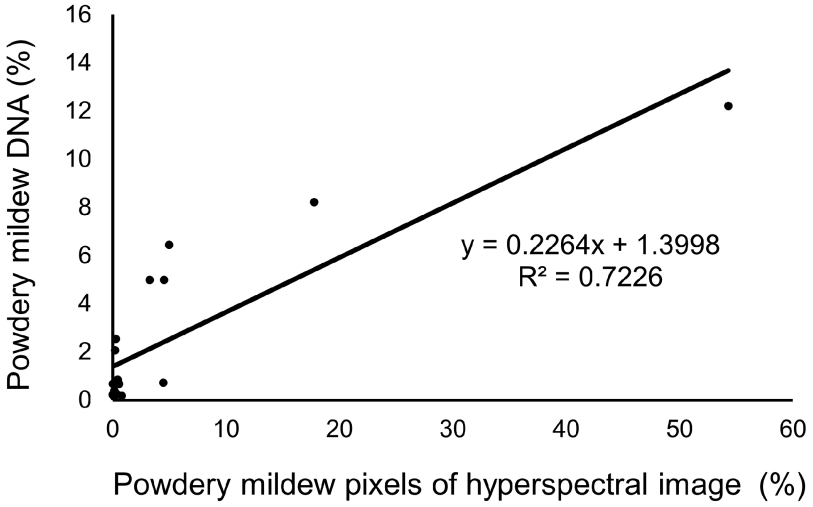


Figure 3.3: Comparison of powdery mildew infection rating based on quantitative real time PCR and principal component analysis. Differences in total amounts registered can be explained due to the different measurement principles (PCR measuring the total amount of plant DNA of the entire leaf; hyperspectral imaging measuring only the surface layer, where powdery mildew is present). The two measurement methods show a correlation of 0.72. (n = 18, measuring period: 3, 6 and 9 days after inoculation).

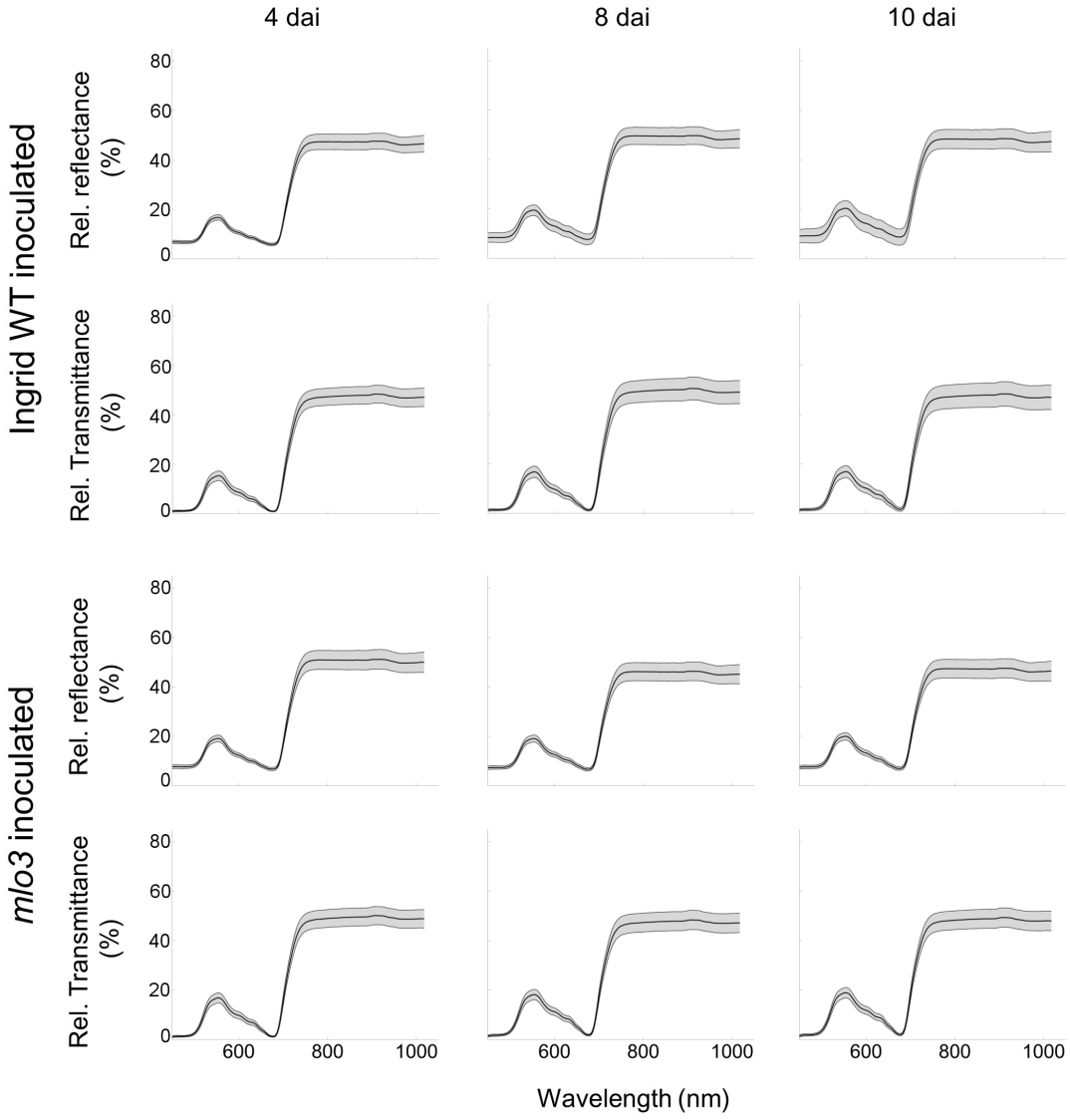


Figure 3.4: Mean spectral signatures for all measured leaves from barley cv. Ingrid plants, inoculated with *Blumeria graminis* f. sp. *hordei*. Reflectance and transmittance, data are shown as relative values. Grey areas represent the *std* of the mean values (n = 6).

range of the spectrum indicated no visible correlation with disease symptoms. These results confirmed the earlier findings, that high variance in the *std* for the range of the spectral signature between 780 and 950 nm was not related to an infection with powdery mildew.

When interpreting the correlation of PCs to specific wavelengths in the dataset it is important to understand that there is no fixed, maximum value for the correlations. In the case of analysing the PCs of a hyperspectral image the maxima is in general defined by the highest value (both positive and negative) available in the PC, which is linked to a specific wavelength range. These, for each PC specific, internal maxima allow an estimation which wavelength ranges from the hyperspectral image are relevant for the variance being explained in the affiliated principal component.

In order to investigate the importance of the first two PCs the pixels of the timeline were plotted into a two dimensional grid according to their value in the PCs, with the PCs functioning as respective x- and y-axes. These scatter plots coincide with the observations from the false colour images. For the susceptible Ingrid WT the second PC had only slight disease specific changes over time, as the values showed minor differences between inoculated and control plants for both reflection and transmission measurement (Fig. 3.6). However, a distinct rise for inoculated plants occurred in the first PC from 6 dai onwards compared with data of control plants. The development from 6 dai onwards coincide with the progression of powdery mildew symptoms (Fig. 3.6). The data of the transmission measurement of the Ingrid WT line did not allow a clear correlation to disease specific changes for both the first and second PC, even at 10 dai the values for inoculated and control plants were not significantly different (Fig. 3.6).

Values of the first PC per pixel were applied to hyperspectral reflection and transmission images and illustrated as false colour image of the leaves in order to confirm the precision of statistical analysis for detecting disease symptoms on the leaves (Fig. 3.7). Areas with correlating values in the first PC matched with symptomatic tissue from the application of the first PC on the reflectance images, as well as with RGB reflectance images. Meanwhile RGB transmittance images did not allow a clear identification of powdery mildew pustules. The first PC applied on the reflection dataset displayed areas with powdery mildew infection already 4 dai, before the first visible symptoms appeared. The first PC from the transmission dataset indicated of powdery mildew infection at 6 dai when first symptoms were visible in the reflectance RGB image (Fig. 3.7).

The values of each pixel in the first and second PC for the resistant *mlo3* genotype were very similar to the control plants of the Ingrid WT line. However, in the later days of the experiment (6–10 dai) some pixels exhibited a similar development in the values of the first two PCs as the pixels of powdery mildew infected tissue of the Ingrid WT line (Fig. 3.6). This trend can be explained by natural necrosis which occurred during later days of the experiment for the plants of the *mlo3* genotype (Fig. 3.8). The development of necrotic spots was visible in both, reflection and transmission based datasets. This distinct change in the first two PCs for pixels of necrotic tissue for both reflection and

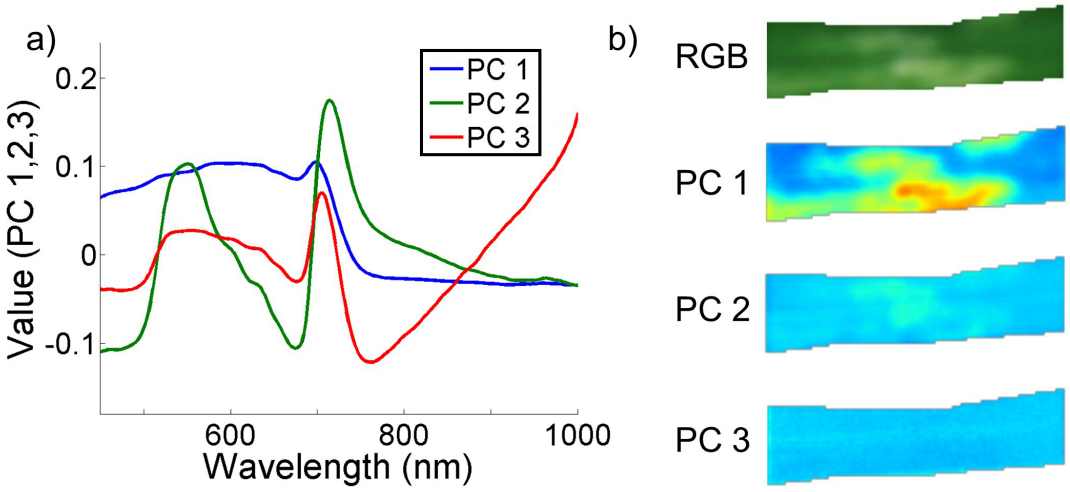


Figure 3.5: (a) The first three principal components (PCs) derived through principal component analysis of the combined mean values for all days from *Blumeria graminis* f. sp. *hordei* inoculated and non-inoculated Ingrid wild-type leaves. (b) Representation of the first three principal components as false colour picture in comparison with a pseudo RGB image. The pseudo RGB image was created from the hyperspectral image, using wavelengths parameters 646, 556 and 456 nm as RGB representation.

transmission images from 6 dai onwards was also noticeable in the scatter plots (Fig. 3.6). The second PC showed only minor differences over the course of the experiment, alike the observations in the dataset of the Ingrid WT line. The slight change in pixel values in the second PC, which represent necrotic tissue on leaves, was inverted when comparing results from the reflection and transmission based datasets.

### 3.1.5 Discussion

The results of this study demonstrate that data gathered by transmission measurement show changes in the hyperspectral profile of barley leaves with developing powdery mildew symptoms and provide additional information to reflection based measurements.

#### Evaluation of transmission based hyperspectral imaging

Hyperspectral transmission imaging has been recently applied for the detection of pertroph pathogens, but so far not for biotrophic pathogens like powdery mildew. Imaging transmission measurement demonstrated to be a promising tool to detect *Cercospora beticola* infestation on sugar beet leaves (Bergsträsser

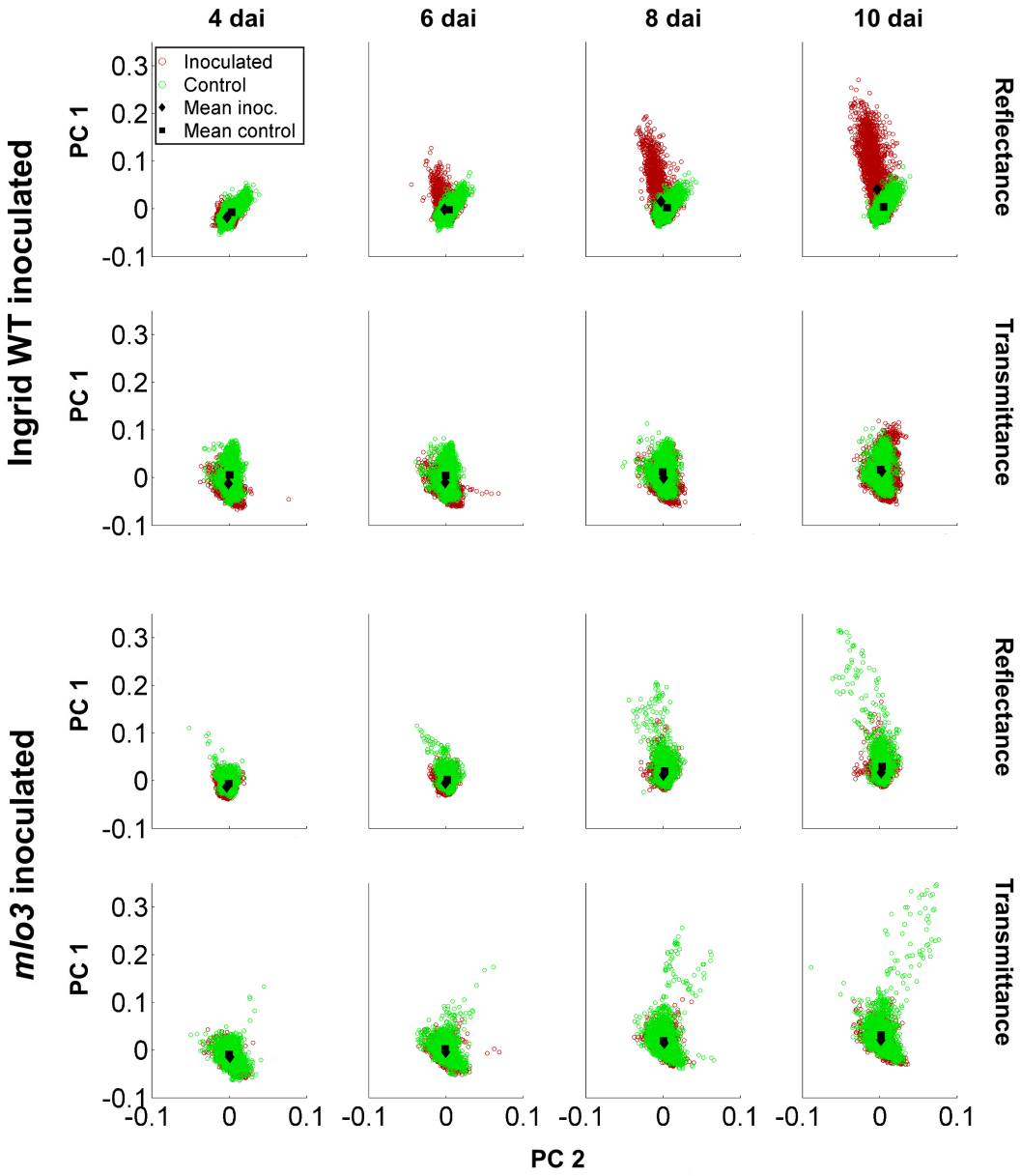


Figure 3.6: Scatterplots of the first and second principal component (PC) values for each pixel from susceptible wild type (WT) and resistant *mlo3* barley leaves in reflection and transmission. Each circle represents a pixel of the images from all measured barley leaves and it's scoring according to first and second PC of the PC analysis.

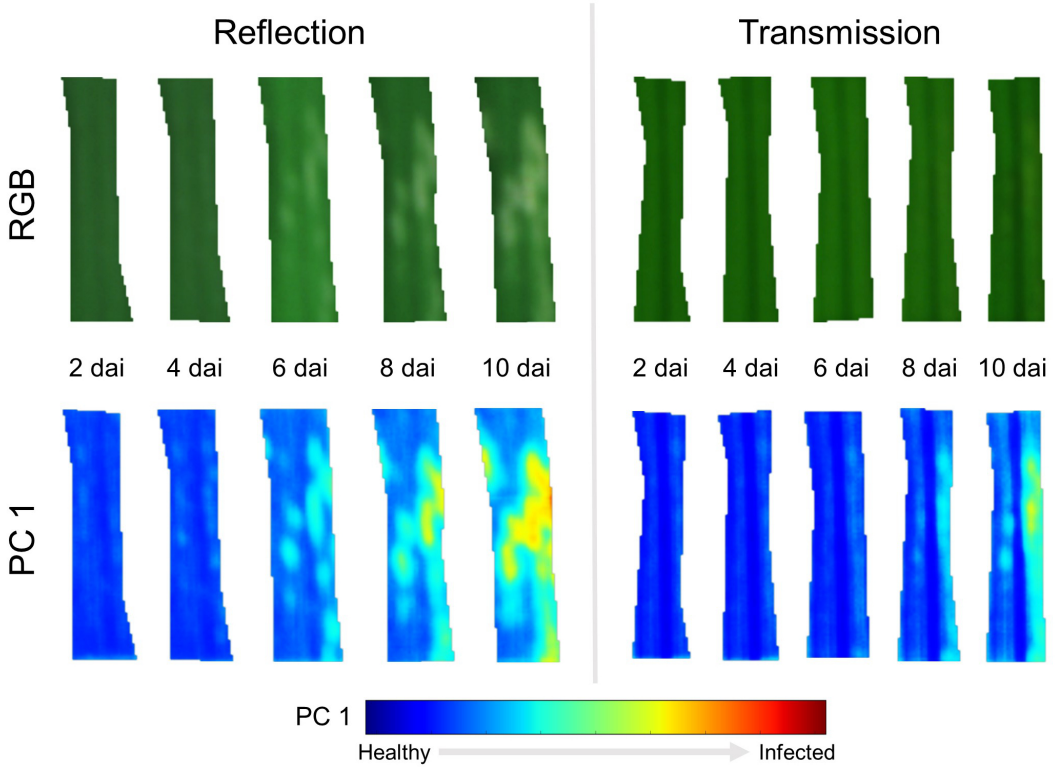


Figure 3.7: Reflection and transmission images of an Ingrid wild type leaf inoculated with *Blumeria graminis* f. sp. *hordei* over time. The pseudo RGB images are compared with false colour images, which represent the value of each pixel in the first principal component (PC) of the PC analysis. The pseudo RGB image was created from the hyperspectral image, using wavelengths parameters 646, 556 and 456 nm as RGB representation. Abbreviation: dai, days after inoculation.

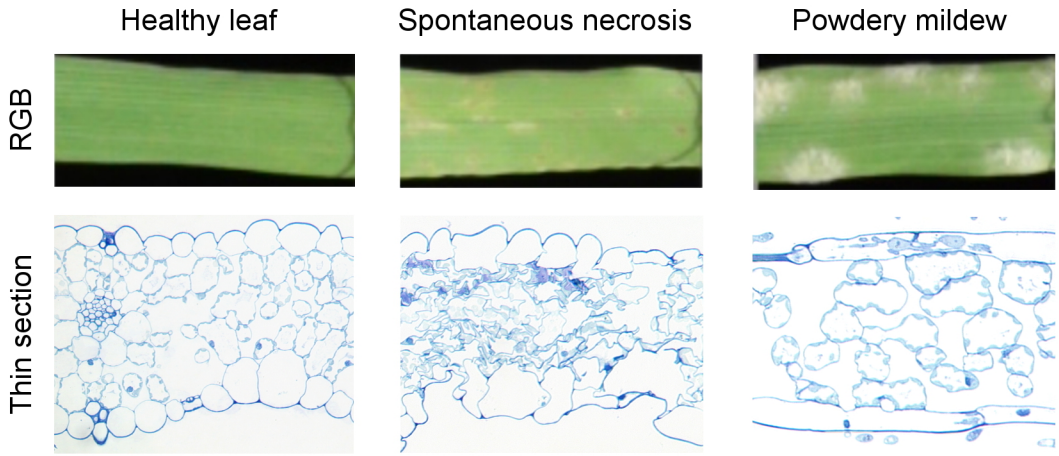


Figure 3.8: RGB images and thin sections of healthy, necrotic and powdery mildew infested barley leaves. The healthy leaves showed a typical cell layer for barley, in the necrotic leaves the cells had collapsed or were deformed through all layers of the leaf (sections crossways, 200×). Powdery mildew symptoms only showed changes in the epidermis cells, were the fungus develops haustoria while lower cell layers remain unaffected (section lengthways, 200×).

*et al.* 2015). These workers were able to make predictions about progressed disease symptoms, influencing a combined reflectance and transmittance profile of the measured plants. In their study a combination of both datasets outperformed analyses based on single datasets derived from reflection or transmission measurement. This coincides with the results of the present study, which shows the advantage of reflection measurement in early detection of powdery mildew. Transmission measurement allows for a sensitive discrimination of powdery mildew symptoms and spontaneous necrosis, which is known to develop in the *mlo* genotypes (Jørgensen 1977).

Bergsträsser *et al.* (2015) suggested that transmission measurements are equally sensitive for stress detection compared with reflection based measurement. The results of this study for powdery mildew infestation coincide only partially with their observations, as reflection based analysis could detect powdery mildew symptoms 2 days earlier then analysis based on transmission datasets. This can be explained as Bergsträsser *et al.* (2015) were measuring *Cercospora* leaf spot symptoms, which appear as necrotic lesions on the infested leaf (Mahlein *et al.* 2012; Leucker *et al.* 2016a, 2016b). In contrast, powdery mildew symptoms develop as small, localised pustules on the leaves and the fungi only penetrates the epidermis cells (Bhat *et al.* 2005; Dean *et al.* 2012; Fig. 3.8). For a detection of spontaneous necrosis the reflection and transmission datasets performed both equally efficient in this study. Unlike the biotrophic pathogen *Bgh* spontaneous necrosis causes tissue damage through all layers of the leaf, similar to *Cercospora* leaf spot symptoms.

It has been shown in several studies that light undergoes scattering, inside the leaf. This is caused by organelles and intercellular air spaces (Vogelmann 1989). This diffuse scattering of the light inside the leaf tissue is beneficial for the plant as light reaching the leaf surface is often reflected back into the leaf, providing increased light for the photosynthesis (Brakke 1994). Light from healthy areas next to small symptoms, which are present at the epidermis layer only, are thereby scattered diffusely while being transmitted through the cell layers of the leaf after passing the symptomatic cell layer. This could provide an explanation for the reduced efficiency of transmission measurement for the detection of biotroph pathogens. In the case of symptoms that develop in all cell layers of the leaves, such as necrotic lesions, the effect of scattered light would not be noticeable. When light is being scattered into the symptomatic area the spectral profile of the light would be affected through the symptomatic tissue. Based on the present results and discussion, transmission measurement is more advantageous for detection of necrotic pathogens, which affect all cell layers of a symptomatic area.

### Early powdery mildew detection through hyperspectral imaging

Minor changes of reflectance mean values over the course of powdery mildew development (Fig. 3.4) emphasise the importance of imaging measurement over non-imaging area measurement. Especially for pathogens with small, discrete symptoms, detection through imaging methods is more accurate compared with

non-imaging sensors. In this case the signal consists to a certain amount of healthy tissue (Mahlein *et al.* 2012). With the use of PCA as data analysis method it was possible to detect powdery mildew infection at a stage where the symptom size is similar to the spatial resolution of the sensor (Fig. 3.7). Powdery mildew symptoms could be identified through false colour pictures of values of the first PC, already at 4 dai, this is 2 days before symptoms became visible on the RGB pictures. This is in accordance with results reported by Kuska *et al.* (2015) who showed that it is possible to use microscopic hyperspectral imaging to detect powdery mildew before the appearance of visible symptoms. The results of the present study show that this can also be achieved on the leaf scale in combination with advanced data analysis.

**Hyperspectral data management and analysis**

The large amount of available data for each pixel of a hyperspectral image makes manual analysis only efficient on small samples of the data. Thus efficient data analysis methods are required (Bauckhage and Kersting 2013; Behmann *et al.* 2015a; Singh *et al.* 2016). Earlier studies have shown that the use of disease-specific indices is suitable (Mahlein *et al.* 2013); however, as indices are based on only few wavebands, relevant information from the hyperspectral image might be neglected. In order to utilise all available information within a dataset, data mining approaches are preferable (Wahabzada *et al.* 2015a; Wahabzada *et al.* 2016).

A first investigation of mean values and standard deviations provides an easy to interpret estimation of the dataset. However, with the use of mean values the advantages of imaging spectroscopy are not applicable. Pathogen-induced stresses usually manifest as small areas around the initial sides of pathogen infestation on the leaves. Therefore the applied data analysis method needs to emphasise the differences between the symptom specific spectral profile and the spectral profile specific for the healthy plant. Principal component analysis, is an excellent method for detecting the variance in a given dataset (Wold *et al.* 1987). It further has the advantage that it is able to work over large datasets with reasonable efficiency. Previous studies have already proven PCA to be an efficient tool for evaluating hyperspectral datasets (Rascher *et al.* 2007; Suzuki *et al.* 2008; Bauriegel *et al.* 2011b; Behmann *et al.* 2015a) as it extracts relevant components of the large amount of present hyperspectral data (Hamid Muhammed and Larsolle 2003; Rascher *et al.* 2007). Besides PCA there are multiple other methods available, which are based on sophisticated machine learning methods (Behmann *et al.* 2015a). For application in plant phenotyping and early disease detection machine learning methods are especially interesting, as it is possible to train the method on a set of training data. This training can happen both unsupervised or supervised by a researcher and allows to analyse plant response to biotic or abiotic stress (Behmann *et al.* 2015a). This aspect, and a further analysis of the reflectance and transmittance dataset of barley will be the subject of future research.

The present study shows that PCA permits early disease detection and has

potential to be performed semi-automated, but there is still a problem in that the derived PCs are difficult to interpret. Nevertheless, a more comprehensive view on plant physiology during pathogenesis could be approached by combining information from different kind of sensors (Berdugo *et al.* 2014). As mentioned recently by Sankaran *et al.* (2012), the accuracy and sensitivity depend strongly on type of data and their quality. For future experiments more advanced data analysis methods, such as simplex volume maximisation (SIVM) should be considered (Thurau *et al.* 2012). SIVM represents the data as only few extreme data points facilitating the interpretability and further processing. In this context, SIVM has shown to work well for the analysis of barley plants under biotic (Wahabzada *et al.* 2015a) and abiotic stresses (Kersting *et al.* 2012a; Römer *et al.* 2012).

**Hyperspectral imaging as phenotyping tool**

Hyperspectral imaging can be used to non-invasively access a multitude of physiologic and structural changes in plants (Fiorani *et al.* 2012). One interesting trait for phenotyping is pathogen resistance (Furbank and Tester 2011; Mahlein 2016). Recent studies have shown that resistance reactions can be monitored with hyperspectral reflectance imaging under a sufficiently high spatial resolution (Kuska *et al.* 2015; Leucker *et al.* 2016a, 2016b).

The results of the present study indicate there is considerable potential for screening different plant genotypes for pathogen resistance. Through the reflection based time series measurements powdery mildew symptoms could be detected in early stages. It was possible to evaluate the disease severity per infested leaf over the course of the experiment. The PCA based estimation of disease severity was then compared in a different experiment with the measurement of powdery mildew DNA in infected leaves. Despite the differences in total amount of powdery mildew detected based on leaf material, the two methods showed a high level of correlation. As both measurement methods are not expected to be 100% accurate the correlation of over 0.72 indicates the possible uses of PCA based disease severity estimation for disease severity. This method has the advantage of being non-destructive and objective compared with the more commonly-used techniques of molecular based analysis and manual rating. PCA is an unsupervised method for data analysis, so improves the throughput of a possible screening process. With automatic hyperspectral measuring platforms for greenhouse and field applications and in combination with easier to interpret, unsupervised data analyses, non-invasive and objective screening for different pathogen susceptibility could be achieved in high throughput (Mahlein 2016).

### 3.1.6 Conclusion

Reflection and transmission based imaging spectroscopy clearly yield complementary data. Reflectance data clearly outperforms the transmission based early detection of the biotrophic pathogen *Bgh*. In contrast, transmission based

data give additional and complementary data also from the plant–pathogen interaction in deeper cell layers. Thus, this study shows there is potential to use transmission measurement as a tool for a comprehensive view on plant physiology during pathogenesis, which will support future phenotyping processes.

## 3.2 Net blotch and brown rust development on inoculated barley leaves

**A research article based on the results of Chapter 3.2 has been submitted for publication:**

**Thomas S**[1], Behmann J[2], Rascher U[3], Mahlein A-K[4] (submitted at 16.04.2021) Evaluation of the benefits of combined reflection and transmission hyperspectral imaging data through disease detection and quantification in plant-pathogen interactions. *Plant Disease and Protection.*

[1]Institute of Phytomedicine, University of Hohenheim, Stuttgart, Germany
[2]INRES-Phytomedizin, University Bonn, Bonn, Germany
[3]IBG2: Plant Sciences, Forschungszentrum Jülich GMBH, Jülich, Germany
[4]Institute of Sugar Beet Research (IfZ), Göttingen, Germany

### Authors contribution

Stefan Thomas, Anne-Katrin Mahlein, and Uwe Rascher designed the study and drafted the manuscript. Stefan Thomas, Jan Behmann, Anne-Katrin Mahlein, and Uwe Rascher interpreted the experiments. Stefan Thomas performed the experiments within the study and carried out manual and statistical analysis. Stefan Thomas and Jan Behmann performed semi-automated preprocessing of the gathered datasets for automated analysis. Stefan Thomas performed the methods for automated hyperspectral data analysis.

### 3.2.1 Abstract

While reflection based measurements of plant-pathogen interactions with hyperspectral imaging sensors are already covered in multiple scientific studies there are only a few studies available which examine the possibilities of transmission based measurements, despite the advantage of transmitted light having passed through every cell layer of the measured plant tissue.

Previous studies which investigated the performance of transmission imaging data compared with reflection based data for disease detection showed inconsistent results. Thomas *et al.* (2017) found that transmittance based imaging performed poorly at powdery mildew symptom detection at barley leaves, while Bergsträsser *et al.* (2015) showed that transmittance based imaging performed similar to reflectance based imaging for the detection of *Cercospora* leaf spot symptoms. In the current study the hypothesis that the disparity between the results of Bergsträsser *et al.* (2015) and Thomas *et al.* (2017) might be correlated with the different interactions of the respective pathogens with the host plants and the way light interacts with plant tissue while passing through it is explored. Two additional pathogens – *Pyrenophora teres* f. *teres* and *Puccinia hordei*, the causative agent of net blotch and brown rust in barley respectively – have been investigated with focus on detection and quantification of symptoms upon barley leaves. The resulting datasets of hyperspectral imaging time-series measurements of barley leaves inoculated with the respective pathogens were analysed in dept through application of multiple data analysis methods (support vector machines; principal component analysis with following distance classifier; spectral decomposition) in order to compare the performance of reflectance and transmittance datasets, as well as the different data analysis methods, for the detection of disease symptoms.

The results of this study allow new insights into the nature of transmission based hyperspectral imaging and its application range. The transmittance datasets of time-series for both diseases in this study outperform the transmittance based powdery mildew detection in Thomas *et al.* (2017), while showing similar results to Bergsträsser *et al.* (2015) – which investigated *Cercospora* leaf spot disease. From these findings it can be concluded that transmittance images are more suited to the detection of plant-pathogen interactions within the deeper cell layers of the plant, while being outperformed by reflectance images when it comes to early disease detection or the detection of pathogens which interact mainly with the epidermis layer of the host plant. The performance differences between the different data analysis methods for the specific diseases in reflection and transmission images indicate that the selection of the most suited data analysis method for specific tasks is important to obtain optimal results.

### 3.2.2 Introduction

Thomas *et al.* (2017) performed a measurement of combined reflection and transmission with focus on plant-pathogen interaction with hyperspectral imag-

ing sensors. The authors investigated barley leaves, which were inoculated with conidia of *Blumeria graminis* f. sp. *hordei*, the causative agent of powdery mildew, with the HyperArt measurement setup (Bergsträsser *et al.* 2015) for simultaneous measurement of reflection and transmission. The results of the study showed, that it is possible to detect powdery mildew infection of barley leaves on leaf level two days before symptoms are visible on RGB images through automatically analysed reflection based hyperspectral data. Furthermore, it could be shown, that the combination of reflection and transmission data was advantageous to distinguish late powdery mildew symptom and spontaneous necrosis of resistant barley leaves. However, the results of the study did show that transmission based detection of powdery mildew symptoms was not possible before symptoms on the leaves were already visible for two days with reflection based RGB imagery. These results stood in contrast to the study of Bergsträsser *et al.* (2015), which performed single measurements of visible symptoms of *Cercospora beticola* infection on sugar beet leaves. Within the study of Bergsträsser *et al.* it was shown, that reflection and transmission based data performed equally for the detection of disease symptoms. Thomas *et al.* (2017) theorised, that this could be explained based on the different interaction of the two pathogens with the plant tissue. While powdery mildew symptoms develop as small pustules on the leaf surface with the fungi only penetrating the epidermis cells of the plant (Bhat *et al.* 2005; Dean *et al.* 2012), *Cercospora* leaf spot symptoms appear as necrotic lesions on the leaves once the fungi switches to its necrotic phase after penetrating the leaf tissue through the stomata and spreading intercellularly (Steinkamp *et al.* 1979; Rangel *et al.* 2020). In this article further studies into the matter and principle of transmission measurement via optical sensors are presented in order to confirm the theory of Thomas *et al.* (2017).

Light interacts with plant leaves in a complex matter. Upon reaching the plant surface (cuticula and epidermis) a significant portion of the light is directly reflected and can be measured, providing information about the plant surface it interacted with (Fig. 3.9). The portion of the light which is neither reflected or absorbed by the plants surface enters the plant tissue, where it is scattered diffusely as it interacts with organelles and intercellular air spaces (Vogelmann *et al.* 1989). During the passing of the plant tissue a small amount of light is reflected back to the upper surface, the majority of light travels through the plants mesophyll layer and the lower epidermis of the leaf. Upon reaching the surface-air border the majority of the diffusely scattered light is reflected back into the plant, with only a small portion is being transmitted through the leaf as it arrives at the surface-air border in the right angle (Fig. 3.9; Brakke *et al.* 2004). The light, which was reflected is scattered diffusely once more as it travels back through the plant tissue layers up to the surface-air border of the upper epidermis, where a small portion is being transmitted and measured together with the surface reflection by reflection based imaging methods, while the larger portion of the light is reflected back into the leaf tissue again (Fig. 3.9). This complex process allows the plant to maximize the usage of incoming light for photosynthesis (Brake *et al.* 2004). These processes provide the reason why it is possible to detect metabolic changes in plants with reflection

based measurement. The Study of Nansen (2018) did also show that hyperspectral measurements have a significant penetration of measured objects. Their study showed that different backgrounds can have significant influence on leaf measurements – especially with multiple layers of leaves being measured.

These factors have to be kept in mind when performing transmission based hyperspectral measurements of pathogens. Due to the diffuse scattering of light inside the leaf and the light passing the leaf multiple times it can be challenging to detect pathogens, which interact mostly with the leaf surface. As demonstrated in figure 3.10, incoming light which interacts with pathogen structures at the plant surface (or the epidermis) can be readily detected due to the direct reflection of light at the structures surface – combined with internal reflection – through reflection based approaches. As the light becomes diffusely scattered while passing the plant tissue it mixes with light scattered from nearby entry points and by the time the light is detected as transmission after exiting the leaf a combined signal of light, which interacted with the pathogen on the plant surface, and light, which did interact solely with health plant tissue, is measured (Fig. 3.10). Thereby, the physical basics of the way plant tissue interacts with incoming light explain why it requires a larger area of pathogen structures covered surface to be detected in transmission based approaches versus reflection based approaches. Consequently, pathogen symptoms interacting with deeper tissue layers of plant leaves, causing necrosis, changes in plant pigmentation, or plant metabolism should be detected through transmission measurements with an increased performance as internal light scattering has a reduced effect on such occurrences.

This study aims to provide insight into the matter through practical experiments. The data of Thomas *et al.* (2017) show the results for tissue with powdery mildew infection, acting on the plant surface and within epidermis cells (Fig. 3.11a). In the current study additional measurements of barley leaves with the HyperArt setup have been performed while selecting pathogens, which interact with deeper layers of the plant tissue, under similar conditions and as time-series.

*P. hordei*, the causative agent of brown rust, is a biotrophic pathogen, which enters infected barley leaves through the stomata (Fig. 3.11b; Voegele 2006). Once inside the plant mesophyll the fungi grows, forming intercellular haustoria to feed upon the plant before finally forming colonies, which break through the epidermis to release new spores (Fig. 3.11b; Voegele 2006).

*Pyrenophora teres* f. *teres* (anamorph: *Drechslera teres*), the causative agent of net blotch, is a necrotrophic pathogen. It penetrates directly through the cuticula, cell wall and cell membrane of the host plants epidermis cells, were it forms a primary and secondary intracellular vesicle (Fig. 3.11c; Liu *et al.* 2011). When the secondary vesicle is formed, the host epidermis cell – as well as nearby epidermis cells – are functionally disrupted. A hypha forms intracellular from the secondary vesicle and breaks into the intercellular space of the mesophyll, where it secretes toxins/effectors which lead to the disruption of nearby mesophyll cells to provide the necrotrophic fungi with nutrients (Fig. 3.11c; Liu *et al.* 2011).

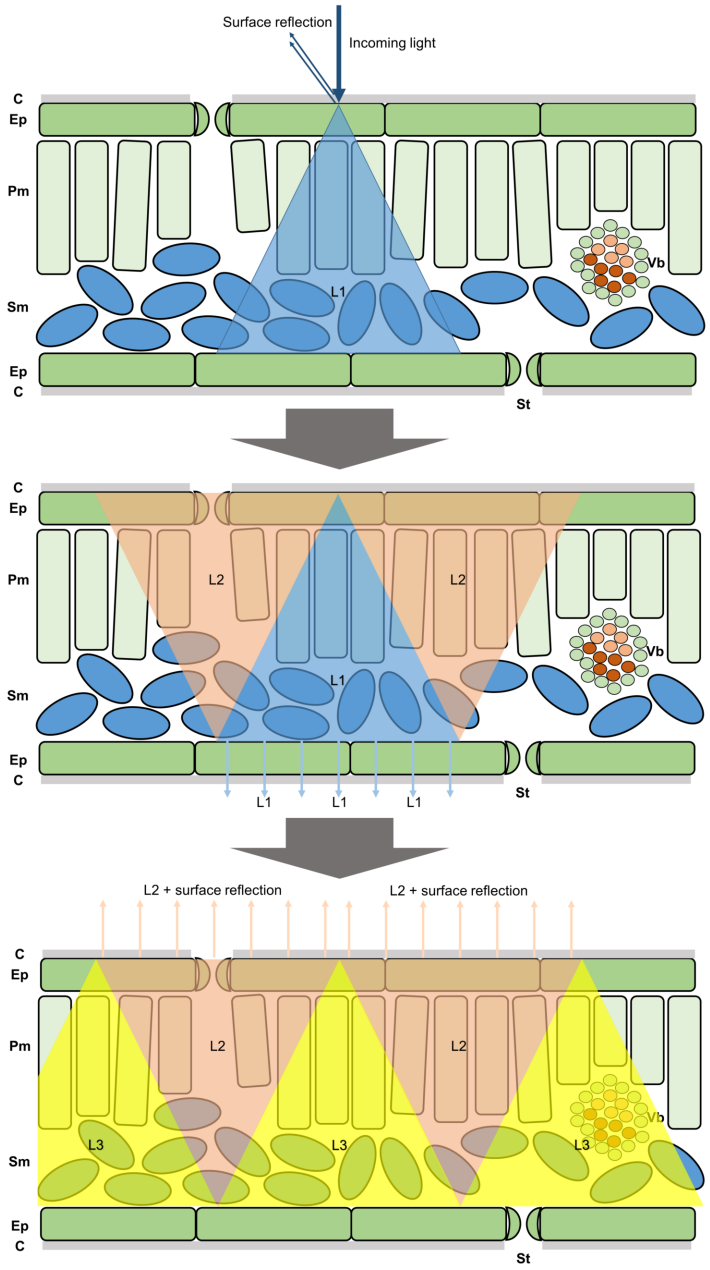


Figure 3.9: Pathway of light when interacting with a plant leaf. Upon reaching the plant's surface a portion of the light is reflected back from the cuticula (C) and epidermis (Ep), while the rest of the light enters the plant tissue in a diffusely scattered manner (L1, blue cone). The light crosses both palisade- (Pm) and spongy mesophyll (Sm) - being partially absorbed and scattered back to the leaf surface as indirect reflection - before reaching the epidermis and cuticula un the bottom of the leaf. Here a portion of the light is transmitted, thereby exiting the leaf as transmitted light (L1, blue arrows), while the rest is being reflected at the leaf surface-air border and traverses the mesophyll tissue again while being diffusely scattered (L2, orange cones). Upon reaching the epidermis and cuticula of the top of the leaf a portion of L2 is transmitted as indirect reflection and would be measured with the light coming from the surface reflection, while the rest is reflected from the leaf surface-air border to continue its path through the leaf (L3, yellow cones). St = stomata, Vb = vascular bundle.

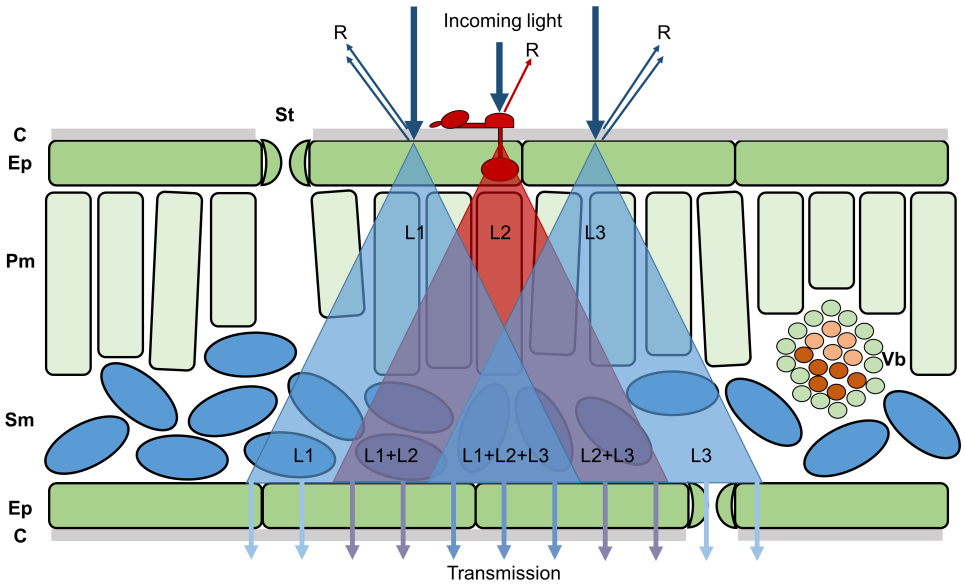


Figure 3.10: Influence of diffuse light scattering inside plant leaf tissue for transmission based measurement of pathogens which interact with the leaf surface and epidermis (Ep). Incoming light is colliding with the cuticula (C) and epidermis of the leaf, where a portion of the light is being directly reflected (R). This leads to a direct interaction of the reflected light with pathogens that grow on the leaf surface, resulting in a significant influence on the reflected lights wavelength. However, the portion of the light which is being transmitted through the leaf is being diffusely scattered (L1, L2, L3). This leads to a significant overlap of light, which did not come in contact with the pathogen, when exciting the leaf tissue as transmitted light (L1+L2+L3). Pm = palisade mesophyll, Sm = spongy mesophyll, St = stomata, Vb = vascular bundle.

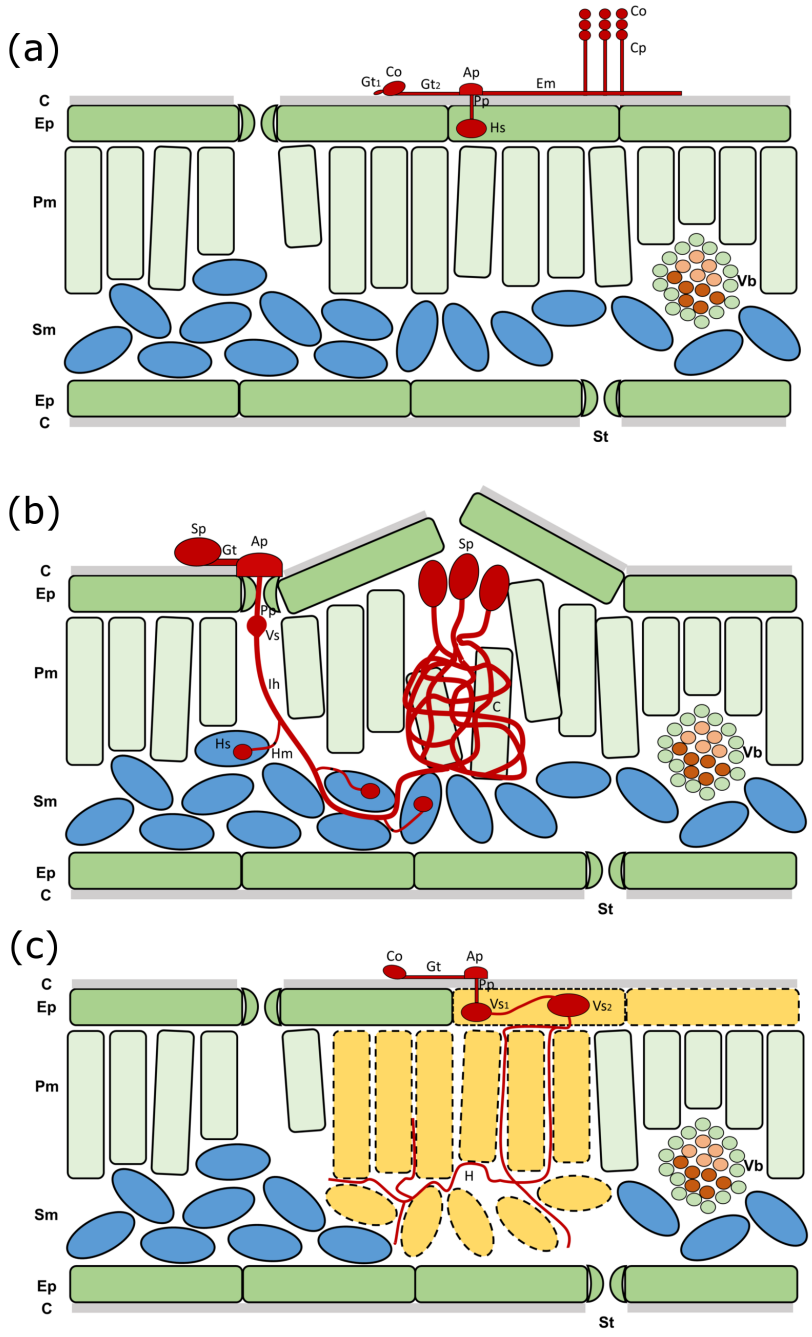


Figure 3.11: Interactions of the pathogens *Blumeria graminis* f. sp. *hordei* (a), *Puccinia hordei* (b) and *Pyrenophora teres* f. *teres* (c) with barley leaves. C = cuticula, Ep = epidermis, Pm = palisade mesophyll, Sm = spongy mesophyll, St = stomata, Vb = vascular bundle, Co = conidia, Gt = germination tube, Ap = appressorium, Pp = penetration peg, Hs = haustorium, Em = epiphytic mycelia, Cp = conidiophores, Sp = Spore, Vs = vesicle, Ih = infection hypha, Hm = haustorial mother cell, C = colony, H = hyphae.

The two pathogens interact in a different way compared to *B. graminis* f. sp. *hordei*. The development of *P. hordei* is relatively subtle at first – before the plant tissue gets disrupted through the fungi breaking through the epidermis. Its growth within the mesophyll should allow for increased detection with transmission based imaging, due to a reduced effect of the light scattering at pathogenic structures deeper within the leaf tissue. *P. teres* f. *teres* finally causes rapid cell death, which should result in similar results as the measurement of spontaneous necrosis in the study of Thomas *et al.* (2017) and should be comparable with the characteristic necrotic lesions in the center of *C. beticola* symptoms, which were investigated by Bergsträsser *et al.* (2015).

The gathered datasets of reflection- and transmission-based leaf images with developing net blotch and brown rust symptoms respectively were analysed with three different data analysis algorithms – Support Vector Machines (SVM, Cortes and Vapnik 1995), Spectral Decomposition (SD, Keshava and Mustard 2002) and a combination of principal component analysis (PCA) with following Distance Classifier (DC, Mahalanobis *et al.* 1996). The SVM represents a supervised approach of data analysis, in which a set of generated training data is used as basis for classification. The SD is an unsupervised method, which generates classes bases on distinct datapoints within the analyzed dataset. The combination of PCA and DC finally represents a mixed approach of reducing data dimensionality with the unsupervised PCA and sorting the resulting correlation of pixels with the principal components into pre-generated classes with the supervised DC. This approach should allow for a comparison of data analysis methods with each other, as well as with disease severity estimation through manual rating (MR).

### 3.2.3 Material and Methods

#### Plant cultivation and pathogen material

*Hordeum vulgare* L. cv. Ingrid wild type (Hinze *et al.* 1991) plants were grown in TEKU VQB 7x7x8 cm pots (Pöppelmann, Lohne, Germany) and filled with commercial substrate (Klasmann-Deilmann GmbH, Geeste, Germany) inside a climate chamber at 20/20 °C (day/night) 60% relative humidity (RH) and day light period of 16 h. At growth stage 12 according to BBCH scale (Hack *et al.* 1992) the plants were inoculated with the respective pathogens and placed in high humidity environment (>90%) and indirect lighting conditions for two days to maximize chance of infection before the second leaf of each plant was fixed within a custom plastic frame. 12 plants were used as healthy control, being inoculated with water, 12 plants were inoculated with a spore suspension (60000 spores/ml) of *P. hordei* (stored field isolate from the area near Bonn) and 12 plants were inoculated with a spore suspension (5000 spores/ml) of *P. teres* f. *teres* from gathered leaves around the area of Bonn. Of the 12 plants which were inoculated with *P. teres* f. *teres* spores six plants had parts of highly infected leaves placed upon their leaves in order to increase the chance of infection. The inoculations were performed by spraying the spore suspensions equally over the

to be inoculated plant leaves.

### Hyperspectral imaging measurement

The HyperArt system was used to measure reflection and transmission of the plants simoultanously during the experiment (Bergsträsser *et al.* 2015; Thomas *et al.* 2017; Patent nr: DE102012005477). The system was modified according to Thomas *et al.* (2017). All leaves were measured in the visible and near infrared areas of the electromagnetic spectrum ($400 - 1050$ nm) in a daily time-series measurement from 3 days after inoculation (dai) to 9 dai. Measurements at earlier times were not possible, due to the requirement of the fungi to have high humility for infection of barley leaves. For each measurement a 99% reflectance white standard (Spectralon, Labsphere Inc., North Dutton, NH, USA) and a white diffuser lambertian transmission foil (Zenith Polymer® $\approx$ 50% transmission, SphereOptics GmbH, Uhldingen, Germany) was acquired, before measuring the leaf sample. These measurements served as white references for reflection and transmission images for the image normalization (Bergsträsser *et al.* 2015). Wavelength dependent differences in the percentage of the reflected and transmitted light of the two white references were taken into consideration during the normalization process. With each measurement a dark current image of the internal camera noise was measured by closing an internal camera shutter.

### Data analysis

The reflectance and transmittance of the images was calculated by normalising the acquired images over the according white references, serving as standards with known reflection/transmission values, with ENVI 5.1 + IDL 8.3 (ITT Visual Information Solutions, Boulder, CO, USA). The normalized images were smoothened through the application of the Savitzky-Golay filter (Salitzky and Golay 1964) to eliminate noise within the hyperspectral datasets for further analysis. Background masking and separating the hyperspectral images to single leaves was performed through an automated algorithm, were the transmission images required manual extraction due to their spectral properties being indistinguishable at places were parts of the frame were covering the plants in order to hold them in place. Due to significant noise within the data at the extremes of the sensor range the analyzed spectral range was reduced to $450 - 1000$ nm.

In order to prepare the dataset for analysis of its variance with principal component analysis (PCA) all spectral signatures were normalized into the unit Euclidian norm to eliminate the influence of non-biologic variance to the measurement. Thereby the signatures/vectors are treated as points on a high dimensional unit sphere (Dhillon and Modha 2001; Leucker *et al.* 2016b), capturing the vectors direction while reducing the variance in the dataset. After these preparations the PCA was performed. PCA is a statistical method which introduced a new axis along the greatest variance into the dataset, thereby trans-

forming it based onto the variance and reducing the data complexity (Wold *et al.* 1987). The PCAs were performed over the healthy control leaves and the respective inoculated leaves within the dataset, including both reflection and transmission-based images. A supervised classification in order to determine disease symptoms on the leaves was performed through the application of the Distance classifier algorithm on the results of the PCA. The DC uses a set of training data in order to classify every pixel of the image based on its distance in the Euclidian space from known classes.

An independent analysis of the data was performed by applying a non-linear support vector machines algorithm on the normalized dataset, which was used for the PCA with following DC. The applied SVM used radial basis function as kernel function to determine linear discriminant functions.

The DC and SVM were both trained with a set of labelled training data, which was generated by an expert, using control- and inoculated leaf images of healthy and inoculated leaves at 7 dai from rust and net blotch datasets in order to classify both early and late stages of disease symptoms. The manually annotated data was ordered into classes and used as reference within the above classifications.

Finally, unsupervised spectral decomposition – based on the mixed pixel approach – was used in order to analyze the datasets. Spectral decomposition factorizes the matrix, which is made up of the to be analyzed hyperspectral dataset, into a canonical form, representing it in terms of its eigenvalues and eigenvectors. This algorithm was applied unsupervised, with the program selecting mixed pixels of the image in order to determine the eigenvalues. The abundance of these eigenvalues within the dataset was then calculated to give out both an abundance map with abundance per pixel, as well as a classification of the image over the generated classes.

All data analysis was performed with the FluxTrainerPro 2.6.2.0 Software (LuxFlux, Reutlingen, Germany).

Leaves were manually rated by an expert at the end of the experiment 9 dai. The manual rating was performed with a Pseudo RGB image as basis with the goal to label healthy and infected leaf tissue. Unlike the generated training data, each pixel of the images was sorted into the classes healthy and symptom during this rating in order to compare disease severity visible by eye with the results of the different data analysis methods. Pixels that showed clearly identifiable disease Symptoms with the bare eye were labelled as Symptom, while other pixels were labelled as healthy.

The results of the manual rating were used as ground truth for post classification of the data through confusion matrices of the classification results from the different data analysis methods on both reflection and transmission datasets. Confusion matrices were computed via a C++ program.

Table 4: Disease severity calculation of net blotch and brown rust inoculated leaves at 9 days after inoculation with different data analysis algorithms and comparison to manual rating.
DC = Distance Classifier, SVM = Support Vector Machines, SD = Spectral Decomposition, r = reflectance, t = transmittance.

| | Net blotch r. | Net blotch t. | Brown rust r. | Brown rust t. |
|---|---|---|---|---|
| Manual Rating | 0.72% | 0.69% | 15.25% | 5.04% |
| SVM | 1.04% | 1.05% | 35.92% | 11.72% |
| DC | 2.4% | 11.18% | 37.9% | 20.75% |
| SD | 1.12% | 0.98% | 27.35% | 13.98% |

### 3.2.4 Results

**Manual assessment of the gathered datasets**

The water-inoculated control plants did not show any development of disease symptoms of either net blotch or brown rust over the course of the experiment.

Of the plants which were inoculated with *P. teres* f. *teres* spores and infected leaf parts only the 6 plants which were treated with direct contact to infected leaf parts during inoculation developed net blotch symptoms, while the 6 plants treated with spore suspension showed no development of disease symptoms over the course of the experiment. First symptoms of the net blotch disease became visible at 5 dai both in reflection- and transmission-based images and slowly progressed until the last measurements were taken at 9 dai (Fig. 3.12). During this time the symptoms developed from the initially infected areas of the host plants leaves, which had direct contact with infected leaf parts during inoculation. Throughout the symptom development the net blotch symptoms proved to be equally visible in reflection and transmission images, showing similar leaf discoloration and symptom area (Fig. 3.12). During manual rating of the disease severity at 9 dai the reflection and transmission data were rated with 0.72 and 0.69 percent of the leaf area showing symptomatic tissue respectively (Table 4).

The plants which were inoculated with *P. hordei* (*Ph*) spore suspension developed without exception brown rust symptoms over the course of the experiment. First disease symptoms became visible at 5 dai in the reflection-based images and 6 dai in the transmission-based images – with the symptoms being easier to distinguish in the reflection-based data (Fig. 3.13). Symptoms developed over the entire leaf area, starting with discrete, small chlorotic spots at the initial infection sites. Typical yellow, chlorotic areas were forming on the leaves at 5 dai and growing, with brown spore colonies breaking through the epidermis and becoming visible from 7 dai until the end of the experiment – this process could be clearly observed in the reflection-based images (Fig. 3.13). Meanwhile, in the transmission-based images this process could only be observed as a slight darkening of the symptomatic leaf areas, which became visible at 6 dai, and the development of brown spots in the middle of the described darkened areas,

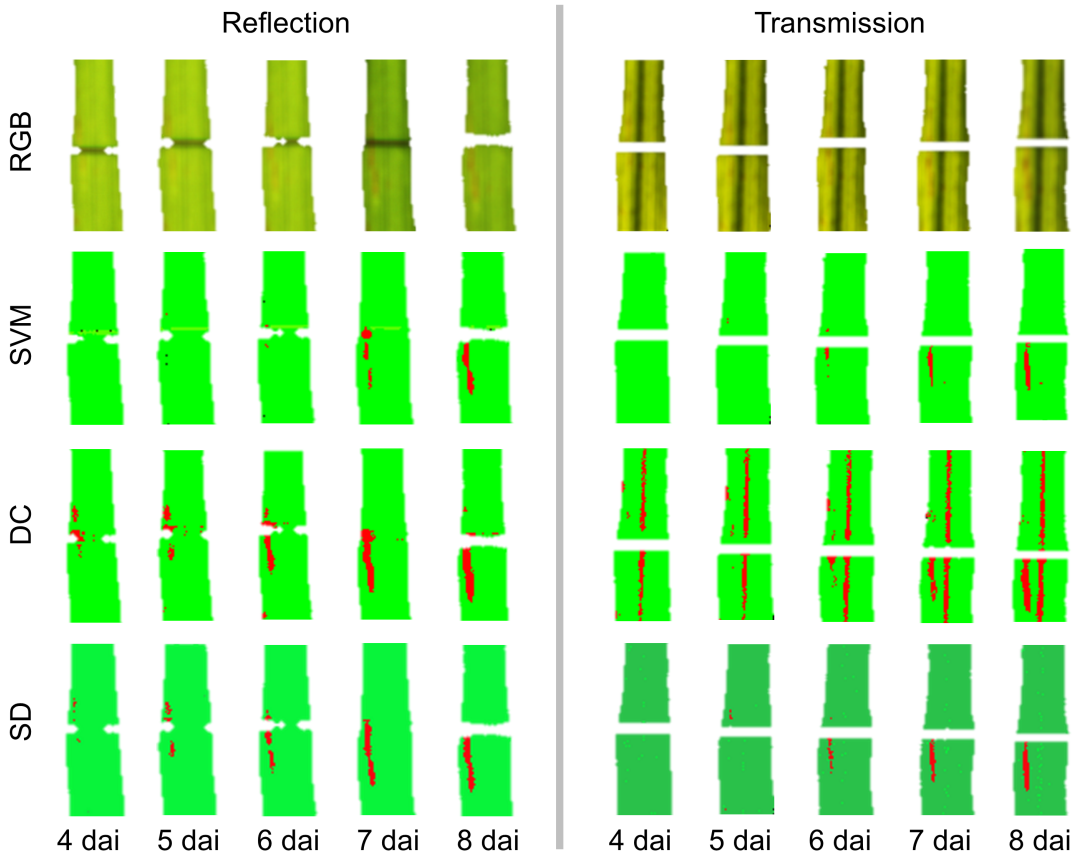


Figure 3.12: Reflection and transmission images of an Ingrid wild type leaf, inoculated with *Pyrenophora teres* f. *teres* over the course of the experiment. The Pseudo RGB images are compared with false colour images, representing the classes healthy (green colours) symptom (red) and artefact (black) of the respective data analysis methods. RGB = Pseudo RGB, SVM = Support Vector Machines, DC = Distance Classifier, SD = Spectral Decomposition.

starting at 7 dai (Fig. 3.13). During manual rating of disease severity – based on reflection and transmission datasets – 15.25 and 5.04 percent of the leaf tissue was rated as symptomatic tissue respectively (Table 4).

**Analysis of the respective reflection- and transmission-based data through three distinctive data analysis methods**

The datasets for the investigated pathogens – for both reflectance and transmittance data – were analysed with the three distinct data analysis methods (SVM, DC, SD) described above.

The leaf images of the control plants were classified as healthy tissue for both reflectance and transmittance with the exception of $<0.1\%$ of the pixels, which were classified as disease symptoms for SVM and SD classification. The falsely classified pixels were located either at the edge of the leaves or in the areas were the frame was covering parts of the leaves during measurement (Fig. 3.14). Thereby, containing mixed information of the respective reflected/transmitted light of both the measured leaf and the black background/frame. The DC algorithm – based on the results of the previously performed PCA – performed noticeably worse, having overall the highest tendency to falsely classify pixels in the above-mentioned areas with up to 0.3% of pixels being falsely classified as symptoms. The DC classification also was unable to differentiate between symptoms and the leaf vein in the transmission-based images of the net blotch dataset, causing pixels of the leaf veins to be classified as disease symptom, increasing the falsely classified pixels up to 10% in this specific case (Fig. 3.14).

Both DC and SD algorithms were able to detect net blotch symptoms within the reflectance images of the *Dt* inoculated leaves at 4 dai – one day before the symptoms were visible with the human eye – and able to track the development of the symptoms during the following measurement days, whereby the DC did show a clearer detection of early symptoms but was also more prone to misclassify pixels containing healthy tissue as symptoms (Fig. 3.12). For transmission-based images the algorithms were able to detect first net blotch symptoms at 5 dai, showing a slightly reduced performance in early disease detection compared to reflectance-based data (Fig. 3.12). The SVM based classification performed notably worse for early detection in reflection-based images. Despite using the same training data set as the DC first symptoms were only detected at 7 dai. Meanwhile, the transmittance images allowed a detection of the symptoms at 5 dai, performing similar to the other two algorithms (Fig. 3.12).

At 9 dai, the final measurement day for the experiment, net blotch symptoms could be classified by all three data analysis methods in both reflectance and transmittance images, correlating with the results of manual labelling of disease symptoms – both in disease severity (Table 4) and location of disease symptoms on the leaf (Fig. 3.14). A notable exception being the DC algorithm for the transmission-based image, as the above-mentioned classification error of the leaf vein persists, causing a disparity of about 10% in disease severity compared to manual rating results and other methods.

When looking in more detail at the classification of the specific pixels within

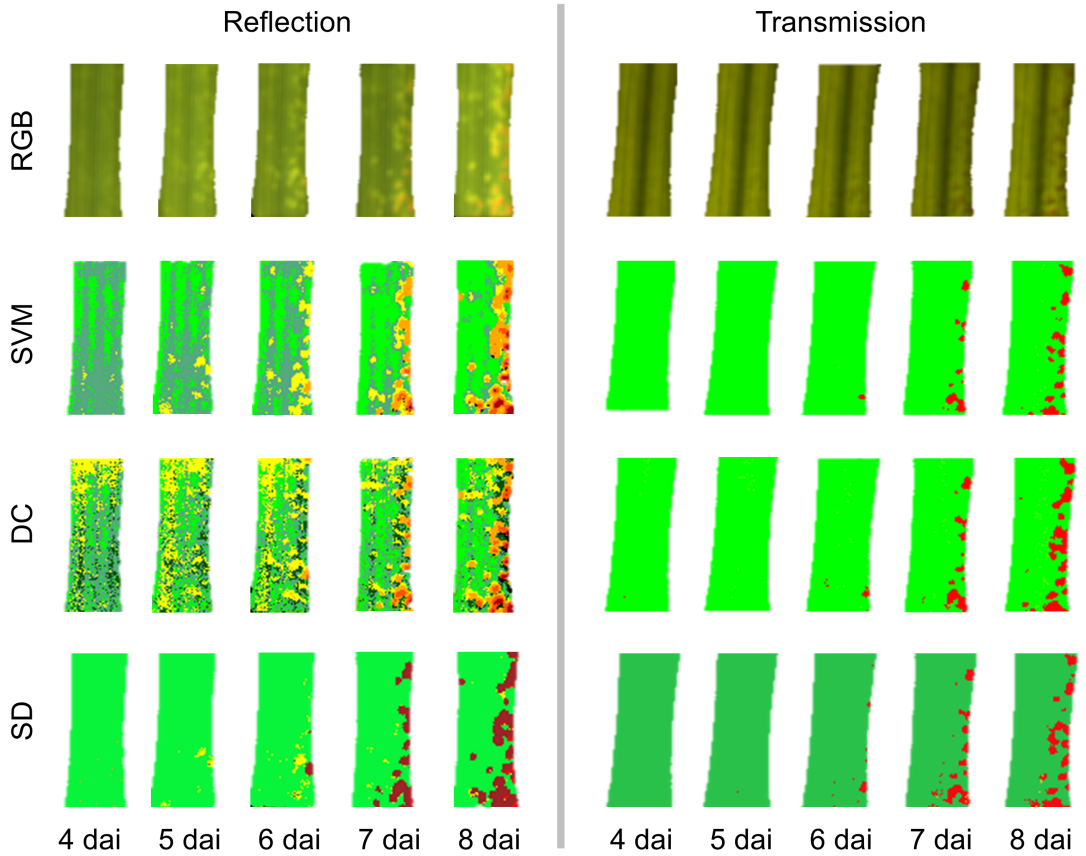


Figure 3.13: Reflection and transmission images of an Ingrid wild type leaf, inoculated with *Puccinia hordei* over the course of the experiment. The Pseudo RGB images are compared with false colour images, representing the classes healthy (green colours) and symptom (yellow and red colours) of the respective data analysis methods. RGB = Pseudo RGB, SVM = Support Vector Machines, DC = Distance Classifier, SD = Spectral Decomposition.

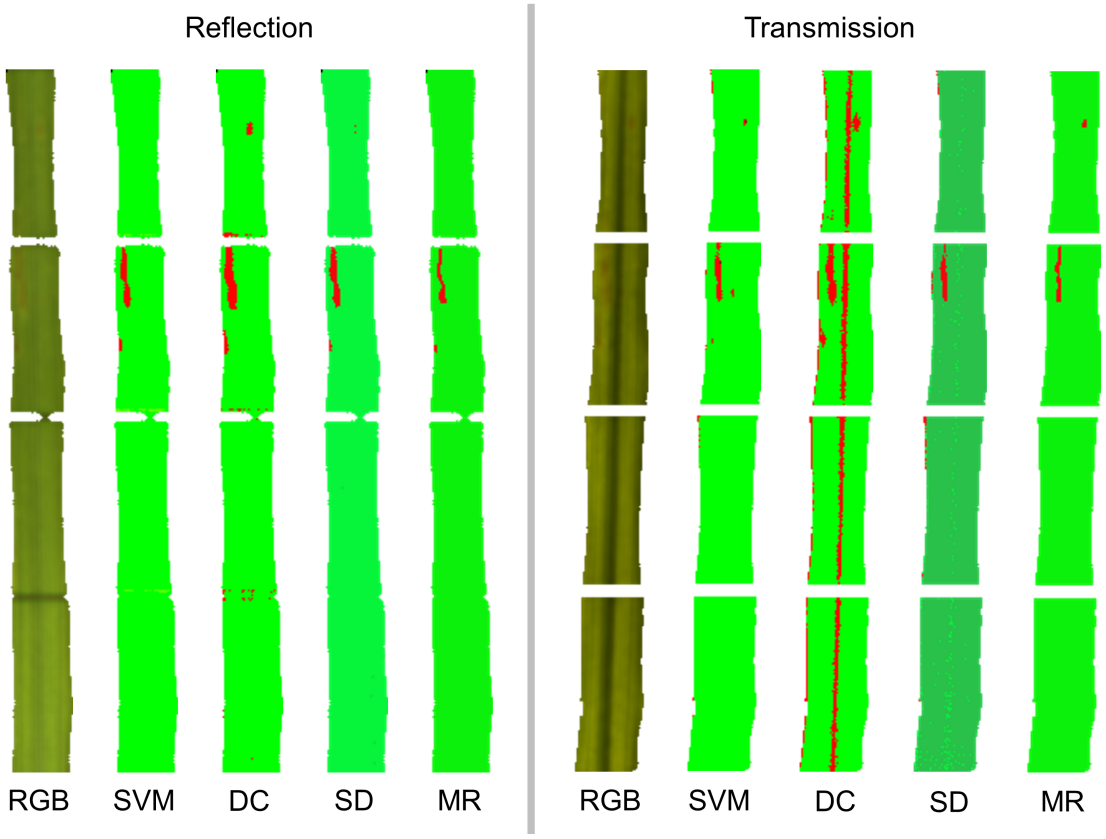


Figure 3.14: Reflection and transmission image of an Ingrid wild type leaf, inoculated with *Pyrenophora teres* f. *teres* at 9 days after inoculation. The Pseudo RGB images are compared with false colour images, representing the classes healthy (green colours), symptom (red) and artefact (black) of the respective data analysis methods, as well as with the results of manual rating of the image by an expert. RGB = Pseudo RGB, SVM = Support Vector Machines, DC = Distance Classifier, SD = Spectral Decomposition, MR = Manual Rating.

Table 5: Results of confusion matrix on images classified with manual rating compared to the applied data analysis methods for net blotch and brown rust infected leaves at 9 days after inoculation. DC = Distance Classifier, SVM = Support Vector Machines, SD = Spectral Decomposition.

| | | | Net blotch | | Brown rust | |
|---|---|---|---|---|---|---|
| | | | Manual rating | | Manual rating | |
| | | | Healthy | Symptom | Healthy | Symptom |
| Reflection | SVM | Healthy | 99.6% | 0.4% | 74.2% | 25.8% |
| | | Symptom | 10.4% | 89.6% | 3% | 97% |
| | DC | Healthy | 98.3% | 1.7% | 69.6% | 30.4% |
| | | Symptom | 0% | 100% | 13.7% | 86.3% |
| | SD | Healthy | 99.4% | 0.6% | 83.5% | 16.5% |
| | | Symptom | 15.5% | 84.5% | 11.7% | 88.3% |
| Transmission | SVM | Healthy | 99.5% | 0.5% | 92.2% | 7.8% |
| | | Symptom | 21.6% | 78.4% | 14% | 86% |
| | DC | Healthy | 89.4% | 10.6% | 84.1% | 15.9% |
| | | Symptom | 2.1% | 97.9% | 4.5% | 95.5% |
| | SD | Healthy | 99.5% | 0.5% | 90.2% | 9.8% |
| | | Symptom | 29.9% | 70.1% | 7.7% | 92.3% |

the images through the application of confusion matrices with the manual rating serving as the ground truth for the different classification results, it shows that all three algorithms have a high accuracy for the correct classification of healthy tissue and symptoms within the reflection data (89.6% for SVM and 84.5% for SD), with the DC algorithm outperforming the other two for disease detection (100%; Table 5). Within the transmission dataset the accuracy of all three algorithms is reduced (78.4% for SVM, 70.1% for SD and 97.9% for DC), with DC showing an uncharacteristically high error margin for misclassification of healthy tissue (10.6%) due to the misclassification of pixels showing the leaf vein as symptoms (Table 5).

Within the brown rust dataset, the SVM classified first pixels in reflectance images as disease symptoms at 4 dai, one day before the disease became visible with the human eye, and classifies symptomatic leaf areas correctly over the course of the experiment (Fig. 3.13). In the transmission-based images the SVM only detects disease symptoms at 6 dai. Due to high difficulties in differentiating early disease symptoms and healthy tissue it was however necessary to create multiple classes of healthy leaf tissue within the training data for both SVM and DC. This explains the early misclassification of pixels showing healthy leaf tissue as disease symptoms at 4 dai for the DC (Fig. 3.13). As shown in figure 3.13 the DC classification increases in accuracy over the course of the experiment, correlating significantly better with the results of the other data analysis methods at 8 and 9 dai. When applied to the transmittance images the DC does not have these issues, accurately detecting disease symptoms from 6 dai onwards like the SVM. The transmission-based dataset could be classified with

only a single class for healthy tissue, showing a more uniform spectral signature over the leaf area when compared with the reflectance dataset. Disease symptom detection with the SD classified first disease symptoms at 5 dai and 6 dai for reflectance and transmittance images respectively and shows accurate detection over the course of the experiment (Fig. 3.13).

Comparison of the classification results for all data analysis algorithms with manual rating at 9 dai shows significantly higher disease severity ratings for both reflectance and transmittance datasets (Table 4), while the spatial distribution of symptomatic pixels within the images matches for data analysis methods and manual rating (Fig. 3.15).

The post classification results of the respective confusion matrices show that the selected algorithms are able to accurately detect disease symptoms, which were labelled in the manual rating, in both reflection (97% for SVM, 86.3% for DC, 88.3% for SD) and transmission (86% for SVM, 95.5% for DC, 92.3% for SD) data (Table 5). The detection accuracy of the SVM for reflectance images being significantly higher than other algorithms. Both DC and SD have a higher accuracy for transmittance image symptom detection, while the accuracy of the SVM decreases when compared with the results of reflection data. All algorithms classified a high percentage of pixels which did not show clearly visible disease symptoms – and where thereby market as healthy tissue in the manual rating – as symptoms (25.8% for SVM, 30.4% for DC, 16.5% for SD) for the reflectance images, while the results of the transmittance images show a lower error margin (Table 5).

### 3.2.5 Discussion

The results of this study show differences within the efficiency of transmission-based measurement approaches, depending on the way pathogens interact with the host plant. Combined with the results of Thomas *et al.* (2017) this allows the estimation of cases in which the addition of transmission-based approaches would be beneficial for increased accuracy in disease detection.

#### Evaluation of transmission-based imaging data for disease detection

The theory postulated by Thomas *et al.* (2017) that light scattering within the leaf influences the disease detection through transmittance images and thereby the interactions of pathogens with the host plant play an important role in detection speed and accuracy is supported by the results of the current study.

It could be shown that net blotch symptoms are detected with no significant differences in disease severity at later stages. This was true for both manual rating of reflectance and transmittance images, as well as classification results with SVM and SD (Table 4). The combination of PCA and DC did classify a significantly higher number of pixels in the transmittance data as diseased, this can be explained due to the inability of the algorithm to discern pixels showing the leaf veins from pixels with disease symptoms (Table 5). Figure 3.16 shows, that the majority of pixels which were classified as showing symptoms in the

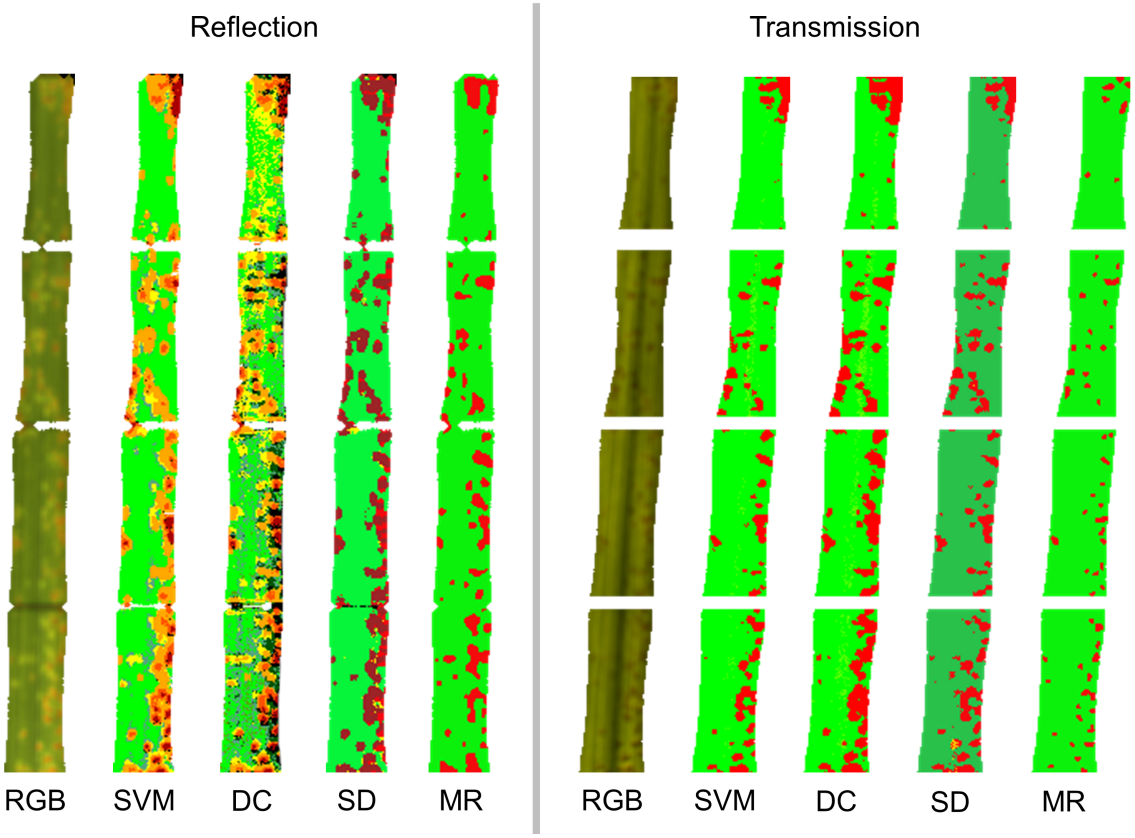


Figure 3.15: Reflection and transmission image of an Ingrid wild type leaf, inoculated with *Puccinia hordei* at 9 days after inoculation. The Pseudo RGB images are compared with false colour images, representing the classes healthy (green colours) and symptom (yellow and red colours) of the respective data analysis methods, as well as with the results of manual rating of the image by an expert. RGB = Pseudo RGB, SVM = Support Vector Machines, DC = Distance Classifier, SD = Spectral Decomposition, MR = Manual Rating.

transmission images of the DC results while being labelled as healthy in the MR align with the leaf vein placement on barley leaves. These results coincide with the findings of Bergsträsser *et al.* (2015), which investigated the advantages of combined reflectance and transmittance measurements for disease severity estimation on developed *Cercospora* leaf spot symptoms. Like the net blotch disease, which was investigated in this study, *Cercospora* leaf spot disease also causes necrotic lesions on infected sugar beet leaves (Mahlein *et al.* 2012, Leuker *et al.* 2016). The results of both studies also correlate with findings of Thomas *et al.* (2017) that transmission-based images allowed for precise detection of spontaneous necrosis on leaves.

In contrast the estimation of disease severity of brown rust on barley leaves within this study showed, that the estimates based on transmittance images were significantly lower compared to reflectance image-based estimates (Table 4). The algorithms did each classify a significant number of pixels, which could not be labelled as symptomatic during the MR, into the symptoms group for both reflectance and transmittance images (Table 5). The location of these pixels shows, that they are mostly located at the outer edges of areas which were labelled as symptoms through MR, hinting at the possibility to detect brown rust infection before visible symptoms appear at a given location (Fig. 3.17). Despite the success of the algorithms for disease detection it showed that the estimated disease severity in transmission based images was significantly lower than reflection based images, with MR and SVM showing the highest discrepancy of about 66% between the results – ~15% and ~35% disease severity for reflectance and ~5% and ~11% for transmittance respectively (Table 4). Visibility of brown rust symptoms with the human eye within the transmittance images was mostly limited to areas were spore colonies had formed and broken through the leaf epidermis, with chlorotic lesions from prior rust development being barely visible only once larger areas were infected. Nevertheless, the detection of brown rust symptoms was more accurate and could be earlier detected within transmission-based data then the powdery mildew symptoms in the study of Thomas *et al.* (2017), with all used algorithms being able to detect disease symptoms one day after they became visible within the reflectance images (Fig. 3.13) compared to two days for powdery mildew in the previous study (see Thomas *et al* 2017, figure 3.7). These findings support the theory that the more intrusive interaction of brown rust with the host plant (Fig. 3.11) – penetrating into deeper tissue layers of the leaf – results in an increased detection possibility through transmittance images.

**Early disease detection through transmission**

It has been shown by multiple studies that hyperspectral reflectance imaging sensors are able to detect disease symptoms before symptoms are visible with the human eye (Kuska *et al.* 2015, Thomas *et al.* 2017, Behman *et al.* 2018). So far this could not be shown for images based on transmission, as studies with time-series measurements that compare the performance of reflectance and transmittance hyperspectral images for early plant disease detection are, to the

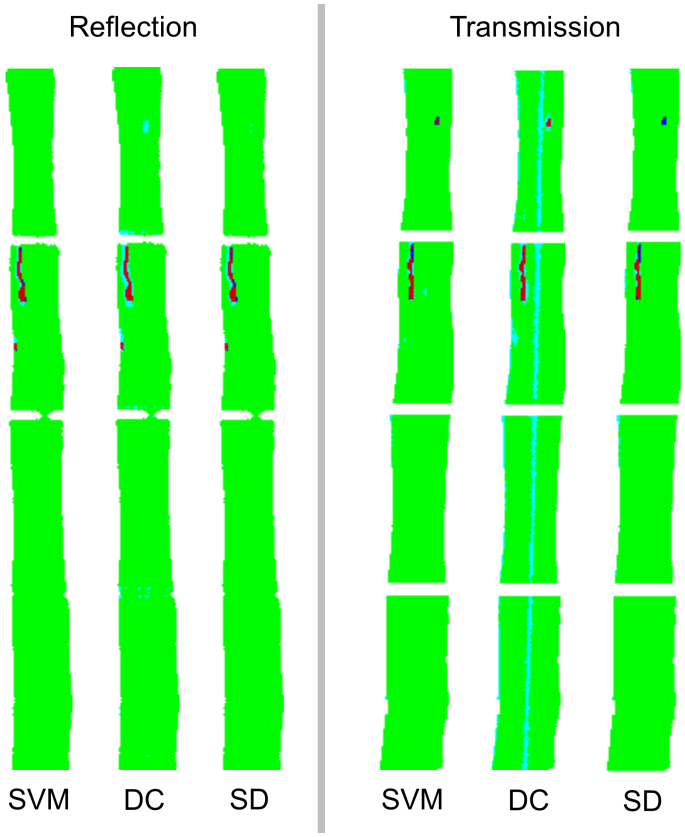


Figure 3.16: False colour visual representation of confusion matrix results on net blotch infected leaves at 9 days after inoculation for reflection and transmission images. The images show the comparison of the respective data analysis method classification outcome compared to manual rating. Green and red pixels representing healthy and symptom classification which showed no difference for manual rating and classification. Light blue coloured pixels represent pixels which were classified as symptoms in the data analysis and healthy in the manual rating. Dark blue coloured pixels respectively represent pixels that were labelled as symptoms in the manual rating and classified as healthy through the data analysis. SVM = Support Vector Machines, DC = Distance Classifier, SD = Spectral Decomposition.

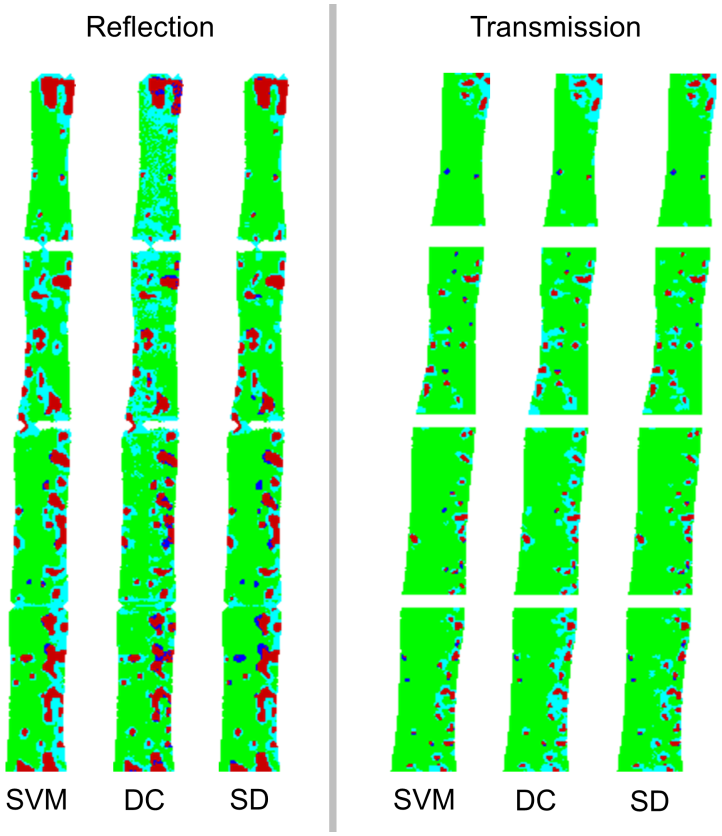


Figure 3.17: False colour visual representation of confusion matrix results on brown rust infected leaves at 9 days after inoculation for reflection and transmission images. The images show the comparison of the respective data analysis method classification outcome compared to manual rating. Green and red pixels representing healthy and symptom classification which showed no difference for manual rating and classification. Light blue coloured pixels represent pixels which were classified as symptoms in the data analysis and healthy in the manual rating. Dark blue coloured pixels respectively represent pixels that were labelled as symptoms in the manual rating and classified as healthy through the data analysis. SVM = Support Vector Machines, DC = Distance Classifier, SD = Spectral Decomposition.

knowledge of the authors, not available – besides Thomas *et al* (2017). Within the study of Thomas *et al.* (2017) powdery mildew infection could be detected based on transmittance images at 6 dai, two days after detection was possible through the reflectance images and at a point when the disease symptoms were already visible by eye in reflection-based RGB images.

In the current study both net blotch and brown rust symptoms in transmittance images could be detected one to two days after detection was possible in reflectance images for all applied data analysis methods – with the notable exception of net blotch symptom detection through SVM, which can be explained as the SVM failed to detect symptoms in the reflection-based dataset before 7 dai while the two other algorithms managed to detect at 4 dai. While this exception shows that under certain circumstances it is possible to achieve earlier disease symptom detection through transmission-based images it would be more suited to use an algorithm that performs better for the detection of net blotch symptoms as the symptoms were visible by eye at 5 dai.

From the results of these studies it can be concluded that transmission-based measurements are not well suited for early disease detection, even from highly invasive pathogens. A possible explanation would be that pathogens like net blotch spread from their entry point at the leaf surface (Fig. 3.10), which might cause changes within the plants spectral signature to be detected in reflectance images while the internal light scattering inside the leaves prevents detection of these early plant/pathogen interactions through transmission-based imaging (Fig. 3.11).

**Comparison of data analysis methods for disease detection and disease severity estimation within this study**

Three different data analysis methods have been used in this study and were compared to MR of the RGB images in order to verify the results of the experiments. In comparison with the MR every algorithm achieved a higher disease severity estimation for both net blotch (Fig. 3.14) and brown rust (Fig. 3.15) symptoms (Table 4). These results, while promising, are posing the question if the classifications of the different algorithms are correct, or misclassifying pixels showing healthy tissue as symptomatic. In order to clarify this issue, the results of each algorithm were investigated twofold. First the classification results of images early in the time-series were compared with pseudo RGB images from later stages for both net blotch (Fig. 3.12) and brown rust (Fig. 3.13) datasets. As the leaves were fixed during the entire timeframe of the measurements it was possible to compare the placement of pixels within different visibility stages. Furthermore, the results of the post classification through confusion matrices with the MR as ground truth were visualized for both net blotch (Fig. 3.16) and brown rust (Fig. 3.17) images at 9 dai. These visualizations show, that the vast majority of the pixels which were classified as showing symptoms through the data analysis are grouped around clusters of pixels that were labelled as symptomatic in the MR. It was expected that the different data analysis methods are able to classify pixels without symptoms being visible to the human

eye, as it is one of the main interests in analysing hyperspectral imaging data to detect disease symptoms before they are visible by the human eye in RGB images (Behman *et al.* 2018).

Among the data analysis methods, the combination of PCA and DC showed the highest estimations of disease severity, but is also the method that has been shown to be most prone to mistakenly classify healthy tissue as symptoms for net blotch (transmission, Fig. 3.16) and brown rust (reflection, Fig. 3.17). In these cases, the SVM was able to clearly differentiate between disease symptoms and healthy tissue, while being trained on the same set of training data. The SVM as a supervised method performed well for both early detection and disease severity estimation, with the notable exception of net blotch reflectance images (Fig. 3.12). The unsupervised SD performed well in all cases, being able to detect symptoms as early as the supervised methods – with the exception of brown rust reflectance, where the SVM was able to detect symptoms one day prior to other methods (Fig. 3.13) – and was overall the least prone to misclassification. SD has the added advantage, that the unsupervised algorithm does not require training data in order to function and did classify disease symptoms and healthy tissue while generating fewer classes then the supervised methods required. However, the SD had in all cases the lowest disease severity estimates when compared with other algorithms, but still outperformed MR (Table 4).

For all algorithms it is difficult to determine which one showed the best results. As the MR labelled only pixels which clearly show disease symptoms as symptomatic it is not surprising that the algorithms outperform the MR for disease detection, as the identification of pixels at high zoom factors is challenging for the human eye. While the DC showed the highest sensitivity for disease detection it is also the one most likely to misclassify healthy tissue as symptomatic. Meanwhile the SVM and SD performed slightly worse in symptom detection but had more robust results regarding misclassification of pixels. The differing results of the data analysis methods suggest that it is advantageous for researchers to use multiple algorithms to analyse experimental datasets and select the one which gives the most reliable results for the intended purposes of the study.

### 3.2.6 Conclusion

The postulated theory that the nature of the plant-pathogen interaction during pathogen infection is related to the possibility to detect disease symptoms through transmission-based imaging is being supported by the results of this study. Thereby, the use of transmission measurement is most suited for invasive pathogens, which cause tissue damage in deeper layers of the leaf, or in order to separate stress factors which show a high similarity within the changes to the spectral signature of reflectance data. Transmission-based measurements seem to be outperformed by reflection-based measurements in general when it comes to early disease detection. The differing results of the utilized data analysis methods within this study highlights the importance of selecting the most suitable analysis method for given experiments.

# 4 Applications of hyperspectral imaging based phenotyping on canopy scale

**Chapter 4 has been published:**

**Thomas S**[1,2], Behman J[1], Steier A[2], Kraska T[3], Muller O[2], Rascher U[2], Mahlein A-K[4] (2018) Quantitative assessment of disease severity and rating of barley cultivars based on hyperspectral imaging in a non-invasive, automated phenotyping platform. *Plant Methods* 14, 45.

[1]INRES-Phytomedizin, University Bonn, Bonn, Germany
[2]IBG2: Plant Sciences, Forschungszentrum Jülich GMBH, Jülich, Germany
[3]Field Lab Campus Klein-Altendorf, University Bonn, Bonn, Germany
[4]Institute of Sugar Beet Research (IfZ), Göttingen, Germany

**Authors contribution**

Stefan Thomas, Jan Behman and Aanne-Katrin Mahlein designed the study and the hyperspectral measurement system. Stefan Thomas, Jan Behman , Angelina Steier, Anne-Katrin Mahlein, Onno Muller and Thorsten Kraksa did help setting up and maintained the measurement equipment. Stefan Thomas performed the hyperspectral measurements. Jan Behman and Stefan Thomas performed the statistical analysis. Stefan Thomas and Jan Behman drafted the manuscript with support from Anne Katrin Mahlein, Aangelina Steier, Uwe Rascher, Thorsten Kraska and Onno Muller.

## 4.1 Abstract

**Introduction:** Phenotyping is a bottleneck for the development of new plant cultivars. This study introduces a new hyperspectral phenotyping system, which combines the high throughput of canopy scale measurements with the advantages of high spatial resolution and a controlled measurement environment. Furthermore, the measured barley canopies were grown in large containers (called Mini-Plots), which allow plants to develop field-like phenotypes in greenhouse experiments, without being hindered by pot size.
**Results:** Six barley cultivars have been investigated via hyperspectral imaging up to 30 days after inoculation with powdery mildew. With a high spatial resolution and stable measurement conditions, it was possible to automatically quantify powdery mildew symptoms through a combination of Simplex Volume Maximization and Support Vector Machines. Detection was feasible as soon as the first symptoms were visible for the human eye during manual rating. An accurate assessment of the disease severity for all cultivars at each measurement day over the course of the experiment was realized. Furthermore, powdery mildew resistance based necrosis of one cultivar was detected as well.
**Conclusion:** The hyperspectral phenotyping system combines the advantages of field based canopy level measurement systems (high throughput, automatization, low manual workload) with those of laboratory based leaf level measurement systems (high spatial resolution, controlled environment, stable conditions for time series measurements). This allows an accurate and objective disease severity assessment without the need for trained experts, who perform visual rating, as well as detection of disease symptoms in early stages. Therefore, it is a promising tool for plant resistance breeding.

## 4.2 Introduction

Phenotyping is a necessary and time intensive step in the process of breeding disease resistant crops (Lobet 2017, Shakoor *et al.* 2017, Tardieu *et al.* 2017). Visual rating by humans, the common non-destructive method of crop phenotyping, has the disadvantage of being a time-consuming, subjective process, which requires experts or trained personnel. The application of optical sensors is a promising approach to overcome the drawbacks of manual visual rating, as – with an adequate analysis algorithm – it is objective and can be automated, while allowing non-invasive measurements directly in greenhouses and fields (Mutka and Bart 2014, Walter *et al.* 2015, Mahlein 2016).

Hyperspectral imaging (HSI) combines these advantages with ability to derive information about a large number of plant traits. Hyperspectral sensors have already been shown to be successfully integrated into automated measurement systems in greenhouses and fields (Humplík *et al.* 2015, Virlet *et al.* 2017). Hyperspectral sensors capture the reflectance characteristics of object in large number of wavelength bands. Similar to RGB cameras, they measure the light which is reflected at the measurement target, but they are sensitive in a larger area of the electromagnetic spectrum (Jensen 2006). As a result, hyperspectral

imaging cameras measure so called hyperspectral datacubes, which show the spatial dimensions of the acquired image and additionally a spectral dimension with the reflectance values per wavelength (Jensen 2006). Hyperspectral imaging has been applied in multiple studies for biotic and abiotic stress detection in plants (Bravo *et al.* 2004, Hillnhütter *et al.* 2012, Wahabzada *et al.* 2012, Thomas *et al.* 2017), as well as pathogen resistance assessment (Kuska *et al.* 2015, Leuker *et al.* 2015a).

However, experiments which are focused on disease detection at the earliest stages in pathogenesis are mostly performed as basic research in the laboratory on leaf scale. In contrast, field studies tend to focus on the detection of diseases at later stages of pathogenesis. In less controlled environments, environmental factors prove to be challenging for accurate hyperspectral measurements. As a result, detecting small symptoms at early stages of pathogen infection is more challenging. Changing light conditions during the measurements are the major environmental factor, reducing the data quality. Other factors, such as wind and rain, play a minor role (Behmann *et al.* 2015b, Damm *et al.* 2016, Pinto *et al.* 2016). As hyperspectral cameras with the highest spatial and spectral resolutions available to date tend to be push/whisk broom scanners, the process of image acquisition takes a certain amount of time (Jensen 2006). During this process, the measurement accuracy is dependent on stable environmental conditions. Furthermore, the angle between incoming light, plant and sensor has influence on the measurement results (Vigneau *et al.* 2011, Behmann *et al.* 2015a).

These problems multiply, when plant canopies are measured instead of leaves. In a dense canopy, the different leaves have individual angles to the light source and hyperspectral sensor. Furthermore, leaves are on different layers in the canopy. This leads to varying distances between measured leaves, sensor and illumination. Main effects are that leaves are less illuminated due to shadowing of the upper canopy layers and multiple scattering at surrounding leaves occurs (Behmann *et al.* 2015b, Sandmeier *et al.* 1998).

Common high throughput field hyperspectral measurement experiments are barely influenced by these factors, as they are either performed airborne or with non-imaging sensors, averaging the effects of canopy diversity over multiple leaves/plants (Hillnhütter *et al.* 2011, Cao *et al.* 2013). Although those procedures have shown to be successful in field monitoring and assessment of disease spread, they lack the spatial resolution to accurately rate the disease severity in early phases of infection and pathogenesis on plants.

Currently available hyperspectral measurement systems focus either on high measurement throughput like canopy measurements on the field with little regard to changes in the environmental factors (Bai *et al.* 2016, Virlet *et al.* 2017), or on plant/leaf level measurements under highly controlled environmental conditions with low throughput (Mahlein *et al.* 2012, Kuska *et al.* 2017, Thomas *et al.* 2017). Both approaches are well suited for their fields of application.

However, the hyperspectral measurement system, which is introduced in this study, offers a new scale, specifically for phenotyping applications in resistance breeding. As it will be shown in this article, the different light conditions in

plant canopies prove to be challenging for modern data analysis approaches even under nearly ideal measurement conditions. The proposed measurement system combines the high throughput of canopy based measurements in fields with the controlled measurement environment of laboratory setups in order to achieve stable data acquisition over the whole time course of disease development.

A greenhouse based phenotyping system, which is based on hyperspectral imaging, has been developed. The system works by growing plants in larger containers (Mini-Plots), which create a field like situation. Each Mini-Plot provides enough space in area and soil depth to grow a canopy consisting of 360 barley plants in similar density as they would be grown in the field. A soil depth of 61 cm allows a more natural development of the plants root systems when compared to commonly used pots. The combination of these factors allows for phenotyping experiments in greenhouses under conditions that resemble those of actual field experiments. The location of the measurement system inside a greenhouse has the innate advantage, that the environmental conditions during the experiment can be controlled at any time. Thereby, the system combines the advantages of phenotyping test plots in the field with the possibility of reliable measurements on a daily basis. This circumvents the problem of plants, which have been grown in pots in the greenhouse, showing different phenotypes compared to being grown under field conditions, due to stable environmental conditions and limited root development (Poorter *et al.* 2012).

Halogen lamps, equipped with diffusors, are implemented in the measurement system, providing stable and diffuse light conditions for the hyperspectral camera. A transportable curtain is attached to exclude natural light, that may interfere with the measurement process. The system can perform automated measurements, allowing for a relatively high measurement throughput with minimal human effort. These factors summarize to the system being a valuable middle ground between field measurements under natural conditions, and low throughput measurements in highly controlled environments. The combination of tightly controlled environment and high measurement throughput with hyperspectral imaging shows the high potential of the presented system for phenotyping applications in resistance breeding.

To the author's knowledge only two comparable systems exist at the time of this publication. Joalland *et al.* (2017) designed a microplot based system, where the response of sugar beet plants to *Heterodera schachtii* inoculation was evaluated with different measurement methods. The microplots, containing three sugar beet plants per plot, were covered with a mobile dark box with a halogen lamp to provide equal light conditions before the average spectrum of the plants was collected with a non-imaging spectrometer. Busemeyer *et al.* (2013) introduced the field based measurement system BreedVision, which can be moved over small plots and perform measurements with multiple sensors. A cover for the whole system provides shading and avoids direct solar radiation influencing the measurements. The system includes a hyperspectral imaging system to measure plant moisture and nitrogen content, which works with a spatial resolution of 3x5 mm. Compared to these systems, the Mini-Plot based system presented in this study features a reduced canopy effect through diffuse

light conditions and a higher spatial resolution, which is important for the early detection of disease symptoms.

The system was tested by evaluating six barley cultivars with different disease susceptibility to powdery mildew. Over the course of the experiment, it could be shown that the gathered hyperspectral data allows an early detection of powdery mildew infection, as well as an accurate estimation of the disease severity for each barley cultivar per measurement day. The estimated values from the hyperspectral data analysis was consistent with the results of visual rating for each cultivar. Furthermore, it was possible to show the spatial distribution and spread of the pathogen over the barley plots during the time of the measurements.

## 4.3 Materials and Methods

### Mini-Plot phenotyping greenhouse

The hyperspectral measurements in this study have been performed in the 'Mini-Plot' facility at Campus Klein-Altendorf of Bonn University, which was developed by the Forschungszentrum Jülich. The facility consists of a large enclosed greenhouse compartment and a fenced-in outside area, where 120 large planting containers, so called Mini-Plots, can be placed. 90 Mini-Plots can be placed inside the greenhouse, while another 30 can be placed in the outside area (Fig. 4.1 a, b). The experiments of this study were performed solely on Mini-Plots inside the greenhouse to be weather independent during the measurement series. An automated sensor positioning system facilitates the precise and robotized positioning of a sensor platform (Fig. 4.1). This allows for the cultivation of relevant crop species in small canopies, while above-ground plant traits can automatically be measured by a modular sensor positioning system, which can be equipped with a portfolio of phenotyping sensors (Fig. 4.1).

Each Mini-Plot is a commercial 535 liter plastic container (inside size 111 x 71 x 61 cm; AUER Packaging, Belgium), that can be filled with local soil or other desired substrates, according to the goal of the experiments. An automated drip irrigation system is attached to each Mini-Plot allowing individual computer-controlled watering. Drainage is enabled by a loose gravel filling at the bottom and a valve in each container, the excess water can be quantified on request. Additionally, multiple environmental sensors are placed in the Mini-Plot area to monitor the environmental conditions and potential gradients; monitoring includes irradiance, air temperature and humidity, as well as soil moisture and temperature. A weather station (Vaisala) is located in the fenced-in area outside the greenhouse to monitor weather conditions and to avoid outside measurements during bad weather conditions.

The automatic positioning system was developed by the Forschungszentrum Jülich in cooperation with Otte Metallbau GmbH & Co Kg (Harkebrügge, Germany) in partnership with Atlantique Automatisierungstechnik GmbH (Ihlow, Germany). A stable and motorized x, y, z rail based traversing unit is installed in the greenhouse and the outside area. This traversing unit moves a universal

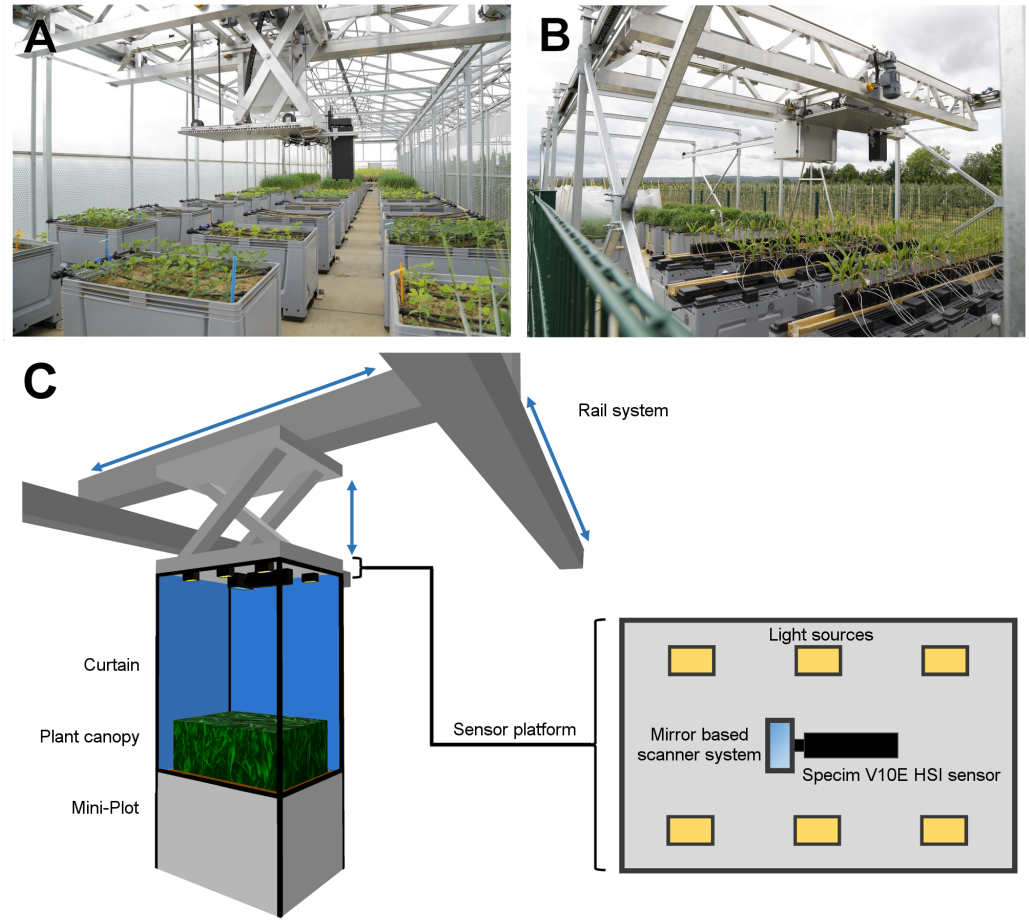


Figure 4.1: Phenotyping greenhouse in Campus Klein-Altendorf with Mini-Plot facility, interior (A) and exterior (B) compartments. Schematic representation of the hyperspectral phenotyping system (C). The rail system of the Mini-Plot facility in combination with diffuse artificial light sources and a curtain allows for automatic measurement approaches under highly controlled environmental conditions. The combination of Specim V10E hyperspectral imaging (HSI) sensor and mirror based scanner system enables fast, high-resolution measurements of the entire Mini-Plot.

base plate, on which various sensors of up to 50 kg can be attached. The baseplate is moved 2 meters above the containers (2.8 meters above ground) and can be positioned with an accuracy of 2 cm using fixed positioning elements at the x and y axis. The universal baseplate (including sensors) can be lowered in z direction to facilitate close range measurements; technically the base plate can be lowered by 1 meter, i.e. bringing sensors in proximity to the plant canopy.

The system is controlled by an in-house developed application based on LabVIEW (National Instruments, USA). Measurements can be scheduled throughout the day, triggering different sensors. The base functions of the system (movement of the traversing unit, switching of the watering valves) are controlled by the Programmable Logic Controller (PLC). These functions can be controlled by the user directly as well. In the automated mode, the communication between the PLC (Siemens, Germany) of the system and the sequence control application (LabVIEW) is facilitated using an OPC server (LabVIEW). The sequence application is commanding the measurement routine, which has been programmed by the user. Within a schedule file, the time when a sensor is triggered, the position/plot and the distance to the container can be configured. It is possible to measure each plot with separate sensors during a single measurement sequence. The acquired data is stored on the acquisition computer located at sensor platform and transferred daily to the server.

**Plant materials and pathogens**

Six barley cultivars with different susceptibility to *Blumeria graminis* f. sp. *hordei* (*Bgh*), based on assessment of the official German cultivar list (Descriptive Variety List; Bundessortenamt, Hanover, Germany), were used in the experiments. The used cultivars are (respective disease susceptibility rating in bracelets): Tocada (7; KWS Lochow GmbH, Bergen, Norway), Grace (7; Ackermann Saatzucht GmbH & Co. KG, Irlbach, Germany), Milford (4; Saatzucht Josef Breun GmbH & Co. KG, Herzogenaurach, Germany), Gesine (4; NORDSAAT Saatzuchtgesellschaft, Halberstadt OT Langenstein, Germany), Eileen (2; KWS Lochow GmbH) and Irina (2; KWS Lochow GmbH). Each cultivar was sown into two Mini-Plots, with 360 seeds per Mini-Plot to simulate barley growth under field conditions. The distribution of the cultivars in the phenotyping greenhouse was randomized to avoid location affects. Directly after sowing, Plantosan fertilizer (20% N, 10% P2O5, 15% K2O, 6% MgO, 2% S, Wilhelm Haug GmbH &Co. KG, Germany) was applied according to the manufacturer's description to each Mini-Plot. The experiment was performed from 16. 09. 2016 – 02. 12. 2016, with low air temperatures in the greenhouse, following the procedure established in the preliminary experiment from 09. 11. 2015 – 18 .01. 2016. The barley cultivars were cultivated for four weeks until sufficient surface cover to perform the experiments was reached. Mini-Plots, which showed development of powdery mildew symptoms prior to inoculation, were treated with sulfur (fungicide Kumulus containing 800g/kg sulfur, BASF, Germany) to prevent further symptom development. Symptomatic leaves were removed from the respective Mini-Plots and sulfur was washed off multiple times before inocula-

tion. Two days before inoculation with *Bgh*, half of the Mini-Plots were treated with the fungicide Vegas (containing 53.1 g/l cyflufenamid, BASF, Germany), to serve as negative control for the experiment. The other half of the Mini-Plots were inoculated with conidia of *Bgh* field isolate from Bonn by shaking heavily infested plants above the Mini-Plots.

### Manual rating of disease development per barley cultivar

Both control and inoculated Mini-Plots of each barley cultivar were visually assessed on every measurement day. Plant and plant disease development were assessed and documented with RGB images. RGB images were taken from above the Mini-Plot – to achieve the same viewing angle as the hyperspectral imaging sensor. Furthermore, close up RGB images of areas with disease symptoms or other anomalies – like necrotic lesions at resistant cultivars – were acquired.

At the last measurement day (30 dai) a visual rating of the inoculated Mini-Plots from each barley cultivar was performed (Moll *et al.* 2009). Three classes of disease severity were defined: Low (up to 5% of the plot showing powdery mildew symptoms), moderate (5% to 20% of the plot showing powdery mildew symptoms) and severe (over 20% of the plot showing powdery mildew symptoms) disease severity.

### Hyperspectral imaging measurement on canopy scale

The hyperspectral reflectance measurements were performed with a Specim V10E hyperspectral push broom sensor (Spectral Imaging Ltd., Oulu, Finland), which was mounted on the rail system based sensor platform in the phenotyping greenhouse (Fig. 4.1). The Specim V10E sensor provides hyperspectral image acquisition in the visual ($400 - 700$ nm) and near infrared ($700 - 1000$ nm) region of the electromagnetic spectrum with a spectral resolution of approximately 2.8 nm. During the measurements, a spatial resolution of 0.3 mm was obtained in a measurement distance of 80 cm. A mirror scanner (Spectral Imaging Ltd., Oulu, Finland) was used to change the field of view of the push broom sensor in order to acquire two dimensional images.

Additionally, 6 halogen lamps (POWLI010 Halogen Floodlight 150 Watt; Varo, Belgium) were symmetrically distributed on the sensor platform to achieve homogenous lighting conditions (Fig. 4.1c). The glass cover of each halogen lamp was replaced by a frosted, highly heat resistant glass cover to diffuse light. Ambient natural light was excluded by the use of a light-proof white curtain covering both the sensor platform and the measured Mini-Plot (Fig. 4.1c). The curtain also provides additional scattering of the light from the halogen lamps, leading to a more homogenous illumination of the measurement samples.

All Mini-Plots were measured in a time-series experiment from 1 dai (days after inoculation) to 30 dai. For each measurement, a barium sulfate 99% reflectance white reference bar (Spectral Imaging Ltd., Oulu, Finland) was measured before the measurement of plant canopy, providing known illumination intensity values for image normalization. After each measurement (both white

reference and plant canopy), a dark current measurement of the internal camera noise was performed with the same exposure time as the previous image, respectively, eliminating inaccuracies during image normalization.

An additional measurement with identical observation parameters as described above was performed two hours before the inoculation of the plants with powdery mildew, in order to ensure that the fungicide treatment of the plants had no effects on the spectral signatures. The confirmatory results were in accordance with previous experiments (Thomas *et al.* 2017). Due to the lack of a pathogen, the data has not been included in the analyzed time series.

### Analysis of the hyperspectral dataset

ENVI 5.1 + IDL 8.3 (ITT Visual Information Solutions) was used to normalize the hyperspectral images against the known values of the white reference standard, while subtracting the dark currents of both images. The normalized images were further smoothed by the application of the Savitzky-Golay filter (Savitzki and Golay 1964) to the spectral domain, in order to reduce noise in the spectral profiles of the images. Areas of the images which were not covered by plants, as well as areas with extremely low light intensity in the lower canopy were masked during the preprocessing of the images. Furthermore, all images were cropped to the designated measurement area of the experiment.

Simplex Volume Maximization (SiVM) was then applied on all preprocessed images. SiVM is an unsupervised data analysis method, which selects extreme hyperspectral signatures of the dataset as archetypes for a re-parameterization of the whole dataset (Fig. 4.2) (Kersting *et al.* 2012a). The application of SiVM leads to a reduction in size of the dataset and a pre-classification of the data based on the abundance level of each generated archetype (Kersting *et al.* 2012a). In this study, the SiVM algorithm was performed with 25 archetypes for the entire dataset of hyperspectral images, including control and inoculated images of each barley cultivar. Thereby, the size of the dataset was reduced to ~27% of the original size. The matrix factorization toolbox PYMF 0.3 (Thurau *et al.* 2012, Python matrix factorization module 2017) was used for this approach.

The SiVM transformed dataset was then classified into healthy tissue, disease symptoms and background by a non-linear Support Vector Machine algorithm (SVM) (Cortes and Vapnik 1995). The applied SVM uses radial basis function as kernel function to determine non-linear discriminant functions. As a supervised method, it is based on training data, i.e. manually selected samples as examples for each class, which were selected for each class by an expert at an unmistakable development state. The required hyperparameters were determined using a cross-validation based grid optimization. LIBSVM 3.21 was used (Chang and Lin 2012). Training data for the SVM classification was selected and annotated – based on a combination of pseudo RGB representation and spectral information of the hyperspectral dataset – by an expert. The inoculated Mini-Plot of barley cultivar Tocada at 22 dai was chosen to collect training data, due to its representative powdery mildew symptoms in different

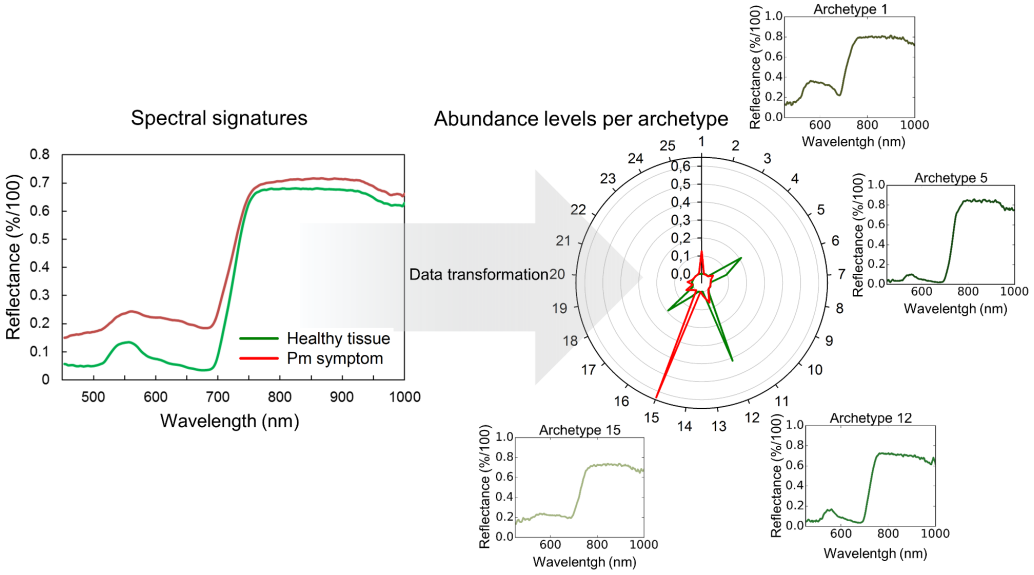


Figure 4.2: Spectral signatures and abundance maps of healthy plant tissue and powdery mildew symptoms (mean values of 50 pixels, each). The spectral signatures (left) represent the mean reflectance of the pixels over the spectral measurement area of the sensor. The abundance map (right) shows the representation of the same mean values based on the abundance of the pixels with the 25 archetypes, which were selected during the transformation of the dataset with the Simplex Volume Maximization. Archetypes with high correlation to healthy or symptomatic tissue are shown separately, each archetype is a real spectral signature from the original hyperspectral dataset (colors of archetype spectral signatures represent the color of the corresponding pixels, which would be visible to the human eye). Pm = Powdery mildew.

development stages and canopy layers. After manual selection of pixels with disease symptoms and healthy tissue in the different canopy layers, the gathered data was used as reference for the above described SVM classification. In order to access the accuracy of the resulting SVM classification the image of the inoculated Mini-Plot of barley cultivar Grace at 22 dai was manually annotated as described above. The manual annotation was compared with the automatic annotation of the SVM classification result for that image, showing the accuracy of the automated data analysis over different cultivars despite the limited training data.

## 4.4 Results and discussion

### Visual observations and manual assessment of the spectral dataset

Both control and inoculated plants developed slower than usual over the course of the experiment and did not produce ears. This was expected due to low temperatures in the greenhouse compared to the usual growth temperatures for summer barley. The slower development of the barley plants and the powdery mildew symptoms enabled long term measurements of the disease progression. Thereby, it was possible to confirm the performance of the non-invasive measurement setup over a prolonged period of time. No plant damage except the effects of the powdery mildew infestation could be detected during the measurement period of 30 days.

The plants in the control Mini-Plots showed no signs of powdery mildew infection from 1 to 24 dai. Starting at 26 dai, the control plants of the susceptible cultivars Milford, Grace and Tocada showed first signs of powdery mildew symptoms at the edges of the Mini-Plot. Meanwhile, the inoculated plants of the cultivars Milford, Tocada and Grace showed sporadic symptoms from 12 dai on the edges of the Mini-Plot and first symptoms of strong powdery mildew infection in the measurement area at 14 dai (Table 6). At 18 dai, moderate infection in early stages could be observed at inoculated Mini-Plots of cultivars Milford, Tocada and Grace, which did increase up to 30 dai. The cultivars Tocada and Grace showed moderate powdery mildew symptoms (Table 6). However, cultivar Milford showed the highest disease severity (severe), despite being listed with moderate susceptibility in the official German cultivar list. Cultivar Eileen showed few visible symptoms at 14 dai, while having a low susceptibility for powdery mildew infection (Table 6). Cultivar Eileen, unlike the three aforementioned cultivars, showed no significant development of powdery mildew symptoms over the course of the experiment. Despite being listed as moderately susceptible to powdery mildew, cultivar Gesine showed no symptoms until 22 dai (Table 6). From this point on, the disease severity steadily increased until the end of the measurements at 30 dai. Some necrotic lesions became visible on the plants, starting at 14 dai. The cultivar Irina showed no signs of powdery mildew infection over the course of the experiment. Severe necrotic lesions over the leaves were visible, starting at 14 dai (Table 6). Overall, the different cultivars showed powdery mildew development and disease severity according to their general rating. Only the cultivars Gesine and Milford interacted different than expected from their assessed susceptibility. Gesine showed a surprisingly high resistance against powdery mildew, with a notable delay in symptom development compared to other susceptible cultivars. Meanwhile, Milford, despite being listed moderately susceptible, showed the strongest disease severity and symptom development of all cultivars. These results were coherent for the Mini-Plot experiment, as well as preliminary experiments in the greenhouse the Mini-Plot facility and microscopic analysis. The explanation is most likely the specific interaction of the cultivars with the used *Bgh* isolate.

Average spectra of pixels with powdery mildew symptoms and healthy tissue

were extracted, unveiling the characteristic changes in the plants spectral signature upon powdery mildew infection when comparing pixels in corresponding canopy layers. Pixels in different canopy layers showed differences in the intensity of their spectral signatures over all measured wavelengths, as changes in the intensity of the incoming light and shadows have a strong effect on the data. The spectral signature of infected leaves shows mostly a general increase in intensity, with a pronounced increase of reflection at 650-700 nm (Fig. 4.3). Both pixels with powdery mildew symptoms and healthy tissue have the highest variety for different canopy layers in the near infrared area between 750 and 1000 nm (Fig. 4.3). The observed variance in the near infrared area of the spectral profiles can be explained by the high sensitivity of near infrared reflection measurements to distance and angle of the target. Thomas *et al.* (2017) showed, that even slight changes of leaf angles in framed leaves lead to high variances in the near infrared part of the spectrum. In the case of canopy measurements, the differences in leaf angle and distance to the camera are greatly increased. The distance and angle of the white reference – serving as standard value for 100% light reflectance – is fixed during the measurement. This leads to an increase in the calculated reflectance in the near infrared area of the spectrum if leaves are closer to the sensor than the white reference. These effects were not corrected in this study, as the study focuses on relative detection of powdery mildew symptoms, rather than their spectral characterization. The changes in the spectral profile of the pixels with disease symptoms are typical for powdery mildew infestation, due to the symptoms are visible as a layer of white mycelia on the leaf with minimal influence on the leaf structure (Thomas *et al.* 2017). Thereby, it proved to be difficult to distinguish spectral signatures of symptomatic and healthy areas, which are located in different layers of the canopy and thereby show differences in the intensity of the reflected light. (Fig. 4.3).

Hyperspectral images acquired under artificial light conditions showed to be superior to images acquired under natural light conditions. The diffuse light of constant intensity did reduce the effects of the canopy structure on the hyperspectral signatures considerably and increased the overall image quality. The image quality, with diffuse light conditions and a spatial resolution of 0.3 mm, was sufficient to distinguish symptoms at 12 dai, when they were first visible with the human eye. These results show the importance of controlled environmental conditions. It was possible to perform stable measurement series over prolonged time periods with comparable results. Additionally, distinct advantages of equally distributed and diffuse lights for an improved measurement quality on the canopy scale could be observed. The results of this study strongly suggest a notable increase in measurement accuracy under diffuse light conditions through a reduced impact of the canopy architecture on the light intensity differences of the individual canopy layers. Furthermore, the measurement system of this study offers a high spatial resolution (0.3 x 0.3 mm pixel size) when compared with similar phenotyping systems in the field (Busemeyer *et al.* (2013) with 3 x 5 mm pixel size) and more comparable to leaf scale laboratory setups (Mahlein *et al.* 2012, Behmann *et al.* 2015b, Thomas *et al.* 2017).

Table 6: Manual rating of disease progression per barley cultivar over the course of the experiment (2016; - = no symptoms appeared). *according to rating of the official German cultivar list.

| Barley Cultivar | Disease susceptability* | First symptoms (dai) | Relative disease severity at 30 dai | Necrotic lesions visible (dai) |
|---|---|---|---|---|
| Tocada | 7 | 14 | Moderate | - |
| Grace | 7 | 14 | Moderate | - |
| Milford | 4 | 14 | Severe | - |
| Gesine | 4 | 22 | Low | 14 |
| Eileen | 2 | 14 | Low | - |
| Irina | 2 | - | - | 14 |

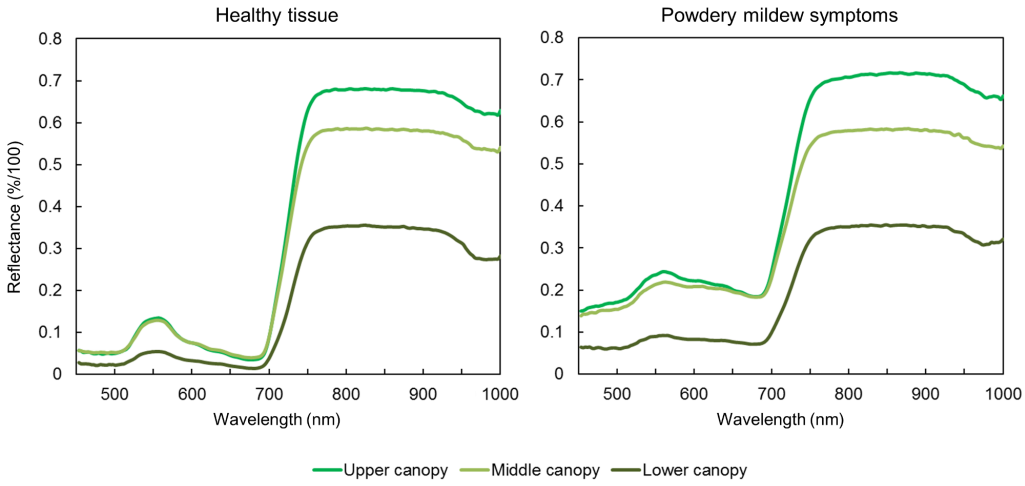


Figure 4.3: Spectral signatures of mean values from 30 pixels on canopy levels, differing in distance to the sensor and illumination system, for both healthy and symptomatic tissue.

### Analysis of the acquired hyperspectral data through SVM

Due to the high data variability across the different layers of the canopy and the extensive amount of the gathered hyperspectral dataset, it was necessary to perform advanced data analysis methods. The application of SiVM significantly reduced the size of the data (from 234 GB to 62 GB) and pre-classified the dataset based on existing, extreme spectral signatures. This approach did increase both speed and accuracy of the SVM based classification. Due to the nature of hyperspectral imaging, techniques for data size reduction are an important part of a functional phenotyping system. When taking into consideration that each image can easily reach the size of several gigabytes, large scale phenotyping experiments are not only requiring a lot of storage space, but also require modern data analysis methods, which tend to be time consuming (Behmann *et al.* 2015a). SiVM has the advantage that the structure of the data is not lost, as each spectrum is classified based on existing data instead of abstract variables (Wahabzada *et al.* 2015a). This allows for a simplified representation with increased separability of the acquired data and a considerable reduction in processing time using the SiVM processed dataset in further data analysis methods.

It was possible to separate pixels showing healthy tissue, powdery mildew symptoms and background into different classes through the combined classification with SiVM and SVM. Classification of the control Mini-Plots showed less than 2% of the pixels in the images being classified as diseased for all cultivars whereas up to 31% of the pixels are predicted as infected for the inoculated plots (Fig. 4.4). Meanwhile, the automatic disease severity estimation of the infected plants of all cultivars in the Mini-Plots, based on the SVM results, show matching results to the visual observations of the disease progression per cultivar at 30 dai (Fig. 4.4). Furthermore, the progression of the disease severity can be accurately tracked across every measurement date during the experiment. Validation of the SVM classification data was based on its application and comparison with a manually labelled hold-out dataset. The dataset was derived from images of the inoculated Mini-Plot of cultivar Grace at 22 dai to verify cross cultivar accuracy. The results show an accuracy of 94.83% for the automatic SVM classification. The results of this study show that the proposed hyperspectral phenotyping system is able to accurately assess the disease severity of each cultivar. Additionally, it is possible to monitor the exact progression of the disease symptoms for each plot at any time during the time series measurement. Combined with the high throughput of the canopy level measurements, the system allows for a quick and objective estimation of barley cultivar susceptibility to powdery mildew. In this study, a high potential of the system to be used for fully automated measurements in the future has been confirmed.

The results of the SVM classification can also be visualized on the pixel scale for each hyperspectral image of the cultivars over the course of the experiment, providing spatial information about disease outbreak and spread over the course of the experiment (Fig. 4.5). In Figure 4.5, the disease progression of the two cultivars with the highest disease severity (Milford and Tocada) is

shown. The differences in disease patterns for the cultivars from the first visual symptoms at 14 dai up to the final stages of powdery mildew infestation can be readily assessed and analyzed for phenotyping purposes. Furthermore, the SVM classification is able to detect first disease symptoms at 12 dai, when they first appeared at the Tocada and Milford cultivars. Due to the similarities of powdery mildew symptoms and healthy tissue with specular reflections, it is difficult to detect such early symptoms without misclassifications. However, such first symptoms contribute only to a small degree to the proportional disease severity estimation. A specific and quantitative evaluation of the early detection was beyond the scope of the experiment and was not specifically regarded in the analysis. Unlike the results of Thomas *et al.* (2017), which detected powdery mildew on barley at leaf scale under laboratory conditions, it was not possible to detect infestation before visible symptoms appeared in the current study. This can be explained as a manual annotation of training data was required due to the SVM classifier. As it was impossible to acquire training data from pixels with powdery mildew infestation before they became visible to the human eye, the SVM algorithm could not be trained to search for these effects. Kuska *et al.* (2015) were able to select powdery mildew infected areas before visible symptoms appeared. However, this was possible due to tracing position on the leaf from later stages in the experiment, when symptoms have become visible. Due to the leaf movement in the partially opened greenhouse, this technique could not be transferred to the current study. Nevertheless, the results show, that powdery mildew symptoms at early stages can be detected in the canopy with the current setup, providing valuable information for resistance breeding.

**Automated assessment of necrosis due to resistance against powdery mildew of cultivar Irina**

Necrotic spots on the leaves of barley cultivar Irina could be spotted in the canopy at 14 dai. Microscopic analysis could identify papillae formation which prevents cell wall penetration of powdery mildew haustoria, as well as hypersensitive response (HR) as response to successful penetration of epidermis cells. Due to the intensity of necrotic lesions on the inoculated plants, it was possible to create training data, based on the plants in the inoculated Mini-Plot of cultivar Irina at 14 dai and perform SVM classification for healthy tissue and tissue with necrotic lesions. As shown in Figure 4.6, it was possible to differentiate inoculated and control plants of cultivar Irina, based on the increase of necrotic lesions in response to powdery mildew inoculation. The training of the SVM classification had to be performed with a small number of samples, which could be identified by the authors due to large amounts of necrotic cells creating visible discolorations on the plant leaves. Nevertheless, these observations are promising for the application of the proposed hyperspectral phenotyping system for the direct detection of resistance reactions in plants as response to pathogen attack. For such experiments, it is possible to reduce the distance between camera and plants inside the Mini-Plots. This would lead to the required higher spatial resolution at the cost of a reduced measurement throughput and more

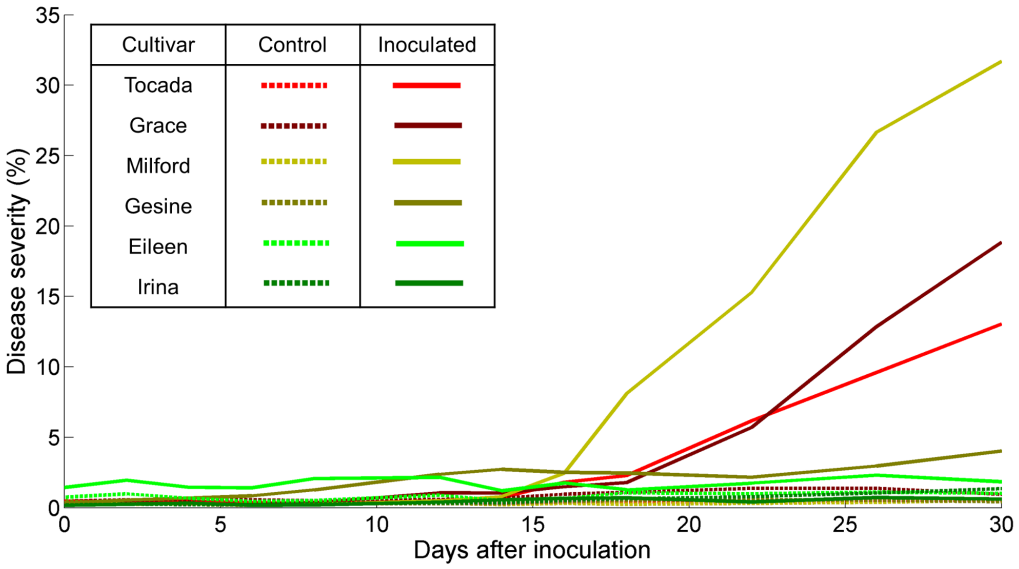


Figure 4.4: Disease severity of the different barley cultivars over the course of the experiment. The disease severity was estimated based on percentage of pixel, which were classified as containing powdery mildew symptoms after Simplex Volume Maximization (SiVM) and following supervised classification by Support Vector Machines (SVM).

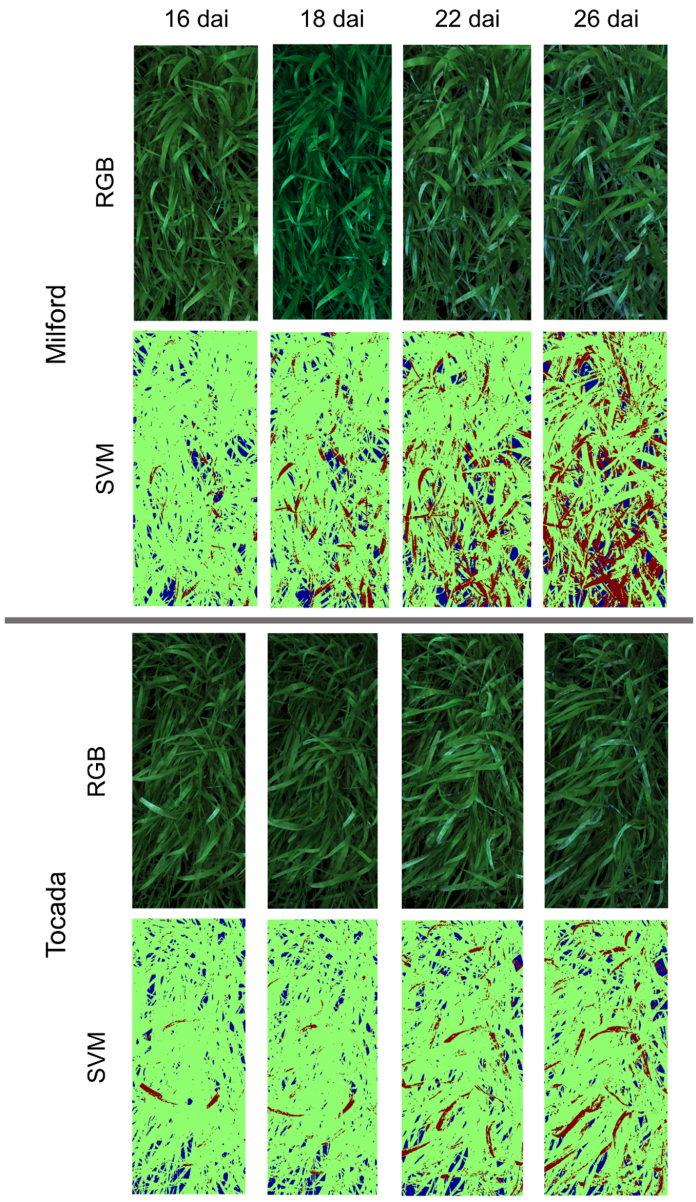


Figure 4.5: Spatial distribution of powdery mildew infestation development over the course of the experiment for highly susceptible cultivars Milford and Tocada through pseudo RGB images and false color images of Support Vector Machines (SVM) classification (green = healthy tissue, red = powdery mildew symptoms, blue = background).

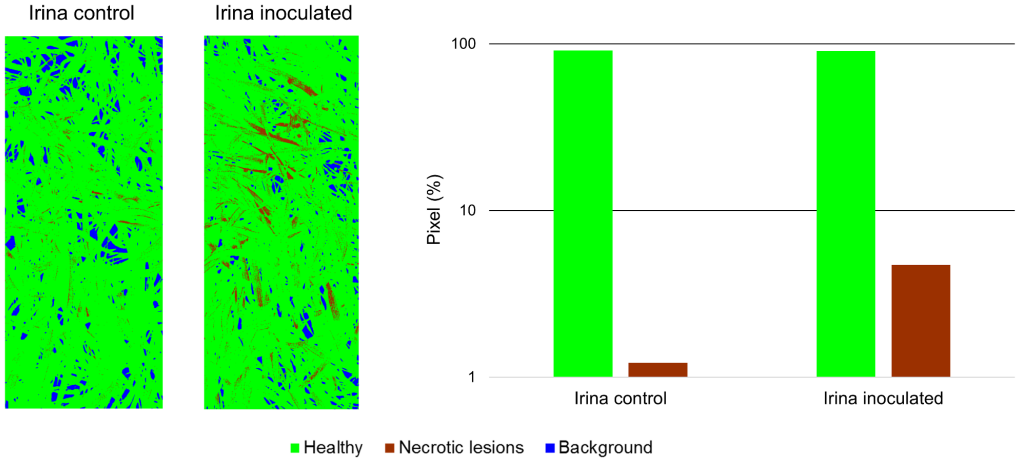


Figure 4.6: Classification of healthy tissue and tissue expressing necrotic lesions as response to powdery mildew infection at the resistant barley cultivar Irina two days after inoculation. False color pictures show the spatial distribution of necrotic lesions over the Mini-Plots of both control and inoculated plants. Additionally, the percentage of total pixels in the image being classified as showing tissue with HR for both plots is shown as bar diagram. The inoculated plot shows a significantly increased number of pixels, which are classified as expressing necrotic lesions.

extreme observation geometries. By the development of modern, more compact hyperspectral cameras, the measurement setup can be further simplified in the future (Behmann *et al.* 2018).

## 4.5 Conclusion

The proposed hyperspectral phenotyping system was designed to enable the accurate measurements of basic research leaf level hyperspectral experiments, usually performed under controlled conditions in the laboratory, at a high throughput with environmental conditions as close to the field as possible. The conducted study shows that, despite the intrinsic difficulties of performing measurements on canopy scale, the system is able to detect disease symptoms at early stages and allow detailed assessment of disease severity and progression over extended periods of time. The achieved results are objectively derived and the measurement process is non-invasive, allowing for repeated measurements without interference with the plants development. Moreover, it was also possible to detect powdery mildew resistance induced necrosis for one of the resistant cultivars, which is a valuable addition for applications in resistance breeding programs. The use of modern data analysis methods enabled automatic extraction of the results and it was possible to analyze the entire dataset,

containing over 234 GB of information, by creating a set of training data from a single hyperspectral image. The proposed hyperspectral measurement system improves efficiency and accuracy of phenotyping procedures and would be a valuable addition in plant resistance breeding programs.

# 5 Summary and outlook

Three main topics have been set for investigation during this thesis. The evaluation of transmission based imaging, both compared and combined with the already well investigated reflection based imaging on leaf scale under laboratory conditions; the practical application of optical sensors for high-throughput early disease detection and quantification on canopy scale under greenhouse conditions. As well as the investigation of comparability of optical sensor data gathered on different scales and measurement conditions for plant disease detection.

## 5.1 Evaluation of transmission based imaging with hyperspectral sensors

The evaluation of transmittance data for plant disease detection – especially within early stages of disease development – was a major focus within this thesis. Building on the promising results of Bergsträsser *et al.* (2015), in which an increased accuracy for the detection of *Cercospora* leaf spot symptoms on sugar beet leaves through a combination of reflection and transmission based data from measurements with hyperspectral sensors was reported, the current thesis has focussed on further examining the possibilities of transmission based measurements – compared to and combined with reflection based data.

Three barley pathogens, which interact differently with the plant tissue during disease development (*Blumeria graminis* f. sp. *hordei*, *Puccinia hordei* and *Pyrenophora teres* f. *teres*) have been selected in order to investigate the possibilities of both reflection and transmission based data in combination with advanced data analysis methods for early disease detection and quantification within the specific plant-pathogen interactions between barley and the chosen pathogens (See Chapter 1.1).

Over the course of the experiments it could be demonstrated, that disease symptoms of all three pathogens could be eventually detected by both reflectance and transmittance data of the measured leaves. However, as this study – unlike Bergsträsser *et al.* (2015) – focussed specifically on early disease detection by means of performing daily time-series measurements over the course of disease development, it could be shown that reflection based datasets outperformed transmission based datasets for early disease detection.

The detection of powdery mildew symptoms showed the greatest disparity during the experiments, with principle component analysis classification based on reflectance data being able to detect powdery mildew symptoms two days before the symptoms were visible with the naked eye – at which point they were also detected based on transmittance data (see Chapter 3.1). Brown rust symptoms could be detected one day before they were visible with the naked eye through the use of support vector machines classification or respectively at the same time through the application of spectral decomposition on reflectance data (see Chapter 3.2). Meanwhile both algorithms were able to classify disease symptoms only one day after they were visible when applied to the transmittance

dataset. Net blotch symptom detection was possible one day before visible symptoms appeared for both reflection and transmission based measurements through the application of a distance classifier on the results of a previously performed PCA, it also showed the highest misclassification of the dataset as it was not possible to distinguish between net blotch symptoms and the leaf vein in the transmittance images (see Chapter 3.2). A notable exception is the classification of net blotch symptoms through SVM, as the transmission based approach actually was able to detect disease symptoms one day before the SVM based on the reflectance dataset. However, it has to be noted that this detection was still one day after symptoms became visible with the naked eye.

In all examined cases reflectance based approaches outperformed transmittance approaches for early disease detection – with the notable exception mentioned above, which does not support the validity of transmittance imaging for early disease detection however, as alternative data analysis methods performed significantly better for net blotch detection.

These results are most likely related to the optical properties of plant leaves, which cause light to spread diffusely when passing through the leaf tissue in order to maximise light availability for energy generation through photosynthesis (see Chapter 3). Especially in the early stages of disease progression light that passed through the symptomatic tissue is spread diffusely during its path through the plant tissue. Additionally, light that interacted with leaf areas next to the symptomatic tissue, which are not yet directly influenced through developing disease symptoms, is equally spread and mixes with the light which interacted directly with the symptomatic leaf tissue. Thereby, the light which is detected through transmission imaging becomes diluted with light that spread from healthy leaf areas at the edges of symptomatic tissue areas within the leaf. This effect is barely noticeable once disease symptoms have developed to a sufficient size, as shown by the measurements of Bergsträsser *et al.* (2015) and the measurements of late stage disease development within the current study. It could be shown to cause a significant reduction in transmittance based disease detection in early stages for all pathogens which were investigated within this study.

Furthermore, this effect was most prominent for the detection of plant diseases which interact mostly with the upper epidermis layers of the leaf, such as powdery mildew, while being the least relevant at the detection of necrotic pathogens (net blotch) and spontaneous necrosis of leaf tissue. These results support the theory that the internal light spreading inside the leaf tissue is the cause for the reduced efficiency in hyperspectral transmission imaging, as changes which are just at the leaf surface would be more prominently affected by light spreading then changes that are present deeper within the tissue layers of the leaf.

The combination of these issues and the additional challenges to the measurement process during hyperspectral imaging of transmitted light in plants make the application of transmittance datasets for pathogen detection in the near future unlikely. Especially the performance of transmission based measurements on canopy layer for practical applications without the possibility to

fixate leaves for precise measurement angles are challenging prospects for future applications. Nevertheless, it could be shown that transmittance data in combination with reflectance data can provide a more detailed approach for especially the differentiation of diseases and other stress factors from each other. These results show potential of transmission based imaging, especially combined with simultaneous reflection based imaging, for the differentiation of causative agents which are highly similar within reflectance data – as well as the detailed investigation of plant metabolic processes and their changes during plant-pathogen interaction.

## 5.2 High-throughput early disease detection on canopy scale for application in resistance breeding

A main goal of the thesis was the establishment of hyperspectral sensor systems that can be applied in practical applications, such as phenotyping procedures during plant resistance breeding. While hyperspectral imaging experiments have shown to be successful in pathogen detection in scientific studies, they are rarely applied outside of the scientific scope. One difficulty being the transition from highly experimental setups under specific conditions to practical applied systems. Another difficulty is the comparatively low throughput of scientific measurements. Finally, most studied about early disease detection are performed on leaf scale, which is not feasible for economic application in agriculture.

In order to remedy these factors a high throughput hyperspectral imaging measurement setup was assembled, which allows rapid measurements of plants on canopy scale (see Chapter 4). The measured mini-plots in which the plants grow furthermore provide similar field-like conditions for the investigated plants, promoting the expression of phenotypes similar to those in field trials. The environmental conditions during measurements of the plants are highly controlled, despite the plants growing in a greenhouse environment or outdoors – causing no interference with plant development outside of the comparably short measurement windows. This allows multiple measurements of different plots over long time periods under highly similar conditions, not only minimizing adjustment time of measurement parameters between measurements but also removing the influence of environmental conditions to both measurement results and ability to perform the actual measurements.

Within the study time-series measurements of six different barley cultivars with varying susceptibility to powdery mildew were performed over a time span of about one month. During these measurements it was possible to detect first plant disease symptoms through a combination of hyperspectral reflectance data and supervised data analysis through a combination of simplex volume maximization and support vector machine at the same day as they became visible with the naked eye, while requiring only a limited set of training data from a single cultivar, which allowed accurate disease detection in all cultivars. Hereby the transition from leaf to canopy level showed a significant impact compared with the earlier measurements within this thesis (see Chapter 3.1). Cross scattering of light and especially the differences in the intensity of reflected light

depending on the plant architecture proved to be challenging for data analysis approaches, with SVM as supervised approach having the advantage that relevant differences between healthy and symptomatic tissue being separated from the generally high data variance through the given training data. A disadvantage of the supervised method was the comparatively late disease detection at the time the first symptoms became visible to the human eye, while leaf based measurements of powdery mildew inoculated plants under laboratory conditions were able to detect powdery mildew infection two days before visible symptoms appeared with unsupervised data analysis methods (See Chapter 3.1). This disparity can be explained through the inability to select areas with developing powdery mildew symptoms before they became visible to the human eye in the canopy level measurements as the leaves did naturally move between measurements times, preventing an exact localisation of areas which would be showing symptoms later during the time-series. Despite these additional challenges, it was possible to automatically access the disease severity of all cultivars at every measurement timepoint automatically. These results showed a high correlation with manual rating of the plants.

The resistant barley cultivar Irina showed necrotic lesions after inoculation with *B. graminis* f. sp. *hordei* spores, but no development of powdery mildew symptoms. Microscopic analysis showed both papillae formation and hypersensitive reaction upon inoculation with spores of the Bgh isolate within the study, linking the observed necrotic lesions to plant resistance reaction against powdery mildew. The combination of SiVM and SVM – as described above – was also able to detect and quantify the appearance of necrotic lesions within the cultivar Irina, based on a separate set of training data, as well as differentiating the necrotic lesions from powdery mildew symptoms. These results show, that detection and quantification of both disease symptoms and resistance reactions is possible on canopy level under greenhouse conditions in high-throughput measurements within the described setup.

The developed system proved to be an efficient tool for plant phenotyping and has the potential to reduce the required manual labour within plant breeding phenotyping through automatization while simultaneously providing objective data about disease severity and resistance reactions. Despite the challenges of close-range canopy measurements, the results could be gathered with minimal requirements for training data and showed to be consistent for the different cultivars, successfully applying the results of previous laboratory studies on a scale which is relevant for practical application with sufficient measurement throughput. Thereby, the proposed system shows the potential for the future application of hyperspectral imaging in both breeding and agricultural practice.

## 5.3 Cross-scale hyperspectral data compatibility

The compatibility of hyperspectral data – which has been generated on different measurement scales – is an important factor for the application of the available results from numerous research studies within the field in agricultural practice.

Within this study powdery mildew symptoms were investigated on leaf scale

within a highly controlled laboratory environment (see Chapter 3.1), as well as on canopy scale within a greenhouse environment (see Chapter 4). It could be shown, that while the changes in environmental conditions and additional factors of canopy measurements – such as plant architecture, different light intensities in the canopy layers, light scattering within the canopy – have significant impact on the data analysis requirements, the changes in the spectral signatures of the plants during plant-pathogen interaction remain the same for both leaf and canopy scale. Comparing these spectral signatures over disease progression with those reported in the study of Kuska *et al.* (2015), which investigated the plant-pathogen interaction of barley with powdery mildew on a microscopic scale, it can be seen that the changes within the spectral profiles during disease development are comparable, despite the detection accuracy being reduced due to changes in the spatial resolution of the measurements when upscaling. These results are further supported by a study of Bohnenkamp *et al.* (2019a), which differentiated between brown rust and yellow rust on wheat leaves with hyperspectral data of rust spores as basis of classification. Bohnenkamp *et al.* (2019b) performed comparative measurements on leaf scale in the laboratory, as well as ground canopy and UAV scale in the field and were able to compare the gathered datasets the detection and quantification of yellow rust. Within their study a notable effect of the plant architecture and cross scattering of light is confirmed to introduce challenges for the canopy based measurements within the field, coinciding with the observations within the current study. While multiple studies about plant pathogen detection on different scales exist (see Chapter 1.2), the studies of Bohnenkamp *et al.* (2019a, b) – as well as the current study (see Chapters 3.1 and 4) in combination with Kuska *et al.* (2015) – show direct compatibility of hyperspectral datasets from the same disease in different scales.

The results of the current study support the thesis that the results of studies using hyperspectral data can be applied to different scales and environments, permitting practice oriented projects to make use of the wealth of available research data from scientific studies. However, it has been shown that increasing the scale from leaf to canopy adds multiple new factors within the dataset, which have to be considered during data analysis. Thereby it is especially important to modify analysis procedures of gathered hyperspectral data to fit the current task.

# References


**Aasen** H, Burkhart A, Bolten A, Bareth G (2015) Generating 3D hyperspectral information with lightweight UAV snapshot cameras for vegetation monitoring: from camera calibration to quality assurance. *ISPRS Journal of Photogrammetry and Remote Sensing* 108, 245–259.

**Anikster** Y (1982) Alternate hosts of *Puccinia hordei*. *Phytopathology* 72, 733-735.

**Anikster** Y, Szabo LJ, Eilam T, Manisterski J, Koike ST, Buschnell WR (2004) Morphology, life cycle biology, and DNA sequence analysis of rust fungi on garlic and chives from California. *Phytopathology* 94(6), 569-577.

**Arens** N, Backhaus A, Döll S, Fischer S, Seiffert U, Mock H-P (2016) Non-invasive presymptomatic detection of *Cercospora beticola* infection and identification of early metabolic responses in sugar beet. *Frontiers in Plant Science* 7, 1377.

**Asner** GP, Nepstad D, Cardinot G, Ray D (2004) Drought stress and carbon uptake in an Amazon forest measured with spaceborne imaging spectroscopy. *Proceedings of the National Academy of Sciences* 101,6039–6044.

**Bai** G, Ge Y, Hussain W, Baenziger PS, Graef G (2016) A multi-sensor system for high throughput field phenotyping in soybean and wheat breeding. *Computers and Electronics in Agriculture* 128, 181-192.

**Baranowski** P, Jedryczka M, Mazurek W, Babula-Skowronska D, Siedliska A, Kaczmarek J (2015) Hyperspectral and thermal imaging of oilseed rape (*Brassica napus*) response to fungal species of the genus *Alternaria*. *PLoS ONE*. doi:10.1371/journal. pone.0122913

**Bauckhage** C, Kersting K (2013) Data mining and pattern recognition in agriculture. *KI - Künstliche Intelligenz* 27, 313–324. doi:10.1007/s13218-013-0273-0

**Bauriegel** E, Giebel A, Herppisch WB (2011a) Hyperspectral and chlorophyll fluorescence imaging to analyse the impact of *Fusarium culmorum* on the Photosynthetic integrity of infected wheat ears. *Sensors* 11,3765–3779.

**Bauriegel** E, Giebel A, Geyer M, Schmidt U, Herpich WB (2011b) Early detection of *Fusarium* infection in wheat using hyper-spectral imaging. *Computers and Electronics in Agriculture* 75, 304–312. doi:10.1016/ j.compag.2010.12.006

**Behmann** J, Steinrücken J, Plümer L (2014) Detection of early plant stress responses in hyperspectral images. *ISPRS Journal of Photogrammetry and Remote Sensing* 93, 98–111.

**Behmann** J, Mahlein A-K, Rumpf T, Römer C, Plümer L (2015a) A review of advanced machine learning methods for the detection of biotic stress in precision crop protection. *Precision Agriculture* 16, 239–260. doi:10.1007/s11119-014-9372-7

**Behmann** J, Mahlein A-K, Paulus S, Kuhlmann H, Oerke E-C, Plümer L (2015b) Calibration of hyperspectral close-range pushbroom cameras for plant phenotyping. *ISPRS Journal of Photogrammetry and Remote Sensing* 106, 172-182.

**Behmann** J, Mahlein A-K, Paulus S, Kuhlmann H, Oerke E-C, Plümer L (2016) Generation and application of hyperspectral 3D plant models: methods and challenges. *Machine Vision and Applications* 27,611–624.

**Behmann** J, Aceborn K, Emin D, Bennertz S, Matsubara S, Thomas S, Bohnenkamp D, Kuska MT, Jussila J, Salo H, Mahlein A-K, Rascher U (2018) Specim IQ: Evaluation of a new, miniaturized handheld hyperspectral camera and its application for plant phenotyping and disease detection. *Sensors* 18(2), 441.

**Behmann** J, Bohnenkamp D, Paulus S, Mahlein A-K (2018) Spatial referencing of hyperspectral images for tracing of plant disease symptoms. *Journal of Imaging* 4, 143.

**Ben-Dor** E, Chabrillat S, Demattê JAM, Taylor GR, Hill J, Whiting ML, Sommer S (2009) Using imaging spectroscopy to study soil properties. *Remote Sensing of Environment* 113,38–55.

**Berdugo** CA, Mahlein A-K, Steiner U, Dehne H-W, Oerke E-C (2013) Sensors and imaging techniques for the assessment of the delay of wheat senescence induced by fungicides. *Functional Plant Biology* 40,677–689.

**Berdugo** CA, Zito R, Paulus S, Mahlein A-K (2014) Fusion of sensor data for the detection and differentiation of plant diseases in cucumber. *Plant Pathology* 63, 1344–1356. doi:10.1111/ppa.12219

**Bergsträsser** S, Fanourakis D, Schmittgen S, Cendrero-Mateo MP, Jansen M, Scharr H, Rascher U (2015) HyperART: non-invasive quantification of leaf traits using hyperspectral absorption-reflectance-transmittance imaging. *Plant Methods* 11, 1–17. doi:10.1186/s13007-015-0043-0

**Bhat** R, Miklis M, Schmelzer E, Schulze-Lefert P, Panstruga R (2005) Recruitment and interaction dynamics of plant penetration resistance components in a plasma membrane microdomain. *Proceedings of the National Academy of Sciences of the United States of America* 102, 3135–3140. doi:10.1073/pnas.0500012102

**Bishop** CM (2006) *Pattern recognition and machine learning*. Springer, New York.

**Blackburn** GA (2007) Hyperspectral remote sensing of plant pigments. *Journal of Experimental Botany* 58, 855–867. doi:10.1093/jxb/erl123

**Blei** DM (2012) Probabilistic topic models. *Communications of the ACM* 55, 77–84.

**Bock** CH, Poole GH, Parker PE, Gottwald TR (2010) Plant disease severity estimated visually, by digital photography and image analysis, and by hyperspectral imaging. *Critical Reviews in Plant Sciences* 29, 59–107. doi:10.1080/07352681003617285

**Bohnenkamp** D, Kuska MT, Mahlein A-K, Behmann, J (2019a) Hyperspectral signal decomposition and symptom detection of wheat rust disease at the leaf scale using pure fungal spore spectra as reference. *Plant Pathology* 68, 1188-1195.

**Bohnenkamp** D, Behmann J, Mahlein A-K (2019b) In-field detection of yellow rust in wheat on the ground canopy and UAV scale. *Remote Sensing* 11, 2495.

**Brakke** TW (1994) Specular and diffuse components of radiation scattered by leaves. *Agricultural and Forest Meteorology* 71, 283–295. doi:10.1016/0168-1923(94)90016-7

**Bravo** C, Moshou D, West J, McCartney A, Ramon H (2003) Early disease detection in wheat fields using spectral reflectance. *Biosystems Engineering* 84, 137–145.

**Bravo** C, Moshou D, Oberti R, West J, McCartney A, Bodria L, Ramon H (2004) Foliar disease detection in the feld using optical sensor fusion. *Agricultural Engineering International: the CIGR Journal of Scientific Research and Development* 6, 1–14

**Busemeyer** L, Mentrup D, Möller K, Wunder E, Alheit K, Hahn V, Maurer HP, Reif JC, Würschum T, Müller J, Rahe F, Ruckelshausen A (2013) BreedVision – a multi-sensor platform for non-destructive field-based phenotyping in plant breeding. *Sensors* 13(3), 2830-2847.

**Cao** X, Luo Y, Zhou Y, Duan X, Cheng D (2013) Detection of powdery mildew in two winter wheat cultivars using canopy hyperspectral reflectance. *Crop Protection* 45, 124-131.

**Carocho** M, Ferreira ICFR (2013) A review on antioxidants, prooxidants and related controversy: natural and synthetic compounds, screening and analysis methodologies and future perspectives. *Food and Chemical Toxicology* 51, 15–25.

**Carter** G, Knapp A (2001) Leaf optical properties in higher plants: linking spectral characteristics to stress and chlorophyll concentration. *American Journal of Botany* 88, 677–684. doi:10.2307/2657068

**Chang** CC, Lin CJ (2011) LIBSVM: A library for support vector machines. *ACM Transactions on Intelligent Systems and Technology*. doi:10.1145/1961189.1961199

**Christiansen** SK, Justesen AF, Giese H (1997) Disparate sequence characteristics of the *Erysiphe graminis* f. sp. *hordei* glyceraldehyde-3- phospahte dehydrogenase gene. *Current Genetics* 31, 525–529. doi:10.1007/s002940050240

**Cortes** C, Vapnik V (1995) Support-vector networks. *Machine Learning* 20, 273-297.

**Damm** A, Guanter L, Verhoef W, Schläpfer D, Garbari S, Schaepman ME (2015) Impact of varying irradiance on vegetation indices and chlorophyll fluorescence derived from spectroscopy data. *Remote Sensing of Environment* 156, 202-215.

**Dean** R, Van Kan JAL, Pretorius ZA, Hammond-Kosack KE, Pietro AD, Spanu PD, Rudd JJ, Dickman M, Kahmann R, Ellis J, Foster GD (2012) The top 10 fungal pathogens in molecular plant pathology. *Molecular Plant Pathology* 13, 414–430. doi:10.1111/j.1364-3703.2011.00783.x

**Deery** D, Jimenez-Berni J, Jones H, Sirault X, Furbank R (2014) Proximal remote sensing buggies and potential applications for field-based phenotyping. *Agronomy* 4(3), 349–379.

**Delalieux** S, Somers B, Verstaeten WW, Keulemans W, Coppin P (2008) Hyperspectral canopy measurements under artificial illumination. *International Journal of Remote Sensing* 29(20), 6051–6058.

**Delalieux** S, Somers B, Verstaeten WW, Vanaardt JAN, Keulemans W, Coppin P (2009) Hyperspectral indices to diagnose leaf biotic stress on apple plants, considering leaf phenology. *International Journal of Remote Sensing* 30(8), 1887–1912.

**Demattê** JAM, Demattê JLI, Camargo WP, Fiorio PR, Nanni MR (2001) Remote sensing in the recognition and mapping of tropical soils developed on topographic sequences. *Mapping Sciences and Remote Sensing* 38, 79–102.

**Devadas** R, Lamb DW, Simpfendorfer S, Backhouse D (2009) Evaluating ten spectral vegetation indices for identifying rust infection in individual wheat leaves. *Precision Agriculture* 10, 459–470.

**Dhillon** IS, Modha DS (2001) Concept decompositions for large sparse text data using clustering. *Machine Learning* 42, 143–175. doi:10.1023/ A:1007612920971

**Elvidge** CD, Keith DM, Tuttle BT, Baugh KE (2010) Spectral identification of lighting type and character. *Sensors* 10(4), 3961–3988.

**Fiorani** F, Rascher U, Jahnke S, Schurr U (2012) Imaging plants dynamics in heterogenic environments. *Current Opinion in Biotechnology* 23, 227–235. doi:10.1016/j.copbio.2011.12.010

**Fiorani** F, Schurr U (2013) Future scenarios for plant phenotyping. *Annual Review of Plant Biology* 64, 267–291.

**Furbank** RT, Tester M (2011) Phenomics – technologies to relieve the phenotyping bottleneck. *Trends in Plant Science* 16, 635–644. doi:10.1016/j.tplants.2011.09.005

**Govender** M, Dye PJ, Weiersbye IM, Witkowski ETF, Ahmed F (2009) Review of commonly used remote sensing and groundbased technologies to measure plant water stress. *Water SA* 35, 741–752.

**Granier** C, Vile D (2014) Phenotyping and beyond: modelling the relationships between traits. *Current Opinion in Plant Biology* 18, 96–102.

**Grieve** B, Hammersley S, Mahlein A-K, Oerke E-C, Goldbach H (2015) Localized multispectral crop imaging sensors: engineering and validation of cost effective plant stress and disease sensors. In: IEEE sensors applications symposium (SAS), Zadar, pp 1–6.

**Großkinsky** DK, Svengaard J, Christensen S, Roitsch T (2015) Plant phenomics and the need for physiological phenotyping across scales to narrow the genotype-to-phenotype knowledge gap. *Journal of Experimental Botany* 66(18), 5429–5440.

**Gubatz** S, Dercksen VJ, Brüß C, Weschke W, Wobus U (2007) Analysis of barley (*Hordeum vulgare*) grain development using three-dimensional digital models. *The Plant Journal* 52, 779–790.

**Gullino** ML, Kuijpers LAM (1994) Social and political implications of managing plant diseases with restricted fungicides in Europe. *Annual Review of Phytopathology* 32, 559-79.

**Hack** H, Bleiholder H, Buhr L, Meier U, Schnock-Fricke U, Weber E, Witzenberger A (1992) Einheitliche Codierung der phänologischen Entwicklungsstadien mono- und dikotyler Pflanzen – erweiterte BBCHSkala. *Allgemeines Nachrichtenblatt des deutschen Pflanzenschutzdienstes* 44, 265–270

**Hamid** Muhammed H, Larsolle A (2003) Feature vector based analysis of hyperspectral crop reflectance data for discrimination of fungal disease severity in wheat. *Biosystems Engineering* 86, 125–134. doi:10.1016/ S1537-5110(03)00090-4

**Hbirkou** C, Pätzhold S, Mahlein A-K, Welp G (2012) Airborne hyperspectral imaging of spatial soil organic carbon heterogeneity at the field-scale. *Geoderma* 175–176, 21–28

**Hillnhütter** C, Mahlein A-K, Sikora RA, Oerke E-C (2011) Remote sensing to detect plant stress induced by *Heterodera schachtii* and *Rhizoctonia solane* in sugar beet fields. *Field Crops Research* 122, 70-77.

**Hillnhütter** C, Mahlein A-K, Sikora RA, Oerke E-C (2012) Use of imaging spectroscopy to discriminate symptoms caused by *Heterodera schachtii* and *Rhizoctonia solani* on sugar beet. *Precision Agriculture* 13, 17–32. doi:10.1007/s11119-011-9237-2

**Hinze** K, Thompson R, Ritter E, Salamini F, Schulze-Lefert P (1991) Restriction fragment length polymorphism-mediated targeting of the *ml-o* resistance locus in barley (*Hordeum vulgare*). *Proceedings of the National Academy of Sciences of the United States of America* 88, 3691–3695. doi:10.1073/pnas.88.9.3691

**Huang** J-F, Apan A (2006) Detection of *Sclerotinia* rot disease on celery using hyperspectral data and partial least squares regression. *Journal of Spatial Science* 51, 129–142.

**Huang** W, Lamb DW, Niu Z, Zhang Y, Liu L, Wang J (2007) Identification of yellow rust in wheat using in situ spectral reflectance measurements and airborne hyperspectral imaging. *Precision Agriculture* 8,187–197.

**Humplík** JF, Lazár D, Husičková A, Spíchal L (2015) Automated phenotyping of plant shoots using imaging methods for analysis of plant stress responses – a review. *Plant Methods* 11, 29.

**Hückelhoven** R, Panstruga R (2011) Cell biology of the plant-powdery mildew interaction. *Current Opinion in Plant Biology* 14, 738–746. doi:10.1016/j.pbi.2011.08.002

**Jacquemoud** S, Verhoef W, Baret F, Bacour C, Zarco-Tejada PJ, Asner GP, François C, Ustin SL (2009) PROSPECT + SAIL models: a review of use for vegetation characterization. *Remote Sensing of Environment* 113, 56–66.

**Jensen,** J. R (2006) *Remote Sensing of the Environment: An Earth Resource Perspective 2/e*. Upper saddle River: Pearson Education.

**Joalland** S, Screpanti C, Liebisch F, Varella HV, Gaume A, Walter A (2017) Comparison of visible imaging, thermography and spectrometry methods to evaluate the effect of *Heterodera schachtii* inoculation on sugar beets. *Plant Methods* 13, 73.

**Jørgensen** JH (1977) Spectrum of resistance conferred by ml-o powdery mildew resistance genes in barley. *Euphytica* 26, 55–62. doi:10.1007/ BF00032068

**Jørgensen** JH, Wolfe M (1994) Genetics of powdery mildew resistance in barley. *Critical Reviews in Plant Sciences* 13, 97–119. doi:10.1080/ 07352689409701910

**Kersting** K, Wahabzada M, Römer C, Thurau C, Ballvora A, Rascher U, Léon J, Bauckhage C, Plümer L (2012a) Simplex distributions for embedding data matrices over time. In 'Proceedings of the 2012 SIAM international conference on data mining, Anaheim'. (Eds J Ghosh, H Liu, I Davidson, C Domeniconi, C Kamath) pp. 295–306. (American Statistical Association: Alexandria, VA, USA).

**Kersting** K, Xu Z, Wahabzada M, Bauckhage C, Thurau C, Römer C, Ballvora A, Rascher U, Leon J, Plümer L (2012b) Presymptomatic prediction of plant drought stress using dirichlet–aggregation regression on hyperspectral images. In: Proceedings of the tetny-sixth AAAI conference on artificial intelligence, pp 302–308.

**Keshava** N, Mustard J F (2002) Spectral Unmixing. *IEEE Signal Processing Magazine* 19, 44-57.

**Kildea** S, Dooley H, Phelan S, Mehenni-Ciz J, Spink J (2017) Developing fungicide control programmes for blotch in Irish winter wheat crops. In 'Modern Fungicides and Antifungal Compounds'. (Eds Deising HB, Fraaije B, Mehl A, Oerke EC, Sierotzki H, Stammler G) Vol. VIII, pp 171-174. (Deutsche Phytomedizinische Gesellschaft, Braunschweig), ISBN: 978-3-941261-15-0.

**Kim** DM, Zhang H, Zhou H, Du T, Wu Q, Mockler TC, Berezin MY (2015) Highly sensitive image-derived indices of water-stressed plants using hyperspectral imaging in SWIR and histogram analysis. *Scientific Reports* 5, 15919. doi:10.1038/srep15919

**Kleinhofs** A, Kilian A, Maroof MAS, Biyashev RM, Hayes P, Chen FQ, Lapitan N, Fenwick A, Blake TK, Kanazin V, Ananiev E, Dahleen L, Kudran D, Bollinger J, Knapp SJ, Liu B, Sorrells M, Heun M, Franckowiak JD, Hoffmann D, Skadsen R, Steffenson BJ (1993) A molecular, isozyme and morphological map of barley (*Hordeum vulgare*) genome. *Theoretical and Applied Genetics* 86, 705-712.

**Knipling** EB (1970) Physical and physiological basis for the reflectance of visible and near-infrared radiation from vegetation. *Remote Sensing of Environment* 1, 155–159. doi:10.1016/S0034-4257(70)80021-9

**Kruse** FA, Lefkoff AB, Boardman JW, Heidebrecht KB, Shapiro AT, Barloon PJ, Goetz AFH (1993) The spectral image processing system (SIPS)-interactive visualization and analysis of imaging spectrometer data. *Remote Sensing of the Environment* 44, 145–163.

**Kuska** M, Wahabzada M, Leucker M, Dehne H-W, Kersting K, Oerke EC, Steiner U, Mahlein A-K (2015) Hyperspectral phenotyping on the microscopic scale: towards automated characterization of plant-pathogen interactions. *Plant Methods* 11, 28. doi:10.1186/s13007-015- 0073-7

**Kuska** MT, Brugger A, Thomas S, Wahabzada M, Kersting K, Oerke E-C, Steiner U, Mahlein A-K (2017) Spectral patterns reveal early resistance reactions of barley against *Blumeria graminis* f. sp. *hordei*. *Phytopathology* 107, 1388-1398.

**LeCun** Y, Bengio Y, Hinton G (2015) Deep learning. *Nature* 521, 436–444.

**Leucker** M, Mahlein A-K, Steiner U, Oerke E-C (2016a) Improvement of lesion phenotyping in *Cercospora beticola*-sugar beet interaction by hyperspectral imaging. *Phytopathology* 1, 1–30. doi:10.1094/PHYTO- 04-15-0100-R

**Leucker** M, Wahabzada M, Kersting K, Peter M, Beyer W, Steiner U, Mahlein A-K, Oerke E-C (2016b) Hyperspectral imaging reveals the effects of sugar beet QTLs on *Cercospora* leaf spot resistance. *Functional Plant Biology* doi:10.1071/FP16121

**Leucker** M, Wahabzada M, Kersting K, Peter M, Beyer W, Steiner U, Mahlein A-K, Oerke E-C (2017) Hyperspectral imaging reveals the effect of sugar beet quantitative trait loci on *Cercospora* leaf spot resistance. *Functional Plant Biology* 44, 1–9.

**Li** H, Lee WS, Wang K, Ehsani R, Yang C (2014) 'Extended spectral angle mapping (ESAM)' for citrus greening disease detection using airborne hyperspectral imaging. *Precision Agriculture* 15, 162–183.

**Liu** Z, Ellwood SR, Oliver RP, Friesen TL (2011) *Pyrenophora teres*: profile of an increasingly damaging barley pathogen. *Molecular Plant Pathology* 12(1), 1-19.

**Liu** Z, Holmes DJ, Faris JD, Chao S, Brueggeman RS, Edwards MC, Friesen TL (2015) Necrotrophic effector-triggered susceptibility (NETS) underlies the barley–*Pyrenophora teres* f. *teres* interaction specific to chromosome 6H. *Molecular Plant Pathology* 16(2), 188-200.

**Lobet** G (2017) Image analysis in plant sciences: publish then perish. *Trends in Plant Science* 22(7), 559–66.

**Lumbroso** E, Anikster Y, Moseman JG, Wahl I (1977) Completion of life cycles of *Pucchinia hordei* and *Uromyces scillarum* on detached leaves of their hosts. *Phytopathology* 67, 941-944.

**Mahalanobis** A, Vijaya Kumar B V K, Sims S R F (1996) Distance-classifier correlation filters for multiclass target recognition. *Applied Optics* 35, 3127-3133.

**Mahlein** A-K (2016) Plant disease detection by imaging sensors – parallels and specific demands for precision agriculture and plant phenotyping. *Plant Disease* 100, 241–251. doi:10.1094/PDIS-03-15-0340-FE

**Mahlein** A-K, Steiner U, Dehne H-W, Oerke E-C (2010) Spectral signatures of sugar beet leaves for the detection and differentiation of diseases. *Precision Agriculture* 11, 413–431. doi:10.1007/s11119-010-9180-7

**Mahlein** A-K, Steiner U, Hillnhütter C, Dehne H-W, Oerke E-C (2012) Hyperspectral imaging for small-scale analysis of symptoms caused by different sugar beet diseases. *Plant Methods* 8, 3. doi:10.1186/1746- 4811-8-3

**Mahlein** A-K, Rumpf T, Welke P, Dehne H-W, Plümer L, Steiner U, Oerke E-C (2013) Development of spectral indices for detecting and identifying plant diseases. *Remote Sensing of Environment* 128, 21–30. doi:10.1016/j.rse.2012.09.019

**Mahlein** A-K, Hammersley S, Oerke E-C, Dehne H-W, Goldbach H, Grieve B (2015) Supplemental blue LED lighting array to improve the signal quality in hyperspectral imaging of plants. *Sensors* 15(6), 12834–12840.

**Mahoney** M, Drineas P (2009) CUR matrix decompositions for improved data analysis. *Proceedings of the Natural Academy of Sciences* 106, 697–702.

**Martinelli** F, Scalenghe R, Davino S, Panno S, Scuderi G, Ruisi P, Villa P, Stroppiana D, Boschetti M, Guolart LR, Davis CE, Dandekar AM (2014) Advanced methods for plant disease detection. A review. *Agronomy for sustainable Development* 35,1–25.

**Melgani** F, Bruzzone L (2004) Classification of hyperspectral remote sensing images with support vector machines. *IEEE Transactions on Geoscience and Remote Sensing* 42, 1778–1790.

**Milton** EJ, Shaepmann ME, Anderson K, Kneubühler M, Fox N (2009) Progress in field spectroscopy. *Remote Sensing of Environment* 113, 92–109.

**Mirik** M, Michels GJ, Kassymzhanova-Mirik S, Elliot NC, Bowling R (2006) Hyperspectral spectrometry as a means to differenciate uninfested and infested winter wheat by greenbug (*Hemiptera: Aphididae*). *Journal of Economic Entomology* 99(5), 1682–1690.

**Moll** E, Flath K, Sellmann J (2009) Schätzen der Befallsstärke – (k)ein Problem. *Journal für Kulturpflanzen* 61(12), 440-442.

**Montes** JM, Technow F, Dhillon BS, Mauch F, Melchinger AE (2011) High-throughput non-destructive biomass determination during early plant development in maize under field conditions. *Field Crops Research* 121, 268–273.

**Moshou** D, Bravo C, Oberti R, West J, Bodria L, McCartney A, Ramon H (2005) Plant disease detection based on data fusion of hyper-spectral and multi-spectral fluorescence imaging using Kohonen maps. *Real Time Imaging* 11, 75–83.

**Mutka** AM, Bart RS (2014) Image-based phenotyping of plant disease symptoms. *Frontiers in Plant Science* 5, 734.

**Nevalainen** O, Honkavaara E, Touminen S, Viljanen N, Hakala T, Yu X, Hyyppä J, Saari H, Pölönen I, Imai NN, Tommaselli AMG (2017) Individual tree detection and classification with UAV-based photogrammetric point clouds and hyperspectral imaging. *Remote Sensing* 9, 185.

**Oerke** E-C, Dehne H-W (2004) Safeguarding production–losses in major crops and the role of crop protection. *Crop Protection* 23, 275-285.

**Oerke** E-C, Mahlein A-K, Steiner U (2014) Proximal sensing of plant diseases. In: 'Detection and diagnostics of plant pathogens'. (Eds Gullino ML, Bonants PJM) pp 55–68. (Springer, Dordrecht). doi:10.1007/978-94-017-9020-8_4

**Petersen** RH (1974) The rust fungus life cycle. *The Botanical Review* 40, 453-513.

**Pinto** F, Damm A, Schickling A, Panigada C, Cogliati S, Müller-Linow M, Balcora A, Rascher U (2016) Sun-induced chlorophyll fluorescence from high-resolution imaging spectroscopy data to dandify spatio-temporal patterns of photosynthetic function in crop canopies. Plant, *Cell and Environment* 39, 1500-1512.

**Plaza** A, Benediktsson JA, Boardman JW, Brazlie J, Bruzzone L, Camps-Valls G, Chanussot J, Fauvel M, Gamba P (2009) Recent advances in techniques for hyperspectral image processing. *Remote Sensing of the Environment* 113, 110–122.

**Polder** G, van der Heijden GWAM, van Doorn J, Baltissen TAHMC (2014) Automatic detection of tulip breaking virus (TBV) in tulip fields using machine vision. *Biosystems Engineering* 117, 35–42.

**Poorter** H, Bühler J, van Dusschoten D, Climent J, Postma JA (2012) Pot size matters: a meta-analysis of the effects of rooting volume on plant growth. *Functional Plant Biology* 39, 839-850.

**Python** matrix factorization module. https://code.google.com/p/pymf/. Accessed 12 May 2017.

**Rangel** LI, Spanner RE, Ebert MK, Pethybridge SJ, Stukenbrock EH, de Jonge R, Secor GA, Bolton MD (2020) Cercospora beticola: The intoxicating lifestyle of the leaf spot pathogen of sugar beet. *Molecular Plant Pathology* 21, 1020–1041. https://doi.org/10.1111/mpp.12962

**Rascher** U, Nichol CJ, Small C, Hendricks L (2007) Monitoring spatiotemporal dynamics of photosynthesis with a portable hyperspectral imaging system. *Photogrammetric Engineering and Remote Sensing* 73, 45–56. doi:10.14358/PERS.73.1.45

**Rascher** U, Blossfeld S,Fiorani F, Jahnke S, Jansen M,Kuhn AJ,Matsubara S, Märtin LLA, Merchant A, Metzner R, Müller-Linof M, Nagel KA, Pieruschka R, Pinto F, Schreiber CM, Temperton VM, Thorpe MR, Dusschoten D, Volkenburgh E, Windt CW, Schurr U (2011) Non-invasive approaches for phenotyping of enhanced performance traits in bean. *Functional Plant Biology* 38, 968–983. doi:10.1071/ FP11164

**Rodionov** A, Welp G, Damerow L, Berg T, Amelung W, Pätzold S (2015) Towards on-the-go field assessment of soil organic carbon using Vis-NIR diffuse reflectance spectroscopy: developing and testing a novel tractor-driven measuring chamber. *Soil and Tillage research* 145, 93–102.

**Römer** C, Wahabzada M, Ballvora C, Pinto F, Rossini M, Panigada C, Behmann J, Léon J, Thurau C, Bauckhage C, Kersting K, Rascher U, Plümer L (2012) Early drought stress detection in cereals: simplex volume maximisation for hyperspectral image analysis. *Functional Plant Biology* 39, 878–890.

**Roscher** R, Behmann J, Mahlein A-K, Dupuis J, Kuhlmann H, Plümer L (2016) Detection of disease symptoms on hyperspectral 3D plant models. *ISPRS Annals of Photogrammetry, Remote Sensing and Spatial Information Sciences* 3(7), 89–96.

**Rouse** JW, Haas RH, Schell JA, Deering DW (1974) Monitoring vegetation systems in the great plains with ERTS. In 'Third earth resources technology satellite-1 symposium. Volume I: technical presentations'. (Eds Freden SC, Mercanti EP, Becker M ) pp 309–317. (Washington DC: NASA SP-351).

**Rumpf** T, Mahlein A-K, Steiner U, Oerke E-C, Dehne H-W, Plümer L (2010) Early detection and classification of plant diseases with support vector machines based on hyperspectral reflectance. *Computers and Electronics in Agriculture* 74, 91–99.

**Sandmeier** ST, Müller CH, Hosgood B, Andreoli G (1998) Physical mechanisms in hyperspectral BRDF data of grass and watercress. *Remote Sensing of Environment* 66, 222-223.

**Sankaran** S, Mishra A, Ehsani R, Davis C (2010) A review of advanced techniques for detecting plant diseases. *Computers and Electronics in Agriculture* 72, 1–13. doi:10.1016/j.compag.2010.02.007

**Sankaran** S, Eshani R, Inch SA, Ploetz RC (2012) Evaluation of visiblenear infrared reflectance spectra of avocado leaves as non-destructive sensing tool for detection of laurel wilt. *Plant Disease* 96, 1683–1689. doi:10.1094/PDIS-01-12-0030-RE

**Sankaran** S, Khot LR, Espinoza CZ, Jarolmasjed S, Sathuvalli VR, Vandemark GJ, Miklas PN, Carter AH, Pumphrey MO, Knowles NR, Pavek KJ (2015) Low-altitude, high-resolution aerial imaging systems for row and field crop phenotyping: a review. *European Journal of Agronomy* 70, 112–123.

**Savitzky** A, Golay M (1964) Smoothing and differentiation of data by simplified least squares procedures. *Analytical Chemistry* 36, 1627–1639. doi:10.1021/ac60214a047

**Schulte** D, Close TJ, Graner A, Langridge P, Matsumoto T, Muehlbauer G, Sato K, Schulman AH, Waugh R, Wise RP, Stein N (2009) The international barley sequencing consortium—at the threshold of efficient access to the barley genome. *Plant Physiology* 149(1), 142-147. doi: 10.1104/pp.108.128967

**Shakoor** N, Lee S, Mockler TC (2017) High throughput phenotyping to accelerate crop breeding and monitoring of diseases in the feld. *Current Opinion in Plant Biology* 38, 184–92.

**Simko** I, Jiminez-Berni JA, Sirault XRR (2017) Phenomic approaches and tool for phytopathologists. *Phytopathology* 107, 6–17.

**Singh** A, Ganapathysubramanian B, Singh AK, Sarkar S (2016) Machine learning for high-throughput stress phenotyping in plants. *Trends in Plant Science* 21, 110–124. doi:10.1016/j.tplants.2015.10.015

**Steinkamp** M, Martin S, Hoefert L, Ruppel E (1979) Ultrastructure of lesions produced by Cercospora beticola in leaves of Beta vulgaris. *Physiological Plant Pathology* 15, 13–26.

**Suzuki** Y, Hiroshi O, Takashi K (2008) Image segmentation between crop and weed using hyperspectral imaging for weed detection in soybean field. *Environment Control in Biology* 46, 163–173. doi:10.2525/ecb. 46.163

**Tackenberg** M, Volkmar C, Dammer K-H (2016) Sensor-based variable-rate fungicide application in winter wheat. *Pest Management Science* 72(10), 1888–1896.

**Tardieu** F, Cabrera-Bosquet L, Pridmore T, Bennett M (2017) Plant phenomics, from sensors to knowledge. *Current Biology* 15(7), R770-R783.

**Thomas** S, Wahabzada M, Kuska M, Rascher U, Mahlein A-K (2017) Observation of plant–pathogen interaction by simultaneous hyperspectral imaging reflection and transmission measurements. *Functional Plant Biology* 44, 23-34.

**Thurau** C, Kersting K, Wahabzada M, Bauckhage C (2012) Descriptive matrix factorization for sustainability adopting the principle of opposites. *Data Mining and Knowledge Discovery* 24, 325–354. doi:10.1007/s10618-011-0216-z

**Tilman** D (1999) Global environmental impacts of agricultural expansion: the need for sustainable and efficient practices. *Proceedings of the National Academy of Sciences of the Unites States of America* 96(11), 5995-6000.

**Underwood** W (2012) The plant cell wall: a dynamic barrier against pathogen invasion. *Frontiers in Plant Science*. doi: 10.3389/fpls.2012.00085

**Ustin** SL, Gamon JA (2010) Remote sensing of plant functional types. *New Phytologist* 186, 795–816.

**Vigneau** N, Ecarnot M, Rabatel G, Roumet P (2011) Potential of field hyperspectral imaging as a non destructive method to assess leaf nitrogen content in wheat. *Field Crops Research* 122, 25-31.

**Virlet** N, Sabermanesh K, Sadeghi-Tehran P, Hawkesford MJ (2017) Field scanalyzer: An automated robotic field phenotyping platform for detailed crop monitoring. *Functional Plant Biology* 44, 143-153.

**Voegele** RT (2006) *Uromyces fabae*: development, metabolism, and interactions with its host *Vicia faba*. *FEMS Microbiology Letters* 259(2), 165-173.

**Voegele** RT, Hahn M, Mendgen K (2009) The *Uredinales*: Cytology, Biochemistry, and Molecular Biology. In: 'Plant Relationships. The Mycota (A Comprehensive Treatise on Fungi as Experimental Systems for Basic and Applied Research)'. (Eds. Deising H.B.) vol 5. (Springer, Berlin, Heidelberg).

**Vogelmann** TC (1989) Penetration of light into plants. *Photochemistry and Photobiology* 50, 895–902. doi:10.1111/j.1751-1097.1989.tb02919.x

**Vogelmann** TC (1993) Plant tissue optics. *Plant Molecular Biology* 44, 231–251.

**Vogelmann** TC, Gorton HL (2014) Leaf: light capture in the photosynthetic organ. In 'The structural basis of biological energy generation'. (Ed. MF Hohmann-Marriott) pp. 363–377. (Springer:Dordrecht,TheNetherlands).

**Wahabzada** M, Kersting K, Bauckhage C, Römer C, Ballvora A, Pinto F, Rascher U, Léon J, Plümer L (2012) Latent dirichlet allocation uncovers spectral characteristics of drought stressed plants. *arXiv preprint*. arXiv:1210.4919.

**Wahabzada** M, Mahlein A-K, Bauckhage C, Steiner U, Oerke EC, Kersting K (2015a) Metro maps of plant disease dynamics – automated mining of differences using hyperspectral images. *PLoS One* 10, e0116902. doi:10.1371/journal.pone.0116902

**Wahabzada** M, Paulus S, Kersting K, Mahlein A-K (2015b) Automated interpretation of 3D laserscanned point clouds for plant organ segmentation. *BMC Bioinformatics* 16, 248.

**Wahabzada** M, Mahlein A-K, Bauckhage C, Steiner U, Oerke EC, Kersting K (2016) Plant phenotyping using probabilistic topic models: uncovering the hyperspectral language of plants. *Scientific Reports* 6, 22482. doi:10.1038/srep22482

**Walter** A, Liebisch F, Hund A (2015) Plant Phenotyping: from bean weighting to image analysis. *Plant Methods* 11, 14.

**Walters** DR, Avrova A, Bingham IJ, Burnett FJ, Fountaine J, Havis ND, Hoad SP, Hughes G, Looseley M, Oxley SJP, Renwick A, Topp CFE, Newton AC (2012) Control of foliar disease in barley: Towards an integrated approach. *European Journal of Plant Pathology* 133,33–73.

**Wei** F, Wing RA, Wise RP (2002) Genome dynamics and evolution of the *Mla* (powdery mildew) resistance locus in barley. *The Plant Cell* 14, 1903–1917. doi:10.1105/tpc.002238

**West** JS, Bravo C, Oberti R, Lemaire D, Moshou D, McCartney HA (2003) The potential of optical canopy measurement for targeted control of field crop diseases. *Phytopathology* 41, 593–614. doi:10.1146/annurev. phyto.41.121702.103726

**West** JS, Bravo C, Oberti R, Moshou D, Ramon H, McCartner HA (2010) Detection of fungal disease optically and pathogen inoculums by air sampling. In: 'Precision crop protection-the challenge and use of heterogeneity'. (Eds Oerke E-C, Gerhards R, Menz G, Sikora RA) pp 135–149. (Springer, Dordrecht).

**Wicker** T, Mayer KFX, Gundlach H, Martis M, Steuernagel B, Scholz U, Šimková H, Kubaláková M, Choulet F, Taudien S, Platzer M, Feuillet C, Fahima T, Budak H, Doležel J, Keller B, Stein N (2011) Frequent gene movement and pseudogene evolution is common to the large and complex genomes of wheat, barley, and their relatives. *The Plant Cell* 23(5), 1706-1718, doi: 10.1105/tpc.111.086629

**Winterhalter** L, Mistele B, Jampatong S, Schmidhalter U (2011) High throughput phenotyping of canopy water mass and canopy temperature in well-watered and drought stressed tropical maize hybrids in the vegetative stage. *European Journal of Agronomy* 35, 22–32.

**Wold** S, Esbensen K, Geladi P (1987) Principal component analysis. *Chemometrics and Intelligent Laboratory Systems* 2, 37–52. doi:10.1016/ 0169-7439(87)80084-9

**Woolley** J (1971) Reflectance and transmittance of light by leaves. *Plant Physiology* 47, 656–662. doi:10.1104/pp.47.5.656

**Yeh** YH, Chung WC, Liao JY, Chung CL, Kuo YF, Lin TT (2016) Strawberry foliar anthracnose assessment by hyperspectral imaging. *Computers and Electronics in Agriculture* 122, 1–9.

**Yin** X, Struik PC, Kropf MJ (2004) Role of crop physiology in predicting gene-to-phenotype relationships. *Trends in Plant Science* 9(9), 426–432.

**Yuan** L, Zhang J, Shi Y, Nie C, Wie L, Wang J (2014) Damage mapping of powdery mildew in winter wheat with high-resolution satellite image. *Remote Sensing* 6, 3611–3623. doi:10.3390/rs6053611

**Zhang** M, Liu X, O'Neill M (2002) Spectral discrimination of *Phytophthora infestans* infection on tomatoes based on principal component and cluster analyses. *International Journal of Remote Sensing* 23, 1095–1107. doi:10.1080/01431160110106078

**Zhao** YR, Xiaoli L, Yu KQ, Cheng F, He Y (2016) Hyperspectral imaging for determining pigment contents in cucumber leaves in response of angular leaf spot disease. *Scientific Reports* 6, 27790.

**Zohary** D, Hopf M (2001) *Domestication of plants in the old world*, Ed 3. Oxford University Press, Oxford, UK, pp 1–12.

# Danksagung

Ich möchte mich ganz Herzlich bei allen meinen Kollegen aus dem INRES der Universität Bonn, sowie dem IGB2 des Forschungszentrum Jülich bedanken, welche mich im Laufe meiner Promotion immer mit guten Ratschlägen, positiver Einstellung und vorbehaltsloser Kooperation unterstützt haben. Ich bedanke mich auch besonders für die stets gute Atmosphäre an beiden Einrichtungen und die Herzlichkeit mit deinen mich alle meine Kollegen aufgenommen haben.

Insbesondere möchte ich mich auch bei Frau Professor Dr. Anne-Katrin Mahlein vom Institut für Zukerrübenforschung der Universität Göttingen bedanken, welche mir als meine Betreuerin stets mit Rat, Tat und viel Geduld zur Seite stand, während sie mich gleichzeitig selbstständig arbeiten ließ und immer für fachliche Gespräche zur Verfügung stand. Anne hat mich nach meiner Bewerbung auf das Projekt in den Bereich der optischen Sensorik eingeführt und mir somit diesen sehr interessanten Aspekt der Forschung, mit dem ich innerhalb meiner vorherigen Studienzeit noch nicht in Berührung gekommen war hervorragend nahegebracht, was sicher auch meine Zukunft in meiner wissenschaftlichen Laufbahn stark beeinflusst hat. Ebenfalls möchte ich mich herzlichst bei Professor Dr. Uwe Rascher vom IGB2 des Forschungszentrum Jülich bedanken, welcher mir als Zweiter Betreuer im Rahmen unserer Kooperation innerhalb des CROP.SENSe.net Forschungsnetzwerks ermöglicht hat im Forschungszentrum Jülich zu arbeiten, wo er mir stets mit guten Ratschlägen, interessanten Diskussionen und den erheblichen Ressourcen des Forschungszentrums begleitet hat. Weiterhin möchte ich mich auch sehr bei Professor Dr. Peter Dörrmann vom Institut für Molekulare Physiologie und Biotechnologie der Pflanzen bedanken, welcher mir die Ehre erwies trotz dem für ihn ungewöhnlichen Forschungsbereich mit hyperspektralen Sensoren als Zweitgutachter für meine Doktorarbeit zur Verfügung zu stehen und der in unseren Gesprächen immer großes Interesse an dem Thema zeigte und mich bei meinem Vorhaben unterstützte.

Weiterhin bin ich Herrn Professor Dr. Heinz-Wilhelm Dehne, Frau PD Dr. Ulrike Steiner und PD Dr. Erich-Christian Oerke vom INRES, sowie Herrn Dr. Onno Müller vom IBG2 zu großem Dank verpflichtet, da sie mich während meiner Arbeit stets mit gutem Rat und konstruktiver Kritik unterstützt haben. Von meinen Kollegen möchte ich mich besonder bei Jennifer Stracke, Kerstin Lange, Carolin Sichterman, Dr. Marlene Leuker und Dr. Matheus Kuska für die vielfältige Unterstützung während des Projekts, sowie Marlene und Matheus auch für die interessanten Interaktionen zwischen unseren jeweiligen Projekten bedanken. Dr. Jan Behmann und Dr. Mirwaes Wahabzada danke ich herzlichst für ihre Unterstützung im Bereich Datenauswertung und Statistik während meines Projekts und die fachliche Hilfe im Bereich Datenanalytik.

Da dieses Projekt im Rahmen des Agroclusters CROP-SENSe.net Kompetenznetzwerk der Phänotypisierungsforschung durchgeführt wurde möchte ich mich auch beim BMBF bedanken, dessen finanzielle Unterstützung die Durchführung des Projekts möglich machte.

Zum Abschluss möchte ich mich noch bei meiner Familie und meinen Freunden bedanken, welche mich immer unterstützt haben und mir verziehen haben,

dass ich während der Promotion stellenweise so wenig Zeit mit ihnen verbringen konnte. Hierbei möchte ich mich ganz besonders bei meinem Vater Manfred Thomas bedanken, der mit den einfachen Worten "Arbeit geht vor" meine Abwesenheit an gleich zwei Weihnachtsfesten wegen Messreihen hinnahm. Sowie meinem Freund André Speelmans, der es auf sich nahm meine Dissertation noch einmal Korrektur zu lesen.